Stiffness Design of Paperboard Packages using the Finite Element Method

Juan Crespo Amigo

KTH Engineering Sciences

Master of Science Thesis

Department of Solid Mechanics

Stockholm, Sweden

KTH Engineering Sciences

Stiffness Design of Paperboard Packages using the Finite Element Method

Juan Crespo Amigo

This thesis is submitted to KTH Engineering Sciences, Department of Solid Mechanics in partial fulfillment for the degree of Master of Science in Industrial Engineering at UPC. The work was carried out at Iggesund Paperboard and Department of Solid Mechanics. Examiner at KTH was Professor Sören Östlund.

Master of Science Thesis

Department of Solid Mechanics

Stockholm, Sweden

July 2012

Acknowledgment

The work presented in this licentiate dissertation was carried out during the period February 2012 – July 2012 at Department of Solid of Mechanics, KTH Royal Institute of Technology, Stockholm, Sweden.

I would like to express my gratitude to my supervisor Sören Östlund, for his guidance, encouragement and support during the course of this work. I would also like to thank Brita Timmermann for her valuable suggestions and for making easy relations with the cooperating company.

Thanks to all the people related at KTH University who selflessly helped me with doubts or testing works. Special thanks go to all my friends and colleagues of Stockholm. Finally, I would like to acknowledge my parents for their constant support.

Abstract

This thesis focuses on FEM analysis of paperboard global stiffness. Simulations in Abaqus and experiments were carried out where the deformation was measured. The experimental results were compared with simulation results in order to verify the FEM simulations. Different types of boxes were used to carry out the empirical experiments. The analyses are based on one model that simulates the mechanic behavior of the used boxes. The influence of the creasing stiffness in the global stiffness is specially analyzed. Different gluing zones, materials and structural geometries were used in boxes.

The model predicted the experimental results well except from the gluing zones that in some experiments had a higher impact concluding in worse results. Moreover, the results of the work indicate that the deformation of the boxes mostly depend on the bending stiffness of the paperboard while the influence of the creasing stiffness is low.

Table of contents

1. **Introduction** 1
1.1 Objectives 1
1.2 Paperboard 1
1.3 Finite Elemental Method 3
1.4 Abaqus 3
2. Modeling 5
2.1 Material 5
2.1.1 Thickness 6
2.1.2 Tensile properties 7
2.1.3 Bending Stiffness 9
2.2 Mesh 9
2.3 Gluing zones 10
2.4 Creases 11
2.4.1 Creasing tests 12
2.5 Boundary conditions 17
2.6 Large deformation analysis 17
3. Experiments 19
3.1 Boxes 19
3.2 Properties of study 19
3.3 Load cases 21
3.4 Summary table 22
4. Experimetal Results 23
4.1 Methodology 23
4.2 Results 27
5. Futher Analysis 34
5.1 Sensibility analysis of creasing stiffness 34
5.2 Sensibility analysis of bending stiffness 39
6. Checkouts 40
7. Conclusions 43
8. Topics for further studies 43
References 44
Appendix 1 45
Appendix 2 54
Appendix 3 64

1. Introduction

1.1 Objectives

The objective of this project work was to analyze the global stiffness properties of packages. Many properties affect package performance so not the least global stiffness. Gluing zones, material properties and creasing stiffnesses are considered as the most important ones and will be investigated in the present work. In order to satisfy the objective, it will be found how to anticipate the packaging performance in mechanical loading situations. In this way, the reaction of any box to a serial of external conditions is known. For this reason, one model was created in Chapter 2 that was analyzed using the commercial finite element software Abaqus.

Tests, and simulations in Abaqus of the same experiments, were done and compared through deformation of boxes which is the best indicator of global stiffness. Simplicity, accuracy and efficiency of the measurement procedure were valued.

1.2 Paperboard

According to tradition, paper was first made in China around the year 105 A.D., using cellulose fibers from flax, cotton and other vegetable sources. Over the centuries, different raw materials have been used and the industrial revolution has facilitated progress from laborious manual operation, one sheet at a time, to continuous production in large quantities, using large machines and computerized process control. The essential properties of paper and paperboard manufacture have, however, remained the same. The raw material for paper is still prepared by separating cellulose fibers from natural renewable raw materials. The basic structure of an interlaced network of fibers still forms the web or sheet of the paper. The process still begins with a very dilute suspension of fibers in water from which most of the water is subsequently removed by drainage and evaporation. Since the mid-19th century the primary source of cellulose fiber has been wood. The fiber is separated by either chemical or mechanical means from naturally occurring species such as spruce, pine or birch.

Paperboard can be made as a single-ply or, more commonly, as a multi-ply construction. For quality reasons paperboard usually requires a combination of several layers of fibers in the wet state. The term paperboard is often used when the grammage of paper is over 200 g/m^2. Multi-ply paperboard is widely used in graphical and packaging applications.

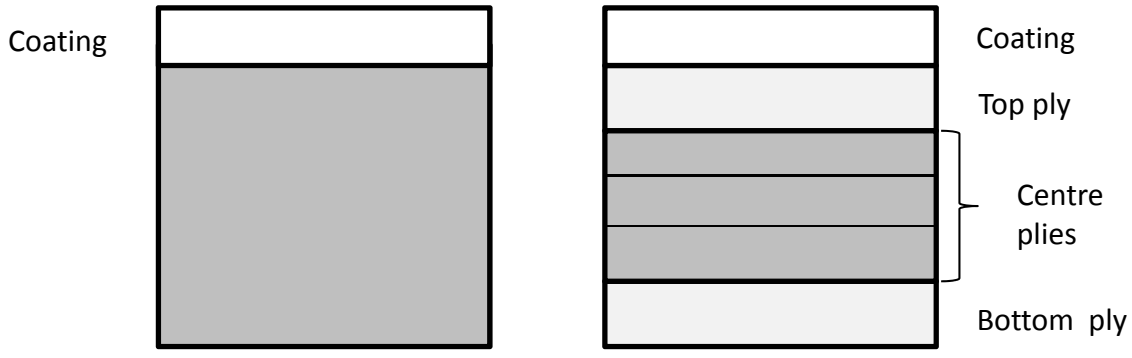

Figure 1.1: Example of the cross-section of two different paperboard designs

Two different types of paperboard properties can be distinguished: the appearance and the performance properties, respectively [1]. The appearance properties are related to the visual impression of the paperboard surface. Printability, whiteness, ink absorption and rub resistance are some of them. The performance properties are related to the physical characteristics of the paperboard. These properties relate to how the paperboard will withstand the surrounding environment. Some of the most important performance properties are discussed below.

Paperboard has a linear elastic behaviour up to a given limit, the elastic limit. This means that the force applied to the paperboard is proportional to the deformation caused by the applied force. If the force is removed the paperboard regains its original dimensions. This is summed up in Hooke's law [2] described in Section 2.1.2.

Paperboard deformed beyond the elastic limit shows elastic-plastic behaviour. This means that the applied force is no longer proportional to the deformation, see Figure 1.2. When the force is removed the paperboard does not regain its original dimensions. The value of the elastic limit is typically 0.2 % relative elongation.

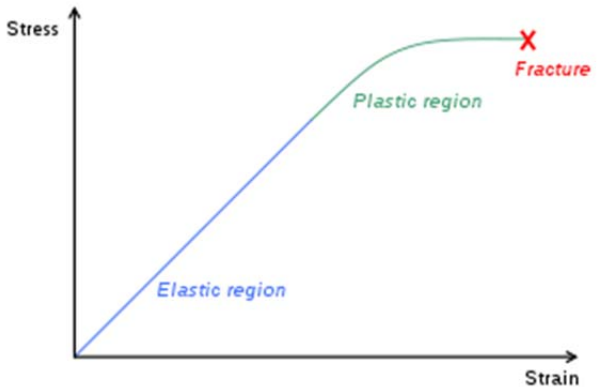

Figure 1.2: Elastic and plastic behavior of typical paperboard [10]

The properties of the fibers and the manufacturing process of paperboard result in a material that to a good approximation can be considered as orthotropic. This means that the materials will have different properties in three orthogonal principal directions; MD (machine direction), CD (cross machine direction) and ZD (thickness direction) as illustrated in Figure 1.3.

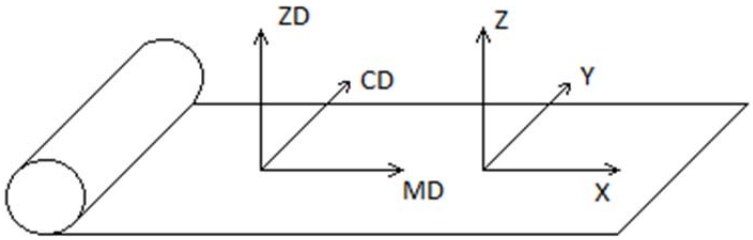

Figure 1.3: Principal material directions of paperboard

1.3 Finite Element Method

The finite element method (FEM) [3] (its practical application often known as finite element analysis (FEA)) is a numerical technique for finding approximate solutions of partial differential equations (PDE) [4] as well as integral equations [4]. The solution approach is based either on eliminating the differential equation completely (steady state problems), or rendering the PDE into an approximating system of ordinary differential equations [4], which are then numerically integrated using standard techniques such as Euler's method [5].

In solving partial differential equations, the primary challenge is to create an equation that approximates the equation to be studied, and is numerically stable, meaning that errors in the input and intermediate calculations do not accumulate and cause the resulting output to be meaningless. The finite element method is a good choice for solving partial differential equations over complicated domains. [3]

FEM uses a complex system of points called nodes forming elements which make a grid called a mesh. The elements of the mesh are programmed to contain the material and structural properties, which define how the structure will react to certain loading conditions. Nodes are assigned at a certain density throughout the material depending on the anticipated levels of stress of a particular area and they transfer the stress from element to element. Points of interest may consist of: fracture points, fillets, corners, complex details, high stress areas, etc. [3]

The finite element method originated from the need for solving complex elasticity and structural analysis problems in civil and aeronautical engineering. Its development can be traced back to the work by Hrennikoff [6]. While the approaches used by these pioneers are different, they share one essential characteristic: mesh discretization of a continuous domain into a set of discrete sub-domains, usually called elements. Starting in 1947, Zienkiewicz [7] from Imperial College gathered those methods together into what would be called the Finite Element Method, building the pioneering mathematical formalism of the method.

1.4 Abaqus

Abaqus FEA [3] is a suite of software applications for finite element analysis and computer-aided engineering, originally released in 1978. Abaqus was initially designed to address non-linear physical behavior; as a result, the package has an extensive range of models for materials such as plastics, metals and woods.

Abaqus is used in the automotive, aerospace, and industrial products industries. The software is popular with academic and research institutions due to the wide material modeling capability, and the program's ability to be customized. Abaqus also provides a good collection of multi-physics capabilities, such as coupled acoustic-structural, piezoelectric, and structural-pore capabilities, making it attractive for production-level simulations where multiple fields need to be coupled.

Every complete finite-element analysis consists of three separate stages. The first stage is called the pre-processing or modeling that involves creating an input file which contains a design for a finite-element analyzer (also called "solver"). The second stage is the processing or finite element analysis that produces an output visual file. The last stage is the post-processing or generating report, image, animation, etc. from the output file.

Abaqus is capable of pre-processing, post-processing, and monitoring the processing stage of the solver; however, the first stage can also be done by other compatible CAD [8] software. Abaqus 6.10 was used in the present work and no CAD software was used for the pre-processing stage.

2. Modeling

In this chapter, the creation of a general box model is explained. In order to understand all the details of the model, the full modeling process will be split into several parts.

2.1 Material characterization

The main objective of this section is to extract the mechanical properties of two different types of paperboard and present them in a form that is applicable in Abaqus. The first material is a SBB (Solid Bleached Board) which is manufactured in by Iggesund Paperboard in Workington, England. It is medium density board with good printing properties. The second material is a FBB (Folding Box Board) manufactured by iggesund, Sweden. It has low density and high bending stiffness. The materials have in the sequel been named materials “S” and “F”, respectively. Both types of paperboard have similar multi-layered paperboard structures, as presented in Section 1.2. Moreover, the thicknesses of the layers and the amount of fibers in each layer are different for the two materials, so different tensile properties, the testing of which are described in Sections 2.1.1 and 2.1.2, respectively, were obtained for the two materials.

Every material is in general characterized by several properties that define its mechanical behavior. There are some features that have a high influence on the material performance. These properties were tested using experiments and defined accurately in order to find a good approximate model for the behavior the paperboard material. On the other hand, there are other properties that are less significant and they were here approximated with literature data and empirical expressions.

Abaqus has many different options to model a structure. In the present case, the paperboard was modeled as a shell structure. This means that the three dimension material was represented by surfaces with a constant thickness. There is no significant difference for the purpose of the present study between using a 3D material model or a shell model, since the deformation in the thickness direction of the paperboard was not considered. The shell model was chosen in order to simplify the modeling work [9].

The paperboard materials were considered to be linear elastic orthotropic [2], so the material deformation is proportional to the applied stress. No plastic behavior [10] was considered as the studied load cases were not supposed to result in such levels of stress. It is obvious then that studies of the failure and fracture behavior [10] were also excluded from the present analysis.

As stated above, paperboard is in general a multi-ply material. This means that the properties in each ply are different. Only three layers were considered in the models of the studied materials, and the contribution from the coating layer to the stiffness properties were neglected. How to set the material characteristics in Abaqus is shown in Appendix 1.

2.1.1 Thickness

The thickness of any paperboard is not exactly constant due to the fibrous structure of the material and small imperfections in the manufacturing process. However, here the paperboards were modelled with a constant cross-section, thus, constant thickness. The average thickness, t, was found through several simple thickness tests with samples of the two different types of paperboard.

To obtain approximate real thicknesses of the three layers, t_1, t_2 and t_3, some samples were previously grinded. This process consists of extracting several thick layers of the paperboard until the sample reaches the desired thickness. The grinded samples of the three layers of the two paperboard materials were facilitated by Innventia [11]. The thicknesses of the layers were tested as $t_{1\text{test}}$, $t_{2\text{test}}$ and $t_{3\text{test}}$. Because of the reliability of the samples of the individual layers was quite low, these values were corrected in order to match with the whole paperboard thickness using the Equation (2.1):

$$t_{\text{i}} = t_{\text{itest}} * \frac{t}{(t_{1_{\text{test}}} + t_{2_{\text{test}}} + t_{3_{\text{test}}})} \;\; ; \;\; i = \{1,2,3\} \qquad (2.1)$$

In Table 2.1, results of the thickness tests, t_{1test}, t_{2test}, t_{3test} and t, and, in Table 2.2, the estimation of the layer thicknesses, t_1, t_2, t_3 and t, are given.

Table 2.1: Thickness measurements of the individual layers and the whole paperboard

Material	Layer	Tested thickness (µm)
F	top ($t_{1\text{test}}$)	124
	middle ($t_{2\text{test}}$)	182
	bottom ($t_{3\text{test}}$)	102
	whole (t)	320
S	top ($t_{1\text{test}}$)	78
	middle ($t_{2\text{test}}$)	134
	bottom ($t_{3\text{test}}$)	77
	whole (t)	305

Table 2.2: Estimated final values of layer thicknesses

Material	Layer	Corrected Thickness (µm)
F	top (t_1)	98
	middle (t_2)	142
	bottom (t_3)	80
S	top (t_1)	82
	middle (t_2)	142
	bottom (t_3)	81

2.1.2 Tensile properties

As stated in Section 1.2, the paperboard is a multi-layered material. In order to characterize the whole paperboard, constitutive parameters must be determined for each layer. The constitutive relation governing the behavior of an orthotropic material (layer) can be written as:

$$\begin{bmatrix} \varepsilon_{11} \\ \varepsilon_{22} \\ \varepsilon_{33} \\ 2\varepsilon_{12} \\ 2\varepsilon_{13} \\ 2\varepsilon_{23} \end{bmatrix} = \begin{bmatrix} \frac{1}{E_1} & \frac{-v_{21}}{E_2} & \frac{-v_{31}}{E_3} & 0 & 0 & 0 \\ \frac{-v_{12}}{E_1} & \frac{1}{E_2} & \frac{-v_{32}}{E_3} & 0 & 0 & 0 \\ \frac{-v_{13}}{E_1} & \frac{-v_{23}}{E_2} & \frac{1}{E_3} & 0 & 0 & 0 \\ 0 & 0 & 0 & \frac{1}{G_{12}} & 0 & 0 \\ 0 & 0 & 0 & 0 & \frac{1}{G_{13}} & 0 \\ 0 & 0 & 0 & 0 & 0 & \frac{1}{G_{23}} \end{bmatrix} \begin{bmatrix} \sigma_{11} \\ \sigma_{22} \\ \sigma_{33} \\ \sigma_{12} \\ \sigma_{13} \\ \sigma_{23} \end{bmatrix} \qquad (2.2)$$

where σ_{11}, σ_{22}, σ_{33}, σ_{12}, σ_{13} and σ_{23} are the components of the stress tensor, conveniently expressed in N/mm^2, E_1, E_2, E_3 G_{12}, G_{13}, and G_{23} are expressed in N/mm^2 and ε_1, ε_2, ε_3, ε_{12}, ε_{13}, and ε_{23} are the components of the strain tensor.

As shown in Equation 2.2, 12 constants need to be determined in order to fully define the material. The variables E_1, E_2 and E_3 are Young's moduli [2] in the three principal directions of the material (MD, CD and ZD). The variables G_{12}, G_{13} and G_{23} are the shear moduli [2] in the principal directions and υ_{12}, υ_{21}, υ_{13}, υ_{31}, υ_{23} and υ_{32} are Poisson's ratios [2]. Although there are six different Poisson´s ratios only, three are independent due to the symmetry of the compliance matrix given in Equation 2.2 [2]. In conclusion, nine constants will have to be determined for each layer.

In order to verify the tensile properties and the thickness values of all the layers, the properties of the whole paperboard was also measured considering the paperboard as a homogeneous material.

Young's moduli E_1 (MD) and E_2 (CD) were determined by tensile tests [12]. The tensile test consists of stretching of one paperboard sample of size 100 x 10 mm and measuring both displacement and applied force. From these results, Young´s moduli in MD and CD were evaluated.

The results of Young's modulus for each layer are given in Table 2.3.

Table 2.3: Young's moduli for all the plies of both paperboards

Paperboard	Layer	E_1 (N/mm^2)	E_2 (N/mm^2)
F	top	4380	1800
	middle	2590	830
	bottom	5460	1500
S	top	7690	3120
	middle	4430	1530
	bottom	6980	3420

Young's modulus in the ZD direction, E_3, was determined by means of Equation (2.3) taken from [13].

$$E_3 = \frac{E_1}{200} \qquad (2.3)$$

The shear moduli for the paperboard, G_{12}, G_{13} and G_{23}, were determined by means of Equations (2.4a), (2.4b) and (2.4c), which also can be found in [13].

$$G_{12} = 0{,}39 \cdot \sqrt{E_1 \cdot E_2} \qquad (2.4a)$$

$$G_{13} = \frac{E_1}{55} \qquad (2.4b)$$

$$G_{23} = \frac{E_2}{35} \qquad (2.4c)$$

Poisson ratios, υ_{12}, υ_{13} and υ_{23} were taken from literature data [13]. Meanwhile υ_{21}, υ_{31} and υ_{32} were calculated from Equations (2.5a), (2.5b) and (2.5c) that follow from the symmetry of the stiffness or compliance matrix.

$$\frac{\upsilon_{12}}{E_1} = \frac{\upsilon_{21}}{E_2} \qquad (2.5a)$$

$$\frac{\upsilon_{13}}{E_1} = \frac{\upsilon_{31}}{E_3} \qquad (2.5b)$$

$$\frac{\upsilon_{23}}{E_2} = \frac{\upsilon_{32}}{E_3} \qquad (2.5c)$$

The results of all these properties for each layer are given in Table 2.5.

Table 2.5: Elastic properties for the plies of both paperboards

Paperboard	Layer	E_3 (N/mm^2)	μ_{12}	μ_{13}	μ_{23}	G_{12} (N/mm^2)	G_{13} (N/mm^2)	G_{23} (N/mm^2)
F	top	21,9	0,458	-2,2	0,54	1080	79,6	51,3
	middle	13	0,519	-2,2	0,54	570	47,1	23,6
	bottom	27,3	0,560	-2,2	0,54	1110	99,2	42,7
S	top	38,5	0,460	-2,2	0,54	1890	139,9	89
	middle	22,2	0,498	-2,2	0,54	1010	80,5	43,8
	bottom	34,9	0,419	-2,2	0,54	1890	127	97,7

2.1.3 Bending stiffness

The bending stiffness is the parameter that quantifies how easy or difficult it is to bend a material. The bending stiffness depends on the geometry of the cross-section of the structure and the through-thickness tensile properties of the paperboard section. This means that once the mechanical properties of paperboard is known, bending stiffness calculation is straight-forward.

If we considered the studied materials as homogenous (same properties in all points of the material) we would be committing a significant error, as the bending stiffness properties of the paperboard cross-section would not be correctly defined. On the other hand, it is not an easy task to define correctly a multi-ply section. The problem stands on how complicated is to measure the thickness of such as thin plies and to correctly determine the properties for each position accurately. Although Carlsson, Feller… [14] show that laminate theory is applicable for paperboard, the properties for each ply are not completely uniform [15]. The multi-ply section was considered in the final model bearing in mind any possible error.

Considering a three layer paperboard, bending stiffness was calculated from the group of Equations (2.6) [16].

$$x = \frac{E_1 \cdot t_1 \cdot \left(\frac{t_1}{2}\right) + E_2 \cdot t_2 \cdot \left(t_1 + \frac{t_2}{2}\right) + E_3 \cdot t_3 \cdot (t_1 + t_2 + \frac{t_3}{2})}{E_1 \cdot t_1 + E_2 \cdot t_2 + E_3 \cdot t_3}$$

$$a = x$$

$$b = a - t_1$$

$$c = b - t_2$$

$$d = c - t_3$$

$$S_b = E_1 \cdot \int_b^a t^2 \cdot dt + E_2 \cdot \int_c^b t^2 \cdot dt + E_3 \cdot \int_d^c t^2 \cdot dt \qquad (2.6)$$

In Equations (2.7), the parameter x is the distance between the top external surface and the neutral axis [16].

The results of the bending stiffnesses of the three layers model are given in Table 2.6.

Table 2.6: Results of bending stiffness

Paperboard	Direction	S_b (Nmm)
F	**MD**	12,7
	CD	4,3
S	**MD**	16,6
	CD	7,3

2.2 Mesh

One of the procedures of the finite element method is to define the finite elements that constitute the model known as the mesh. There are infinite possible meshes for the same body and many of them may be an appropriate choice. The problem is to choose the mesh that is best suited for the particular problem. In general, the smaller element size, the more accurate results will be obtained. On the other hand, if too small elements are

used, the simulation time will be longer. In conclusion, there is a trade-off between accuracy and simulation time.

Each type of box has its own geometry so different meshes were used for each type of box. In Figure 2.1 the mesh of a general box is shown. How to mesh the different boxes is explained in Appendix 1.

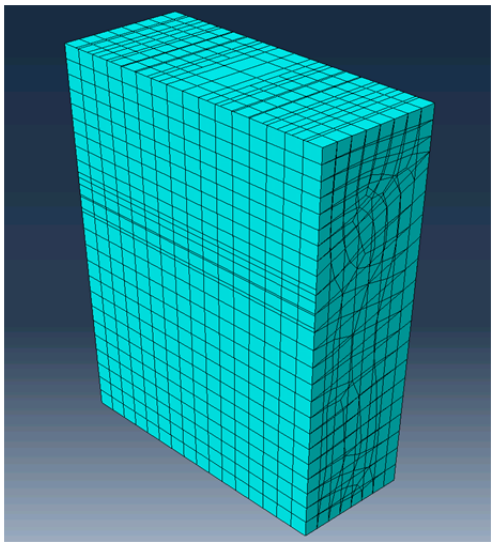

Figure 2.1: Example of a mesh for a general box

2.3 Gluing zone

The gluing zone is the area where two different paperboard surfaces are tied to each other. In the real case, glue is used to attach these two surfaces to each other. In the model, a constraint between the surfaces was added. This constraint ties the two surfaces to each other completely so no movement is allowed between them. How to use this constraint is explained in Appendix 1 and one example is shown in Figure 2.2.

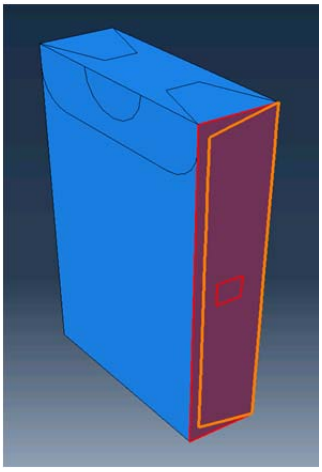

Figure 2.2: The orange line delimits one gluing zone.

It is important to notice that real glue does not tie the two surfaces to each other completely since the glue is not perfectly rigid, while the constraint does. Glue may allow any sort of displacements between the two surfaces that despite being locally small can affect the final performance of the box. This means that in such case the model may not necessarily represent the general performance of the box correctly.

2.4 Creases

In order to correctly model a crease, it should first be defined. A crease is the separation line created when paperboard is folded [17]. If we consider this paperboard as two joined surfaces, it is a difficult task to define the relation between them. The connection between the two surfaces is defined by six degrees of freedom, three displacements and three rotations as illustrated in Figure 2.3.

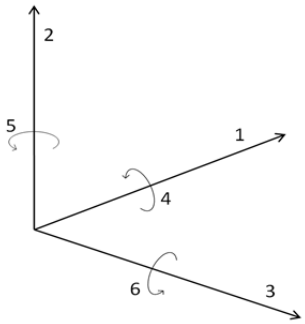

Figure 2.3: General degrees of freedom.

However, five degrees of freedom will be eliminated as they are supposedly insignificant. The only degree of freedom that will be considered is the rotation in the fold direction. In conclusion, the only relative movement between two surfaces joined by the crease will be the rotation in the fold direction (degree of freedom 4), see in Figure 2.4.

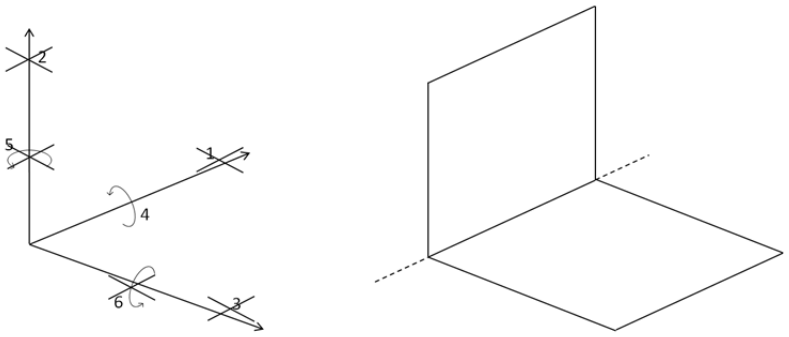

Figure 2.4: Degree of freedom at edge between two surfaces

Moreover, the only remaining degree of freedom may have a particular behavior. This unknown creasing performance will depend on the material properties and the angle of

the fold as well as the geometry of the scoring operation [18]. It is essential to define this creasing property with accuracy high enough to model the stiffness performance of boxes without being too costly from a computational point of view.

The tool of Abaqus that will allow the model to incorporate these requirements (eliminate five from the six degrees of freedom and add a particular behavior to a certain folding geometry) is called CONNECTOR [9]. One connector adds conditions between two nodes. However, the objective is to join two edges instead of two points. It is explained in Appendix 1 how have connectors been applied to solve this problem.

Creasing stiffness depends on many unknown features and there is not any formula that quantifies this property. Tensile material properties, bending stiffness, angle of the crease, folding process, folding geometry of the of the sample and the creasing equipment, and many other features will affect the creasing performance [18]. As stated previously, connectors will represent the creasing behaviors. A spring function, $K_{44}(\theta)$ was added to the connector in order to define the appropriate behavior. In order to define K_{44}, creasing stiffness tests were carried out.

2.4.1 Creasing tests

The creasing measurement consists of folding one creased paperboard sample of size 50 x 25 mm at the crease according to the settings as defined in Figure 2.5. The creasing testing equipment measures the applied force, $F(\theta)$, for angles, θ, from 0 to 135 degrees during loading (forward) and unloading (backwards).

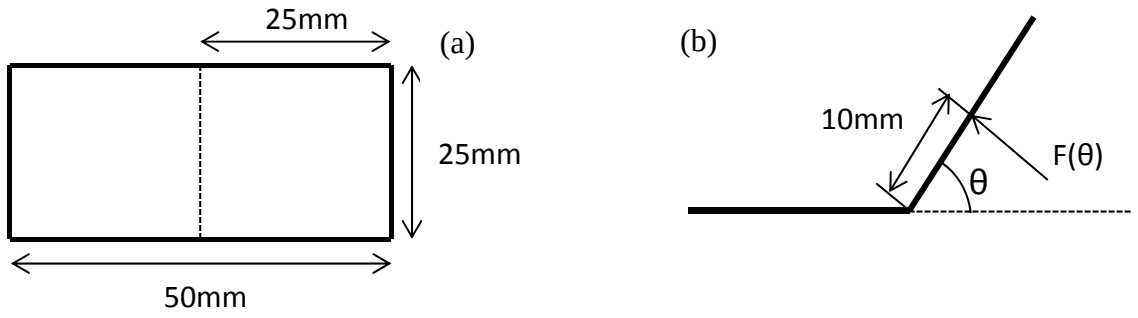

Figure 2.5: Measures of the sample of the creasing test (a) and paramaters (b)

Four complete folding tests were carried out to characterize the creases, one for each material (F, S) and each direction (MD, CD). One full test consisted of five folding measurements, calculation of the mean value of the five series and analysis of the particular behavior around 90 degrees since this is the angle of importance for the rectangular boxes considered in this work. The results for Material S in MD are given in Figures 2.6a, 2.6b and 2.6c. The results for Material F and in CD are given in Appendix 2.

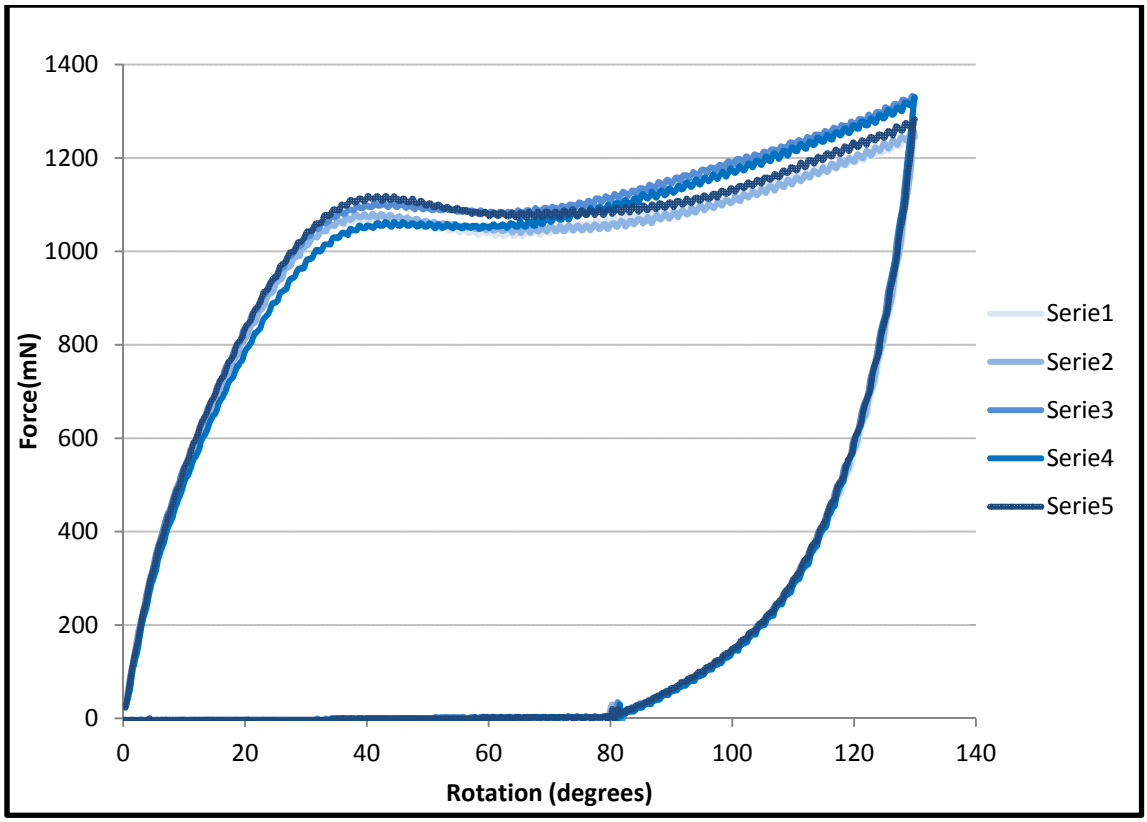

Figure 2.6a: Five creasing tests in MD for material S

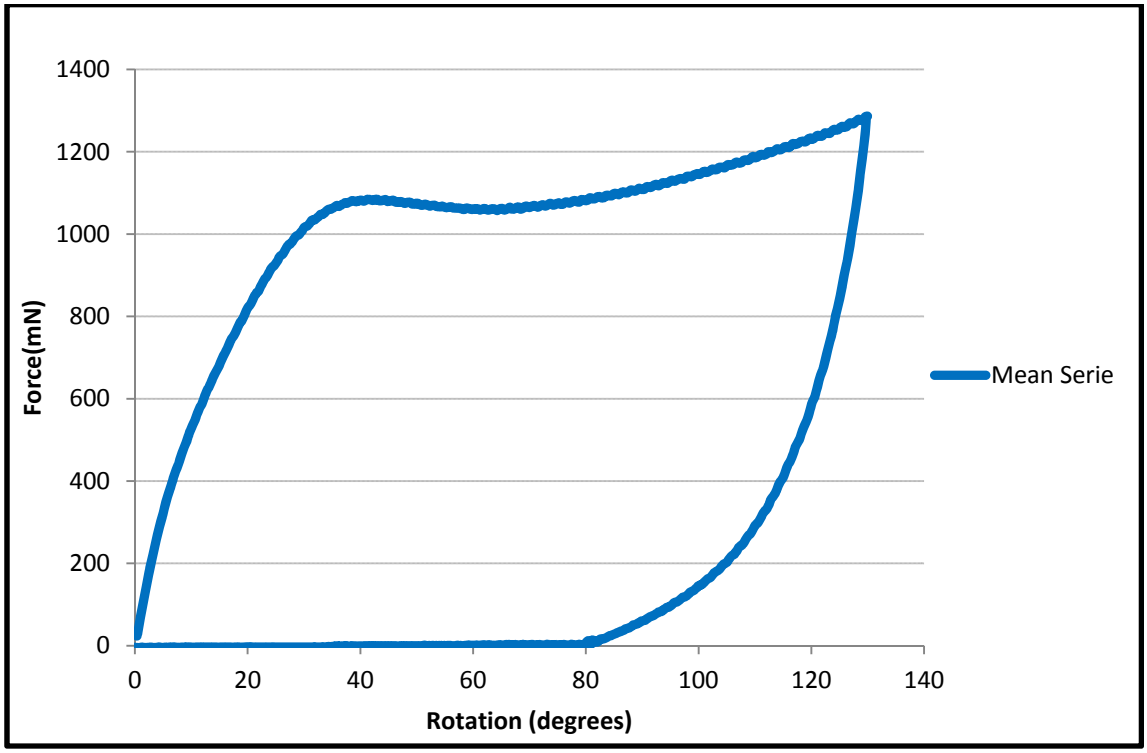

Figure 2.6b: Mean value of the five creasing tests in MD for Material S

In Figure 2.6b two different curves can be distinguished. The top curve corresponds to the loading and the bottom curve corresponds to the unloading.

The number of times that one crease has been folded can affect the creasing stiffness. In the manufacturing process of boxes, the creases are supposed to be folded just one time. For this reason, the loading curve (which has been folded once in the creasing test) was considered and the unloading measurements (which have been folded twice) were not considered.

In Figure 2.6c, for this particular material and direction (S, MD), an approximate linear behavior was observed so a linear tread line was added. For the other three tests, Material S in CD, Material F in MD and Material F in CD, no linear behavior was detected; even so the results were approximated as linear.

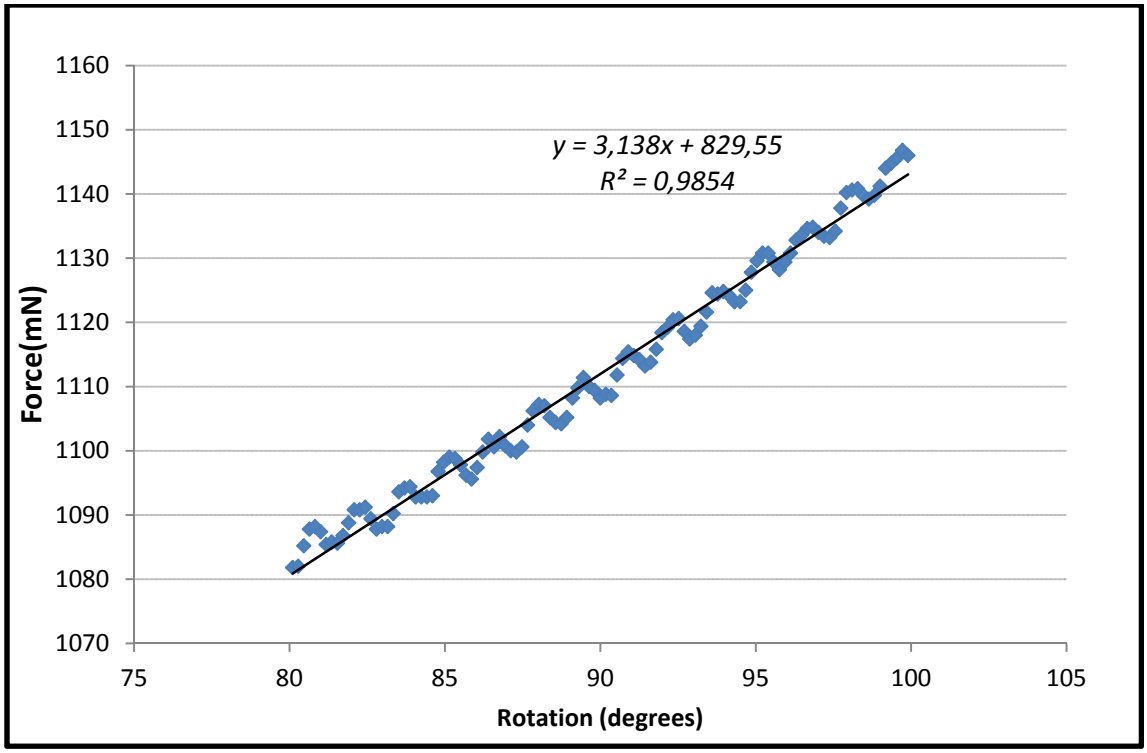

Figure 2.6c: Mean values of the five folding tests during loading from 80 to 100 degrees with a linear tread line in MD for Material S

In parallel, the model of the creasing experiment shown in Figure 2.7 was designed.

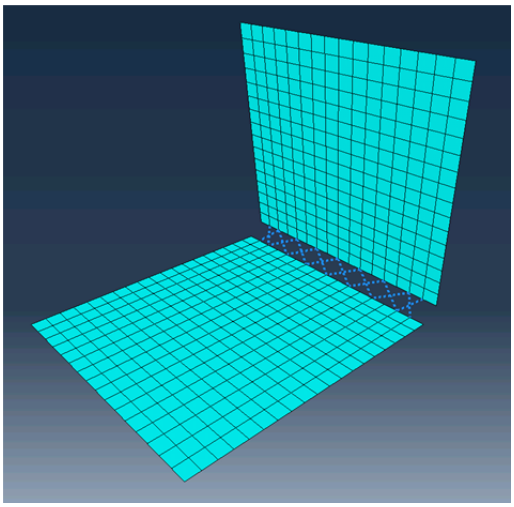

Figure 2.7: Model of the creasing experiment

In order to represent the linear behavior observed in Figure 2.6c, a linear spring constant was added in the connectors as explained in Section 2.4. The value of the constant value was found by comparing the results from the tests with the behavior of the model.

The mesh of the model was changed in order to verify if the element size had any effect on the spring constant. Several element sizes were investigated and for each element size a suitable value of K_{44} was found. The results are given in Figure 2.8.

It is important to notice that the element size was not the same for all the elements in a general mesh. The size values given in Figure 2.8 are the approximate mean value, Z, of the sizes of all the elements in the crease. This means that areas where elements have different size than Z will not work well. However, in Chapter 6, it is deduced that the error caused for the variance of the element sizes can be neglected.

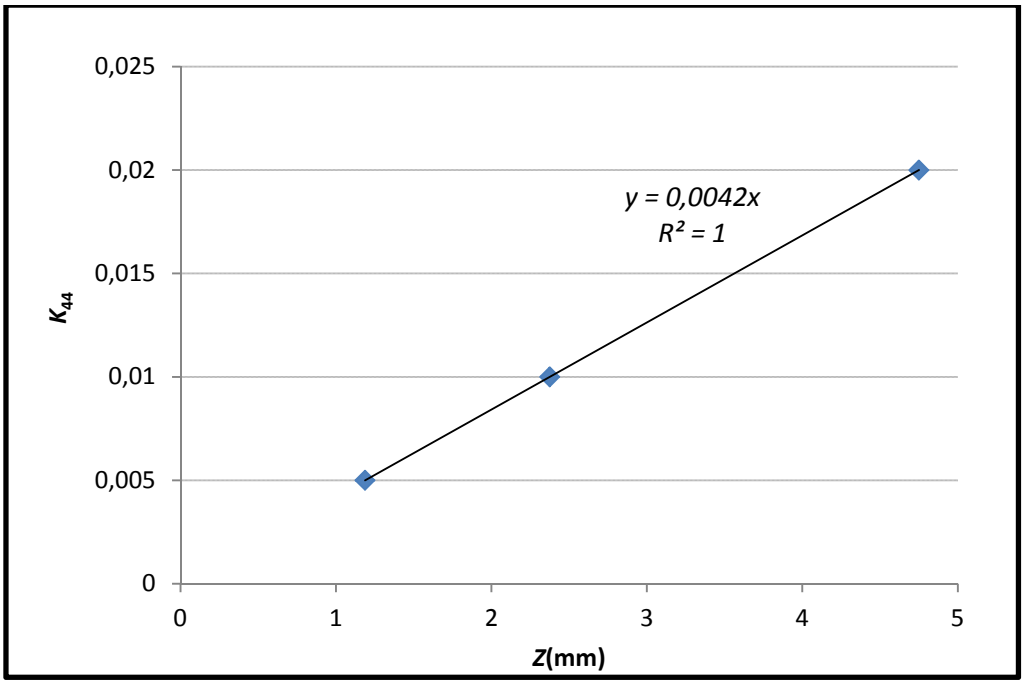

Figure 2.8: K_{44} values for 3 different element sizes

In Figure 2.8 is observed that K_{44} is proportional to the element size. In Table 2.7, K_{44} values are compared for each material and loading direction at a certain element size, Z = 2.375 mm (16 elements in a crease of width 38mm).

Table 2.7: Values of K_{44} for the model for each material and direction with a mean element size, Z = 2.375 mm

Material	Direction	K_{44} (Nmm/degree)
F	MD	0,01
	CD	0,165
S	MD	0,116
	CD	0

The five creasing tests in Material S in CD (Appendix 2, Figure F) had a negative slope around 90 degrees. This is an impossible elastic behavior and for this reason, the value of K_{44} was approximated as zero, see Table 2.7.

These constants had to be adjusted to the element sizes of the mesh used in the analysis of each box, respectively. The results of the values used for each box are given in Table 2.8.

Table 2.8: Adjusted values of K_{44} for each type of box

		K_{44} (Nmm/degree)			
Material	Direction	Model	Cigarette Box	Pill Box	Square Box
F	MD	0,01	0,015	0,017	0,021
	CD	0,165	0,243	0,278	0,347
S	MD	0,116	0,171	0,195	0,244
	CD	0	0	0	0
	Z (mm)	2,375	3,5	4	5

2.5 Boundary conditions

The boundary conditions define an experiment. This set includes loads and displacement boundary conditions. The loads will represent the applied forces on the box while the displacement boundary conditions represent the experimental fixture.

Loads were modeled as pressures on surfaces of size 5 x 5 mm. Point forces can distort results because they accumulate high stress concentrations that are unlikely to occur in practice, so they were not used. How to set the boundary conditions is shown in Appendix 1.

2.6 Large deformation analysis

NLGEOM is one option of Abaqus that can stay “off” or “on”. When NLGEOM is “off”, the orientation of the properties of the material stay fixed even if the material has rotated in any simulation, this is classical small displacement analysis well-known from basic courses in solid mechanics and strength of materials. If NLGEOM is “on”, the orientation of the properties of the material co-rotate with the deforming structure. With this option activated, the simulation time is longer but the results are more accurate. An early experiment was carried out in order to appreciate the difference. One box was pressed with different loads and the maximum deformation was measured. In parallel, two simulations of the test were carried out, one with NLGEOM “off” and the other with NLGEOM “on”. The results are shown in Figure 2.9. How to configure NLGEOM in Abaqus is shown in Appendix 1.

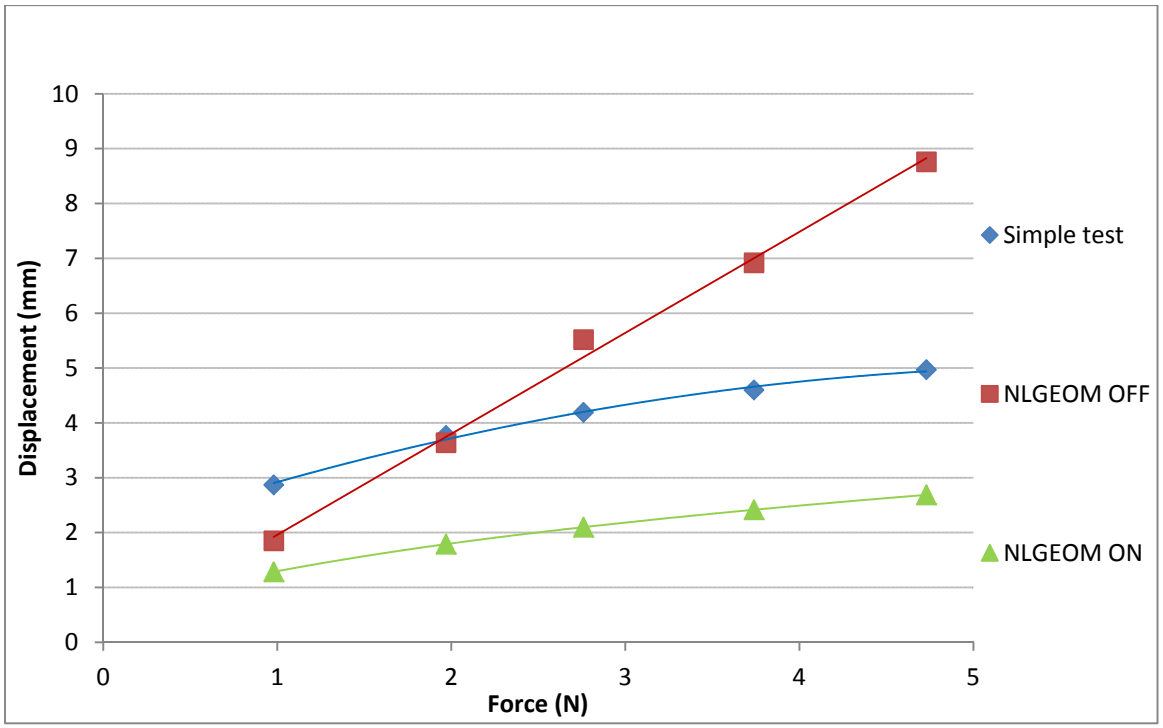

Figure 2.9 Early experiment with the cigarette box in Material F with full glue (see Section 3.2) and simulations with NLGEOM on and off

Although none of the simulations adjust well to the test, the simulation with NLGEOM "on" shows a trend similar to the experiments, while NLGEOM "off" give an expected linear trend in the result. For this reason, in the following experiments NLGEOM was always activated.

In theory, the results between simulations with NLGEOM off and on should give the same results. However, the more the box is deformed, the more the side panels are rotated, the larger is the discrepancy between simulation and test. As shown in Figure 2.9, simulations with NLGEOM off have better results when the maximum deformation is lower. The results for NLGEOM on for small deformation are as good as results for large deformation. The curving trend for larger deformation observed for NLGEOM on in Figure 2.9 is similar to the experimental results.

3. Experiments

Experiments were carried out to verify the model and to analyze the global stiffness of the boxes considered. In this chapter, the experiments that have been done are explained and their features are described.

3.1 Boxes

Three types of boxes were chosen to carry out the experiments and are shown in Figure 3.1: the cigarette box (left), the pill box (middle) and the square box (right). The names are introduced to help the reader to identify which box that is referred due to its shape or performance. In Appendix 3, the geometries of the three boxes are given in detail.

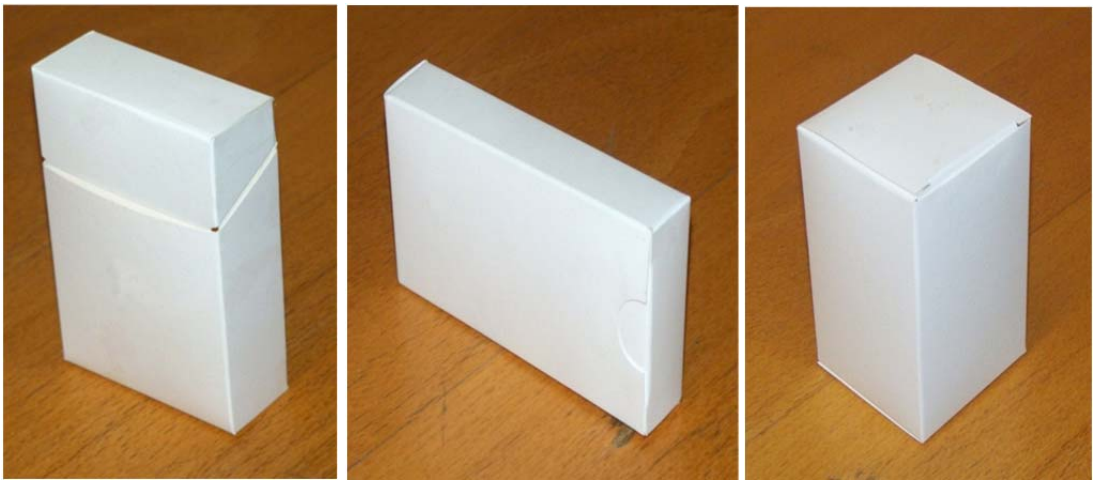

Figure 3.1: Cigarette box (left), pill box (middle), square box (right)

3.2 Properties of study

For each type of box, the influence of one model parameter was investigated. If no reference is given, the box is in Material F, with glue all over the gluing zones and with the creasing stiffnesses as estimated in Section 2.4.1.

For the cigarette box type, two boxes with different gluing zones were considered. The first box had glue all over the gluing zones as shown in Figure 3.2a, while for the second one, for each gluing zone, the glue was only applied along the edges of the surfaces as shown in Figure 3.2b.

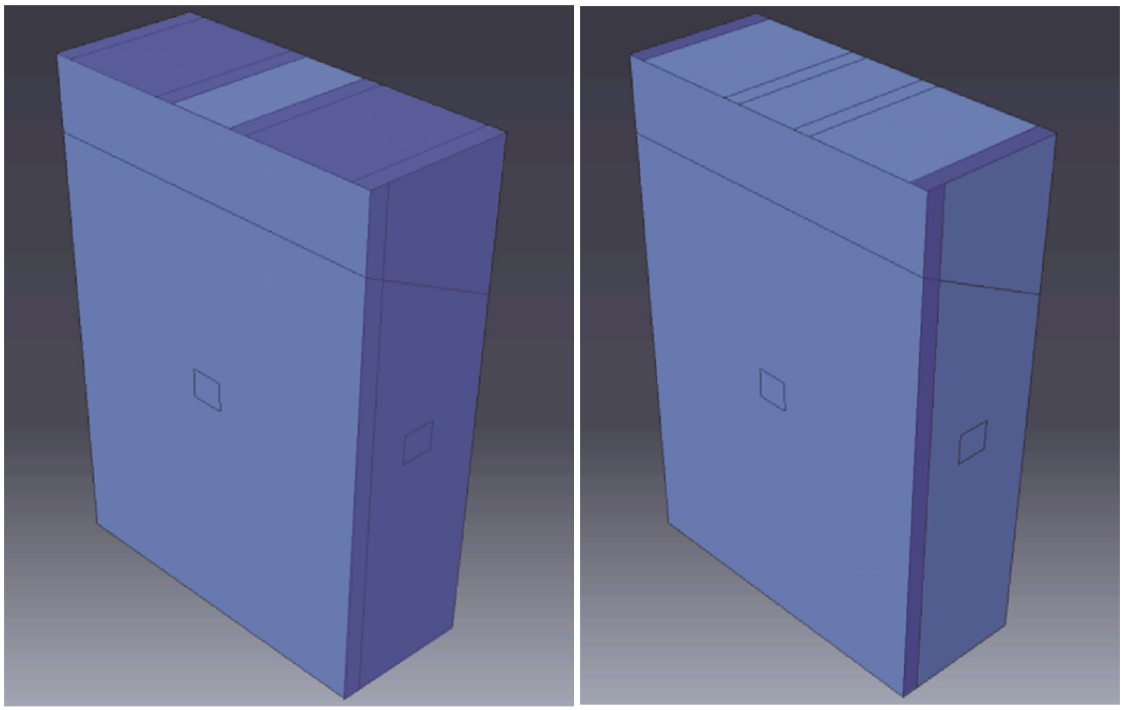

(a) (b)

Figure 3.2: Two different gluing zones for the cigarette e box. The dark regions represent the gluing zones.

The pill box was analysed for two different levels of creasing stiffness. In the first experiment, the box had the standard values of the creasing stiffness. In the second experiment, the creasing stiffness was reduced, considerably, to a negligible level. In order to reach a non-rigid stiff crease in the experiments, all the creases were folded several times. Meanwhile, the creasing stiffness constant of the connectors in the model were set to zero. It is understood that it is impossible to completely remove the creasing stiffness in both model and experiment, so there will be an accepted error between them.

For the square box, tests were carried out with the two different types of materials “S” and “F”, respectively.

3.3 Load cases

All the tests were carried out in the same way. The box was placed on a rigid plate just making contact with the lower surface. After that, a variable load was applied at the middle point of the top surface as shown in Figure 3.3.

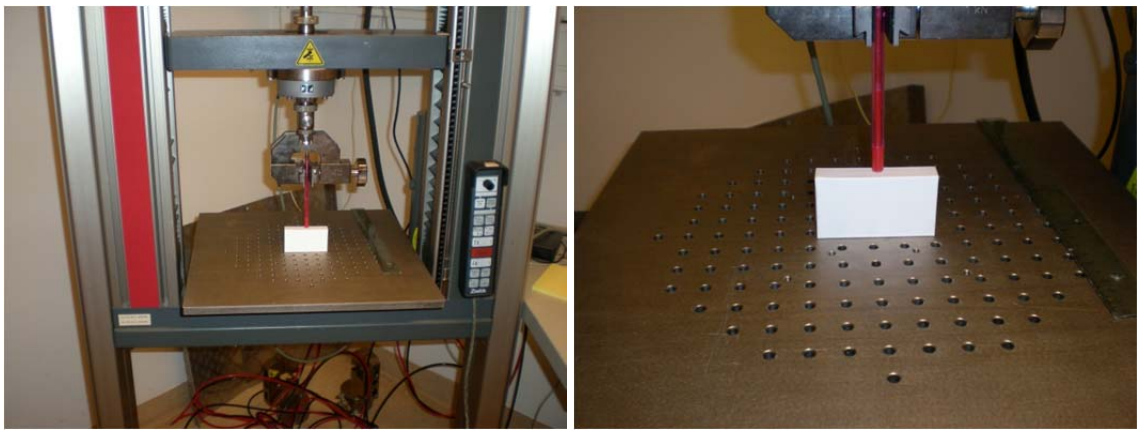

Figure 3.3: Photographs of the experimental set-up

The load took values from 0 to approximately 5.5 N (the machine was manually stopped) and the displacement was measured for all load cases. The measured displacements correspond to the point of the box with the maximum displacement. In all the tests that point was close to the middle point of the top surface, where the load was applied.

For each box, two different experiments were done, where the position of the box was changed between each experiment as illustrated in Figure 3.4.

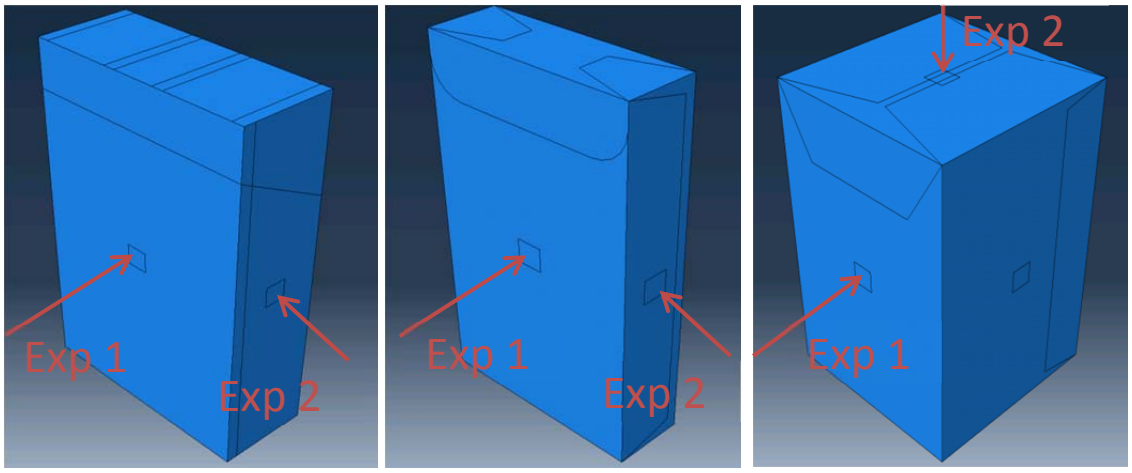

Figure 3.4: Illustration of the two load cases for each box. The arrows represent the directions of the applied loads.

3.4 Summary of experiments

In conclusion, twelve experiments were carried out according to Table 3.1, where the identifications for each experiment also are introduced.

Table 3.1: Notations used for the twelve different experiments

	CIGARETTE BOX		**PILL BOX**		**SQUARE BOX**	
	Full glued	Half glued	Stiff creases	Hinge creases	Material S	Material F
Experiment 1	A.1	A.3	B.1	B.3	C.1	C.3
Experiment 2	A.2	A.4	B.2	B.4	C.2	C.4

4. Experimental results

In this chapter, the results of the experiments described in Chapter 3 are presented and compared with the results of the simulations using Abaqus.

4.1 Methodology

Test A1 with the fully glued cigarette box was used to develop the analysis procedure that later was used for all tests. The experimental results of these tests are shown in Figure 4.1a while the experimental results of the other eleven tests are given in Appendix 2. Two different behaviors can be distinguished in Figure 4.1b.

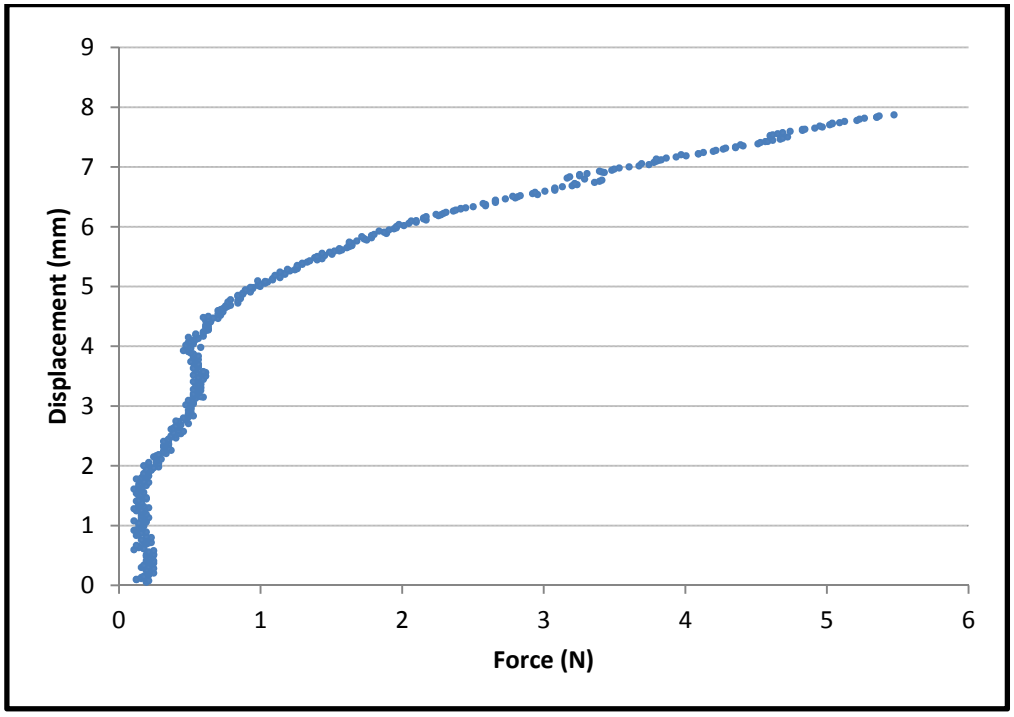

Figure 4.1a: Force-displacement curve for a fully glued cigarette box in experiment 1

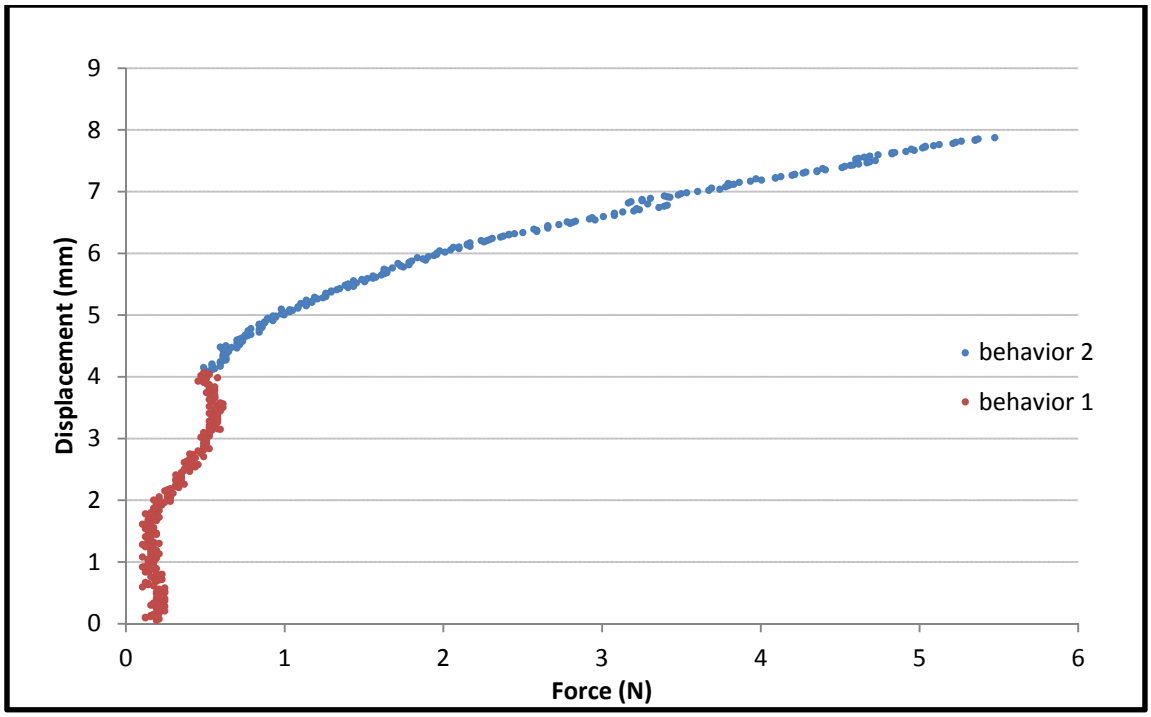

Figure 4.1b: Behavior 1 and 2 for a fully glued cigarette box in Experiment A1

If both behaviors are compared, the average slope for behavior 1 is considerably higher than for the second part (behavior 2) and behavior 1 is also more unpredictable than behavior 2. This means that the global stiffness of the box is low and difficult to predict for the first few millimeters of displacement. The global stiffness of behavior 2 is higher and seems to follow a logarithmic behavior.

To analyze the experiments, it was observed that the first behavior is the result of the concave shape of the box due to the manufacturing process and possible flattening of the irregularities of the bottom panel of the box. Besides, the beginning of behavior 2 was supposed to coincide with the original prismatic shape of the box. For this reason, behavior 2 was further studied and behavior 1 was not considered in the comparison with the simulations. In Figure 4.1c, behavior 2 is re-plotted after removal behavior 1.

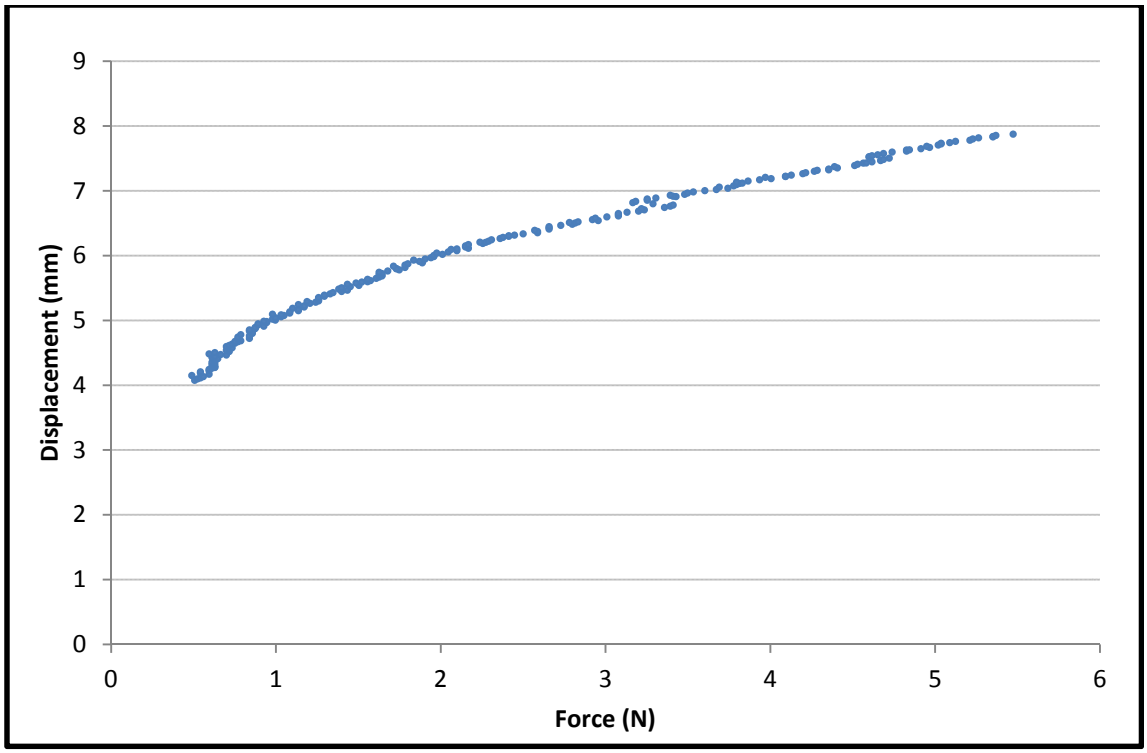

Figure 4.1c: Behavior 2 for a fully glued cigarette box in Experiment A1

Since behavior 1 was removed, all the experimental measurements were corrected so that the initiation of behavior 2 became the initial position. This means that the first measurement of behavior 2 corresponds to displacement zero and force zero. The corrected values of behavior 2 are given in Figure 4.2.A1 in blue. The red dots are the result of the simulations using Abaqus for the same type of box and experiment.

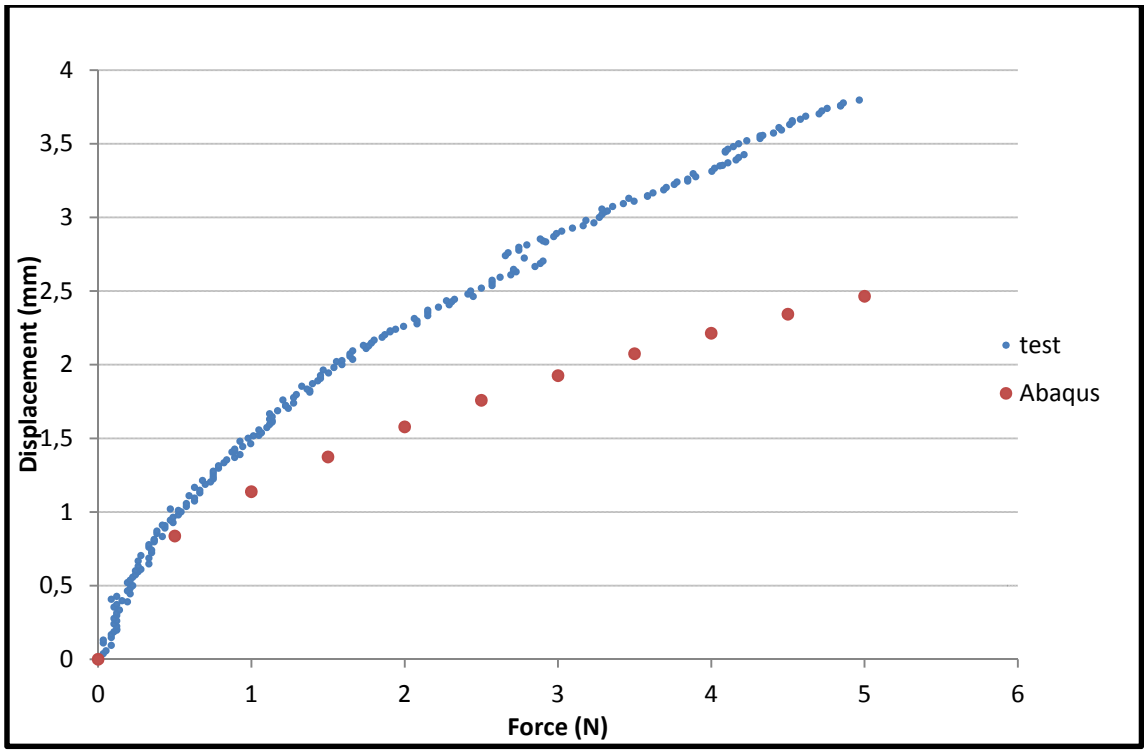

Figure 4.2.A1: Comparison of simulation and experimental results for a fully glued cigarette box in Experiment 1 (test A1)

4.2 Results

In this section, the results of all the experiments presented in Chapter 3 are analyzed considering the procedure explained in Section 4.1.

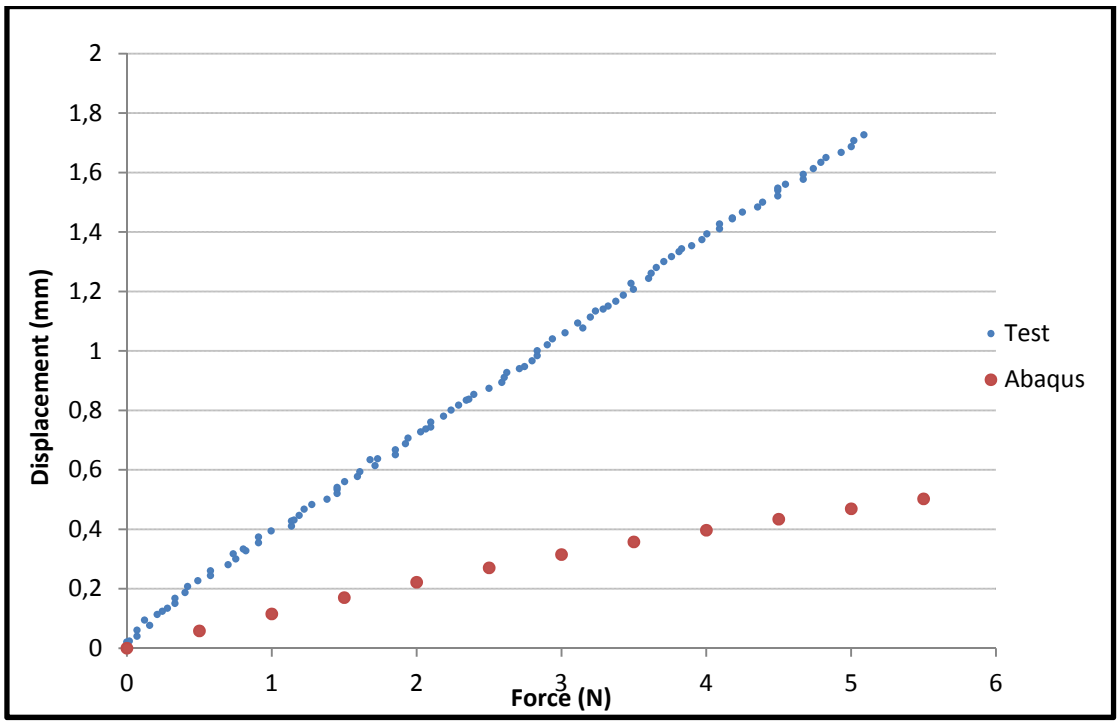

Figure 4.2.A2: Comparison of simulation and experimental results for a fully glued cigarette box in Experiment 2 (test A2)

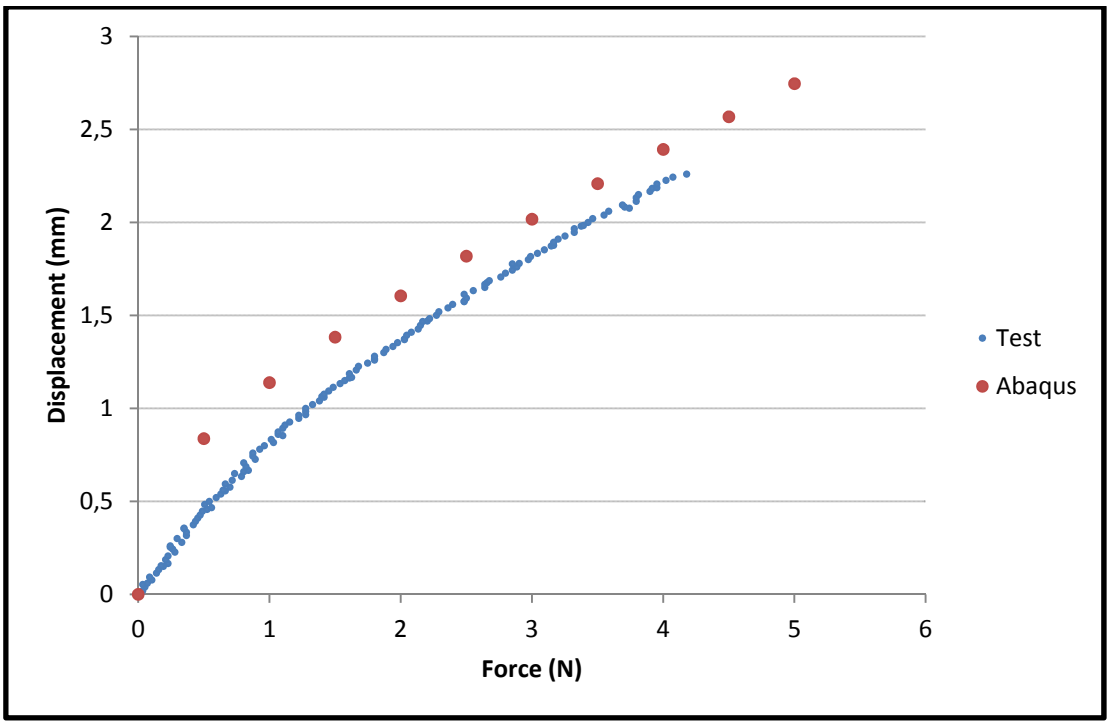

Figure 4.2.A3: Comparison of simulation and experimental results for cigarette box with half glue in Experiment 1 (test A3)

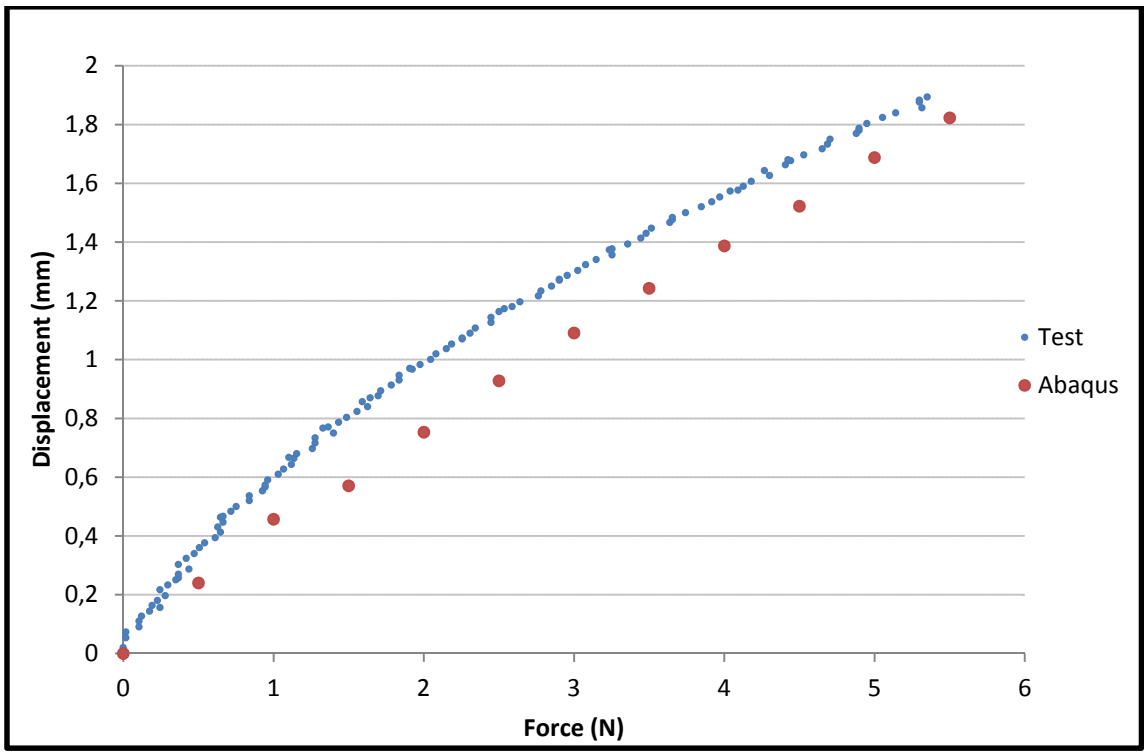

Figure 4.2.A4: Comparison of simulation and experimental results for cigarette box with half glue in Experiment 2 (test A4)

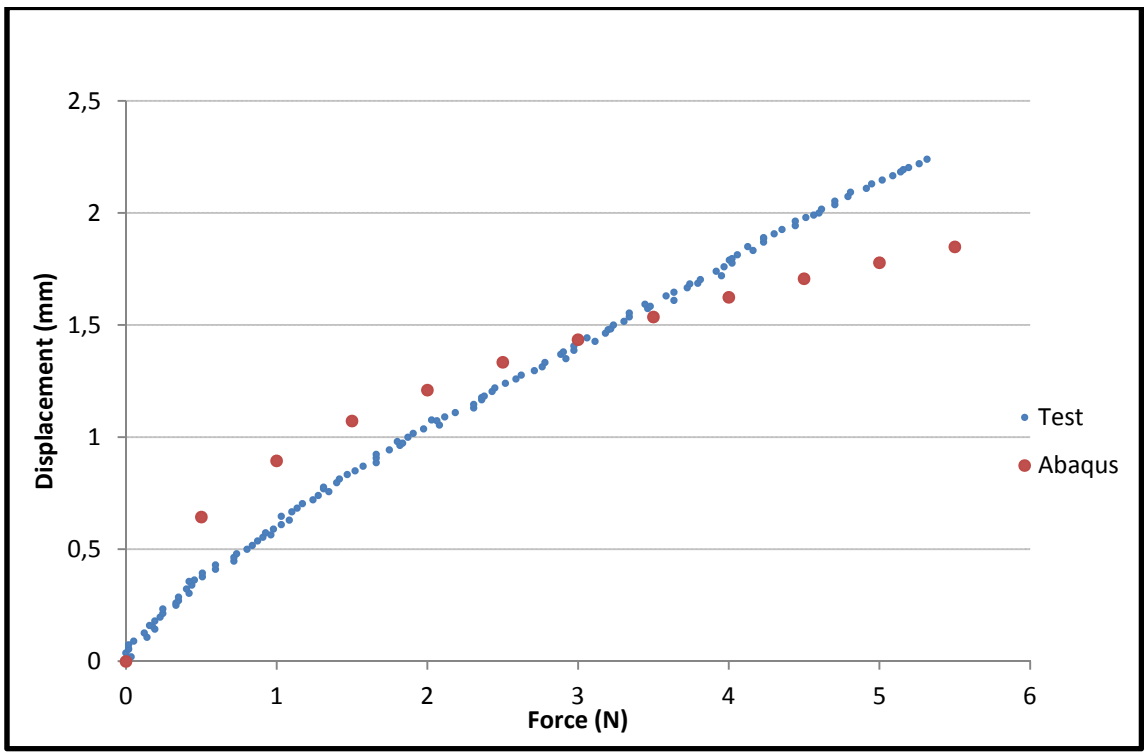

Figure 4.2.B1: Comparison of simulation and experimental results for pill box with stiff creases in Experiment 1 (test B1)

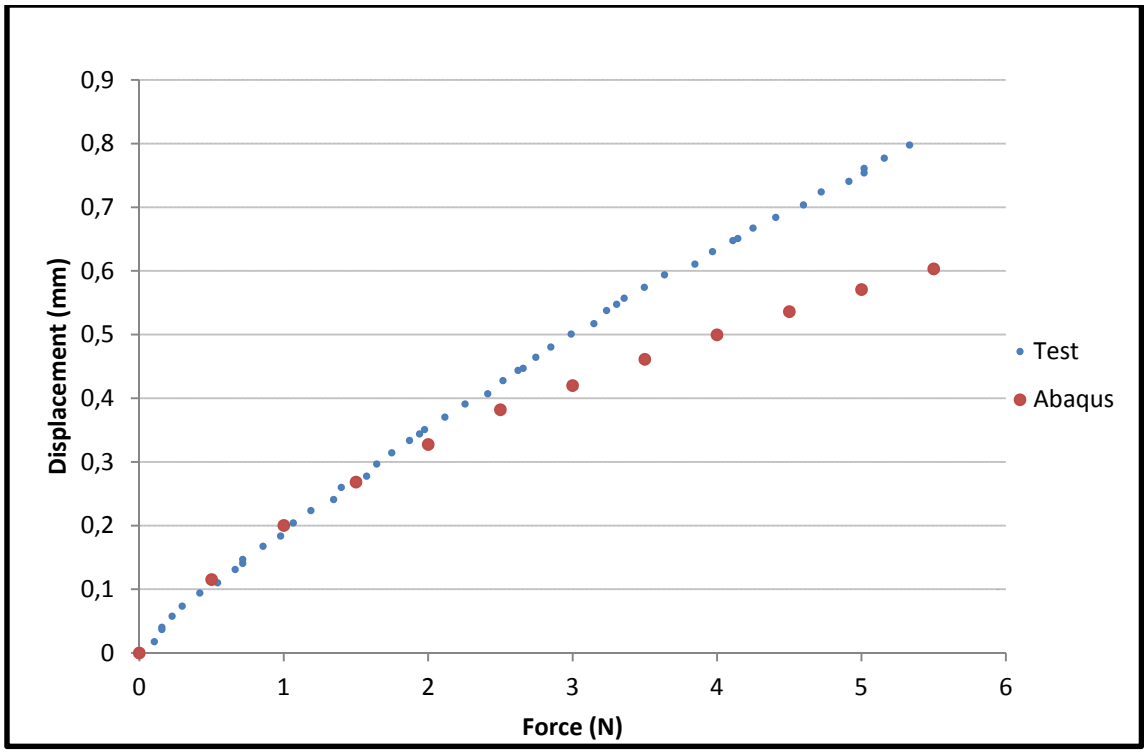

Figure 4.2.B2: Comparison of simulation and experimental results for pill box with stiff creases in Experiment 2 (test B2)

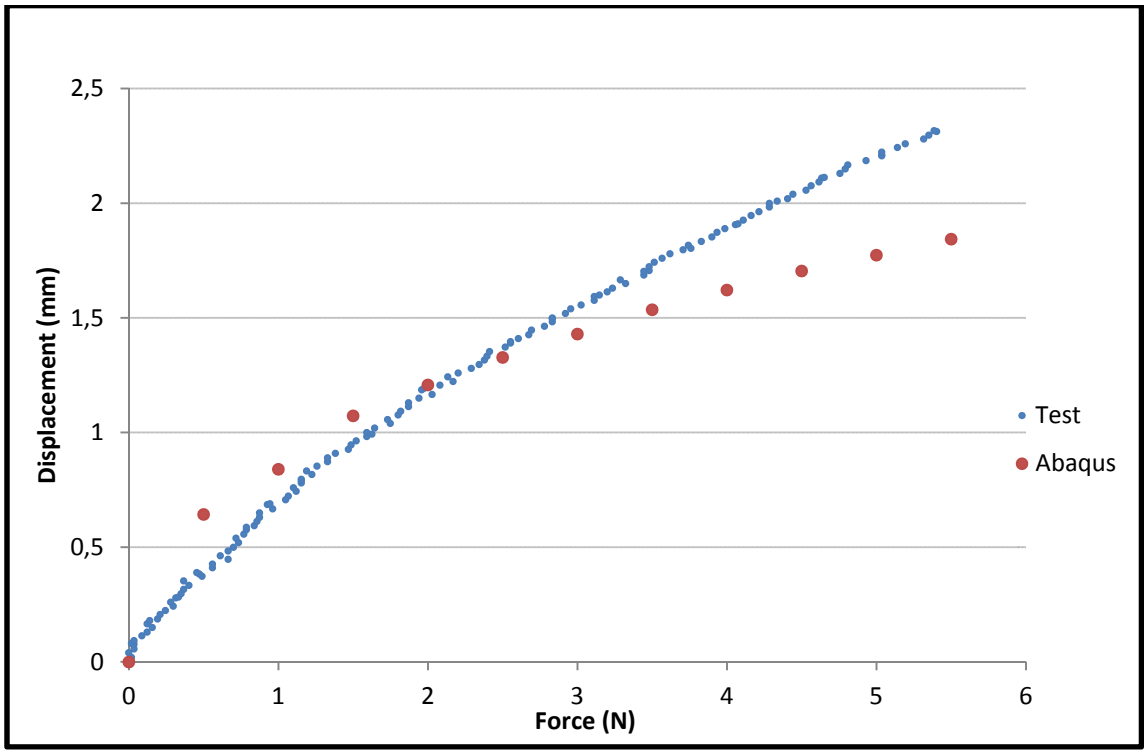

Figure 4.2.B3: Comparison of simulation and experimental results for pill box with hinges as creases in Experiment 1 (test B3)

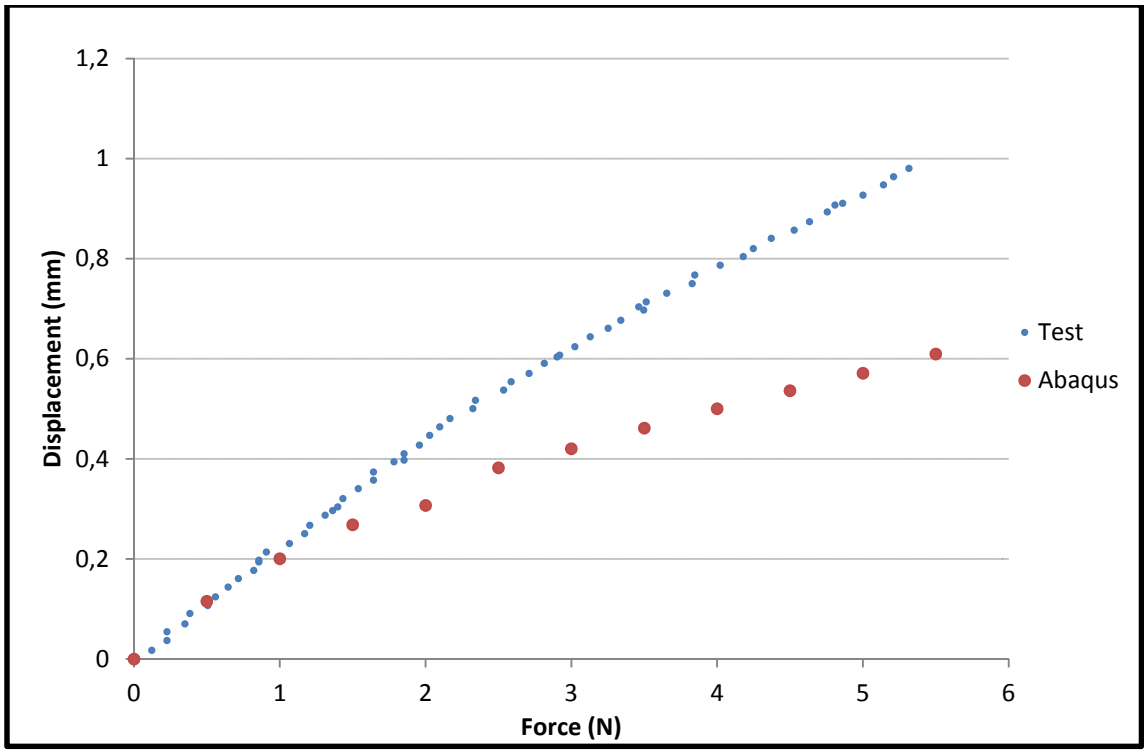

Figure 4.2.B4: Comparison of simulation and experimental results for pill box with hinges as creases in Experiment 2 (test B4)

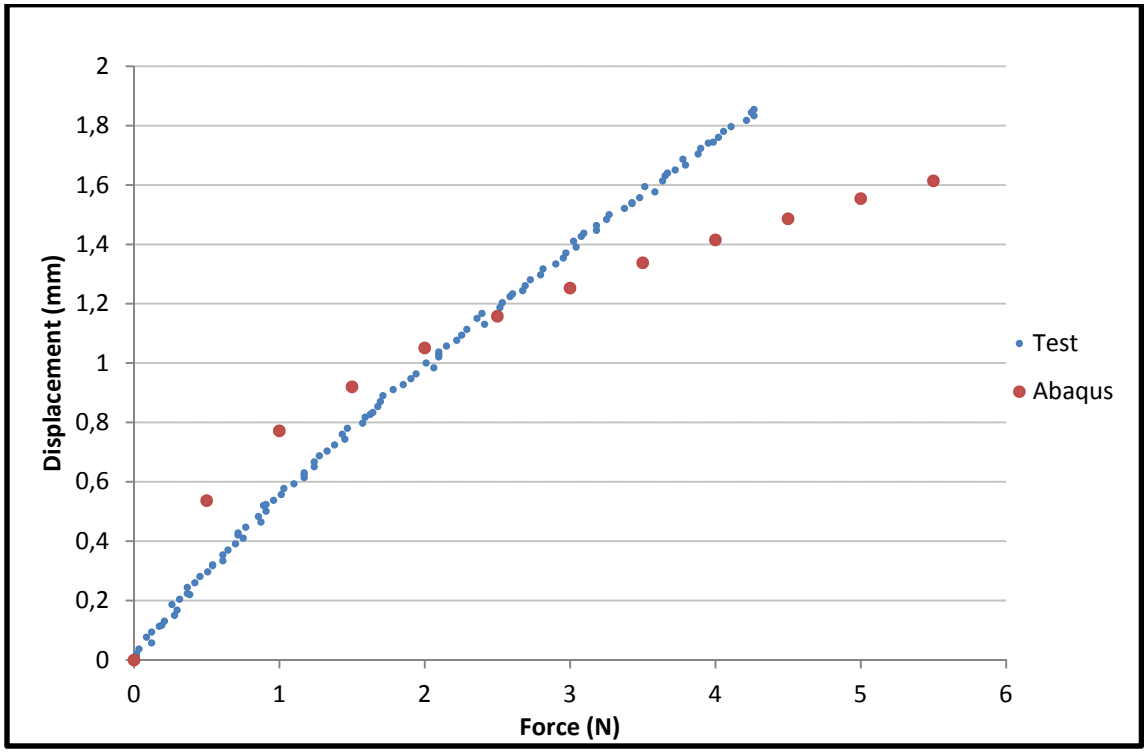

Figure 4.2.C1: Comparison of simulation and experimental results for square box of material S in Experiment 1 (test C1)

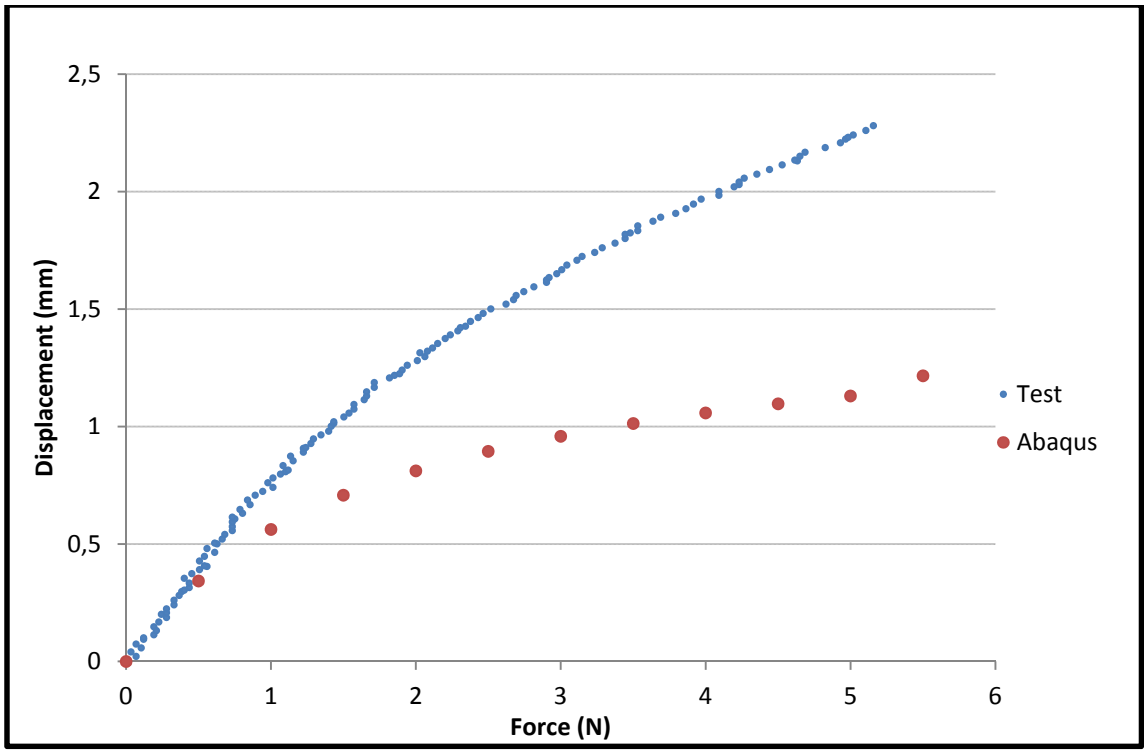

Figure 4.2.C2: Comparison of simulation and experimental results for square box of material S in Experiment 2 (test C2)

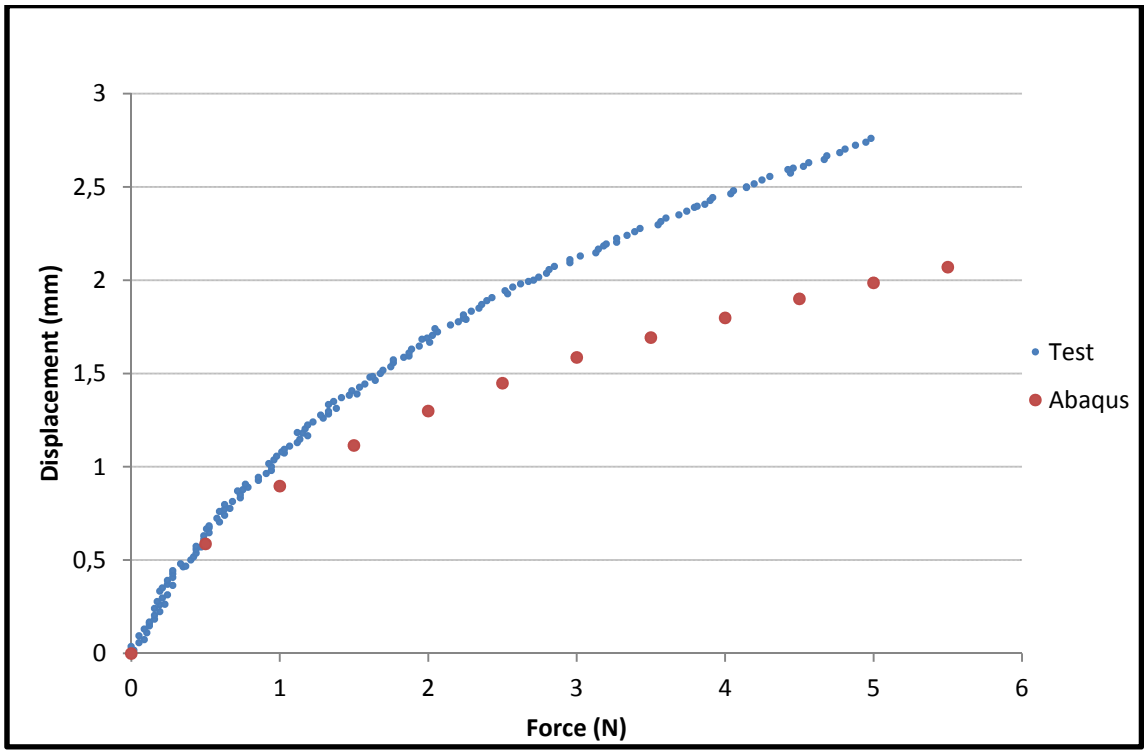

Figure 4.2.C3: Comparison of simulation and experimental results for square box of material F in Experiment 1 (test C3)

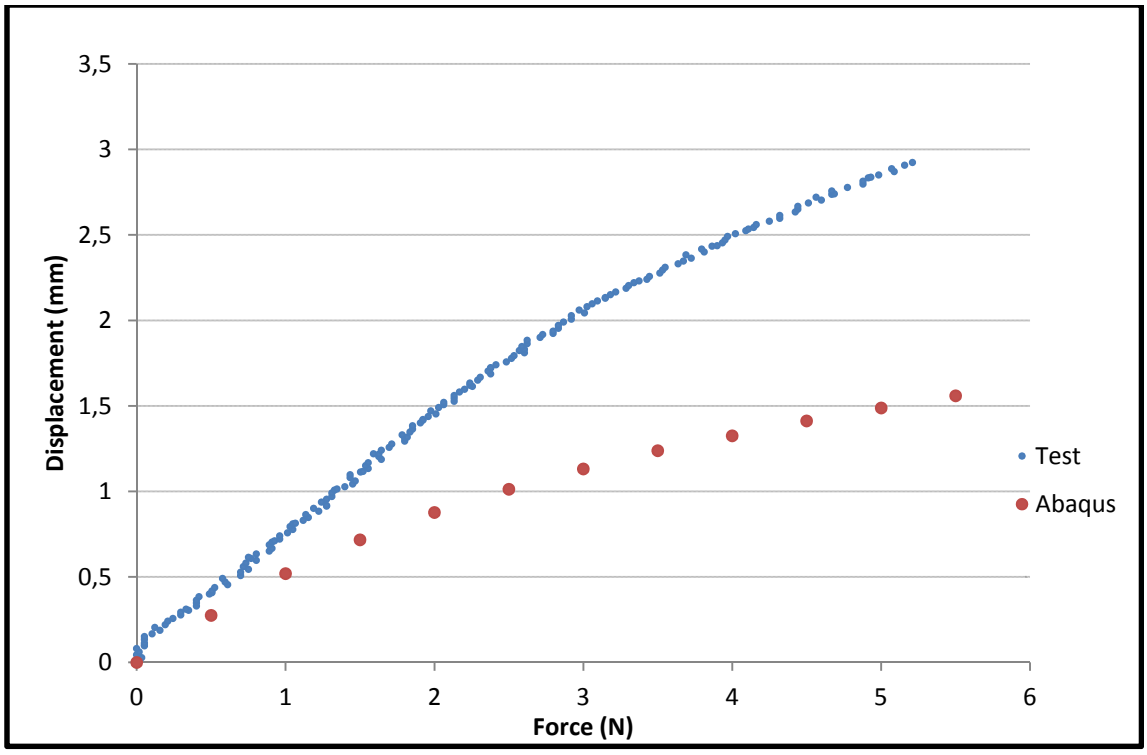

Figure 4.2.C4: Comparison of simulation and experimental results for square box of material F in Experiment 2 (test C4)

If the graphs are analyzed in a global way, three different types of graphs are distinguished. In the first type of graph, the measurements of the test and the values of the simulations coincide excellently. Accordingly, the Abaqus model is appropriate for the tests in Figures 4.2.A3 and 4.2.A4. These tests correspond to the cigarette box with half glue for both experiments.

In the second group of graphs, there is a huge discrepancy between experiments and simulations. The tests A2, C2 and C4, shown in Figures 4.2.A2, 4.2.C2 and 4.2.C4, belong to this group. Test A2 shows a higher error than C2 and C4. These three tests have one feature in common; the load is applied to a paperboard surface which is fully glued to another paperboard surface. This means that the maximum deformation takes place in a double thickness paperboard surface. Why test A2 is higher than C2 and C4 cannot be explained with the present experiments.

In the third type of graphs, the measurements of the test and the values of the simulations have a relatively small discrepancy between experiments and simulations, and their appearances, Figures 4.2.A1, 4.2.B1, 4.2.B2, 4.2.B3, 4.2.B4, 4.2.C1 and 4.2.C3, belong to this group.

The most important features from the model, general paperboard properties, creasing properties, geometry, gluing zones and the general setup of Abaqus, are further analyzed in this section.

Some conclusions can be deduced from the twelve tests. Firstly, there were two experiments that were completely successfully, i.e. experiments from the first group, A3 and A4, as stated above. This means that there are two reasonable options for each feature of the general model of the boxes: the feature is correctly modeled or it is

incorrectly modeled but it does not affect the final results in these two tests. The features that are modeled differently in the other test are possible reasons for the discrepancy since they can be incorrectly modeled. The general paperboard properties, the creasing properties and the general setup of Abaqus remain constant in almost all the experiments so they can be considered as appropriately modeled.

In order to verify if the box geometries affect the results of the tests, Tests A1 and A3 were compared. The only difference between these two experiments was the gluing zone but the error was much higher in A1 so the geometry is most likely not responsible for the error between both tests. If Tests A2 and A4 are compared, the same conclusion is deduced. In conclusion, the geometry is also correctly modeled.

This concludes that the gluing zones are the only candidates for being incorrectly modeled. In Tests A3 and A4 the gluing zones were small so there was almost no error. In tests A2, C2 and C4 the maximum deformations were in the gluing zones so the error was significant. In the other tests the gluing zones (that were not situated where the force was applied) had a medium influence and so this was reflected in the error. Real glue allows two glued surfaces to slide relative to each other, if only little, so the glue was considered completely rigid in the model. However, such a small relative displacement between surfaces can have significant influence on the deflection when both surfaces are bending and for this reason the deflections of the model are lower than the deflections in the tests.

5. Further analysis

The deformation of a general box for a general load case basically depends on three properties of the paperboard material: in-plane tensile stiffness, bending stiffness and creasing stiffness. The objective of this chapter is to break down the causes for the deformation and associate it to one of these three previous features. Then, the maximum displacement, L, is the sum of three terms: displacement contributed to in-plane tensile stiffness, L_{tensile}, the displacement contributed to bending stiffness, L_{bend}, and the displacement contributed to creasing stiffness, L_{crease}.

$$\mathrm{L} = \mathrm{L}_{\text{tensile}} + \mathrm{L}_{\text{bend}} + \mathrm{L}_{\text{crease}} \qquad (5.1)$$

Because of the shell structure of the boxes, tension and compression efforts are not significant. For the range of forces studied, if any laminate of the paperboard is submitted to compression or traction in ZD, the thickness does not practically change. If the laminate is submitted to compression or tension in MD or CD, the maximum deformations are due to the bending. This means that the paperboard does not get compressed in practice; the paperboard bends. For this reason, tensile properties were not further considered.

$$\mathrm{L}_{\text{tensile}} = 0 \qquad (5.2)$$

Considering the model described in Chapter 2, two sensibility analyses were carried out.

5.1 Sensibility analysis of creasing stiffness

Nine simulations with different creasing stiffness were carried out. The simulations were done using the pill box in Experiment 2 with a constant force of 5 N. The maximum deflection was measured and the results are given in Figure 5.1. The values of the creasing stiffness K_{44} are on logarithmic scale on the horizontal axis and the red symbol corresponds to the standard bending stiffness, which was the approximate mean of the bending stiffness in MD and CD.

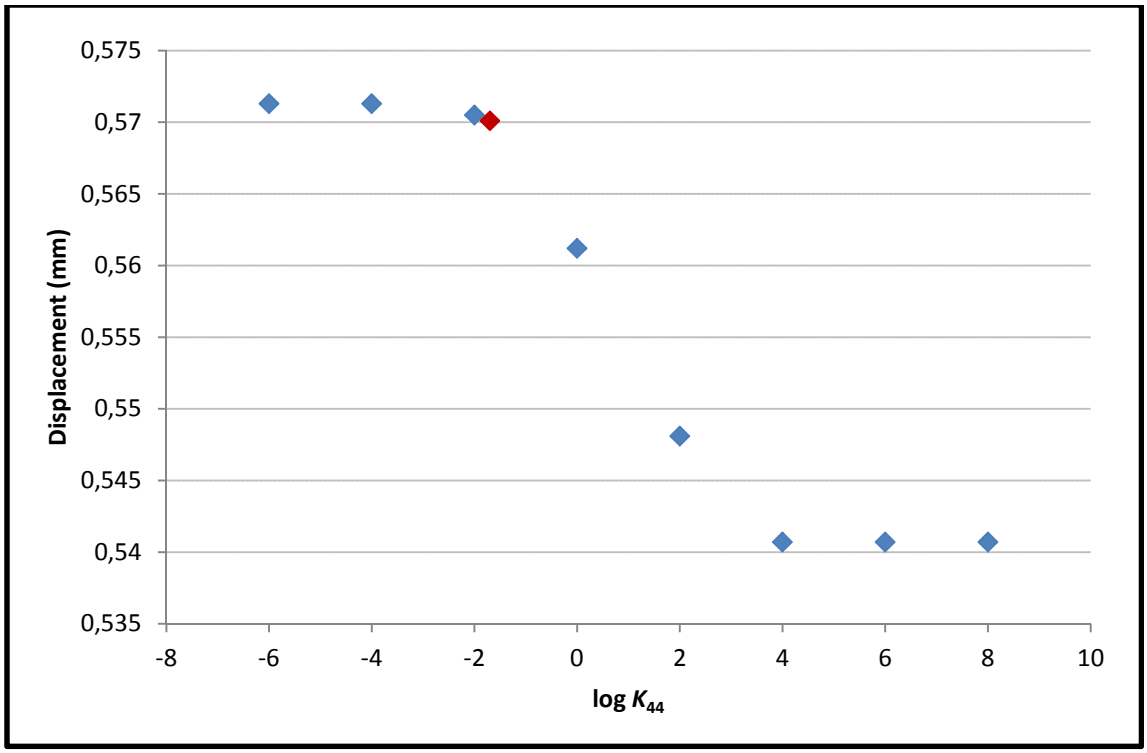

Figure 5.1: Sensibility analysis of creasing stiffness for the pill box in Experiment 2 with a 5 N force

The resultant curve converges to constant values for both high and low values of K_{44}. For high values of K_{44} larger than 4 the deflection is almost constant indicating that the creasing stiffness can be approximated as infinite. The crease stiffness values are so high that the creases are considered completely rigid, meaning that the creases do not fold noteworthy. In these cases the displacement, L_{min} = 0.541 mm, is due to the bending stiffness. Thus, in Equation (5.1)

$$L_{bend} = 0.541 \text{ mm} \qquad (5.3)$$

$$L_{crease} = 0 \text{ mm} \qquad (5.4)$$

For the low value of the creasing stiffness displacement converges to L_{max} = 0.571 mm. In this case, the creases are folded but they do not introduce any resisting moment so the creases behave as hinges. If the displacement associated to the bending stiffness is assumed as constant, from Equation (5.1) and Equation (5.2) it can be deduced that

$$L_{bend} = 0.541 \text{ mm} \qquad (5.5)$$

$$L_{crease} = 0.03 \text{ mm} \qquad (5.6)$$

The deformation of the box when creases behave as hinges is 100.2 % of the standard deformation, L = 0.57 mm for boxes with estimated creasing stiffnesses. On the other hand, the deformation of the box when K_{44} tends to infinity is 94.8 % of the standard deformation. The range of behaviors for all the possible creasing stiffness values is illustrated in Figure 5.2a.

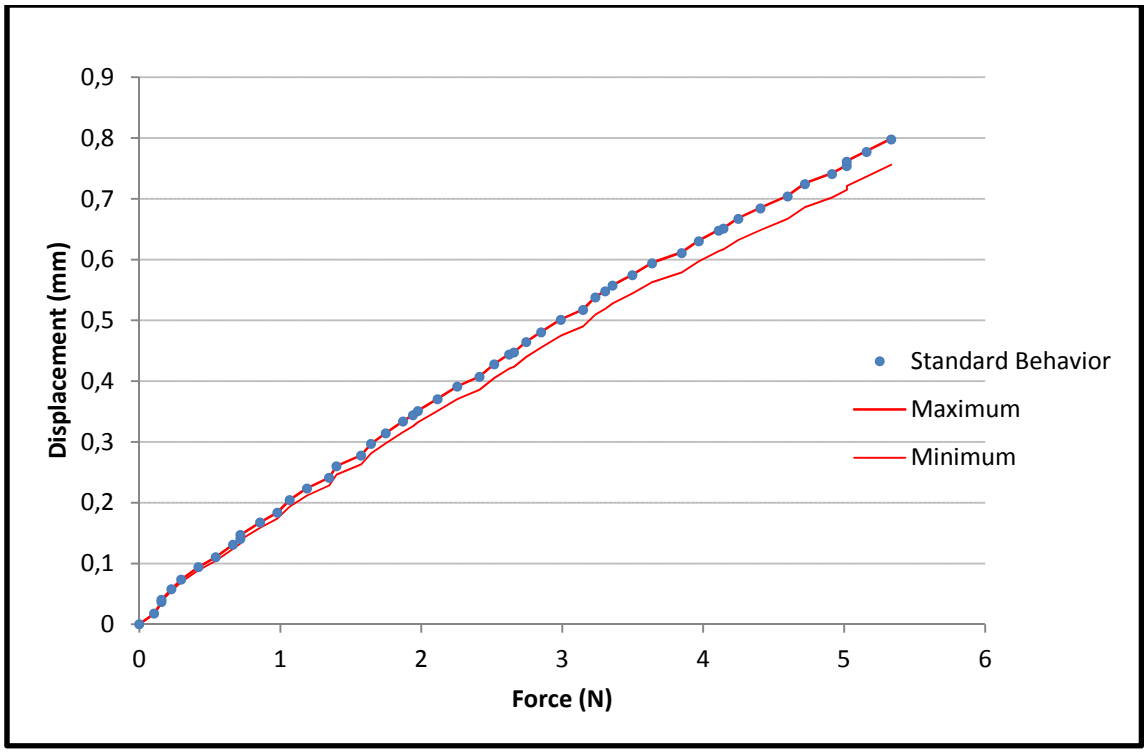

Figure 5.2a: The graph shows the range of behaviors for the pill box in Experiment 2 considering the sensibility analysis of crease stiffness with a load of 5 N. The red lines limit the range of behaviors.

The procedure explained above was applied to three other experiments. The numerical results are given in Table 5.1 and the graphical results are given in Figures 5.2a, 5.2b, 5.2c and 5.2d.

Table 5.1: Limits of the range of behavior for four types of experiments

	Cigarette_exp1_1N	Cigarette_exp1_5N	Pill_exp2_1N	Pill_exp2_5N
L (mm)	1,321	2,882	0,2	0,57
L_{min}/L (%)	83,6	86,7	91,3	94,8
L_{max}/L (%)	100,4	100,1	100,0	100,2

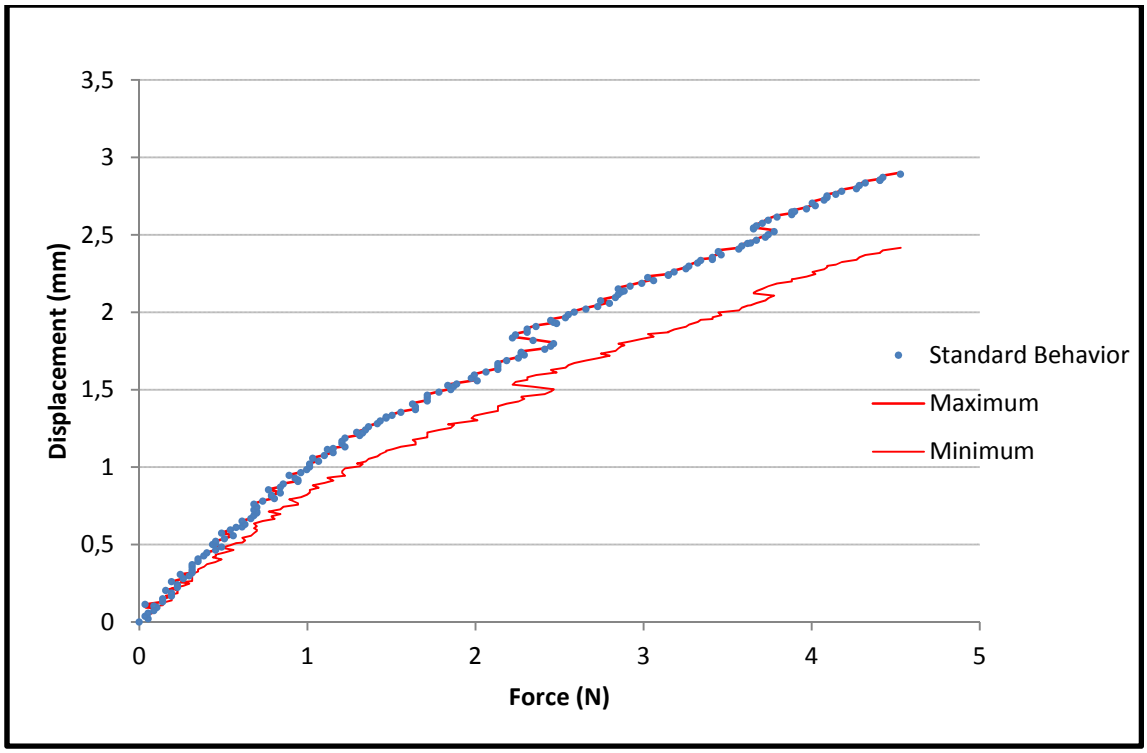

Figure 5.2b: Range of behaviors of creasing stiffness for the cigarette box in Experiment considering the sensibility analysis of crease stiffness with a 1 N

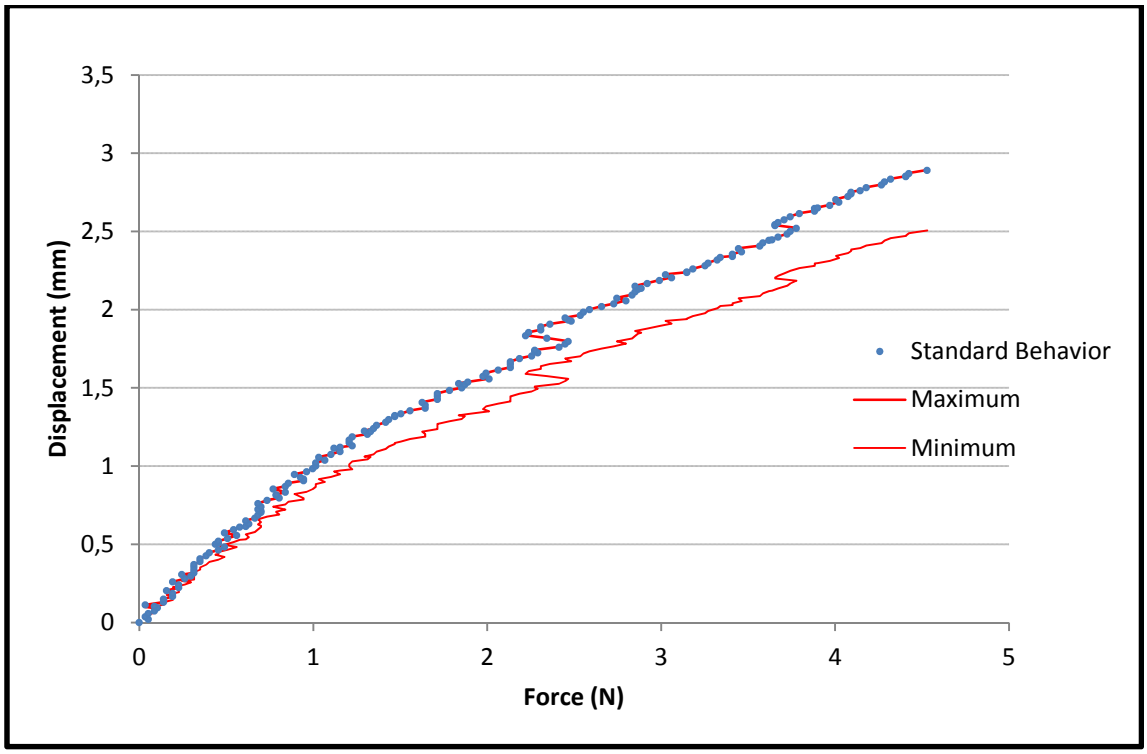

Figure 5.2c: Range of behaviors of creasing stiffness for the cigarette box in Experiment 1 considering the sensibility analysis of crease stiffness with a 5 N

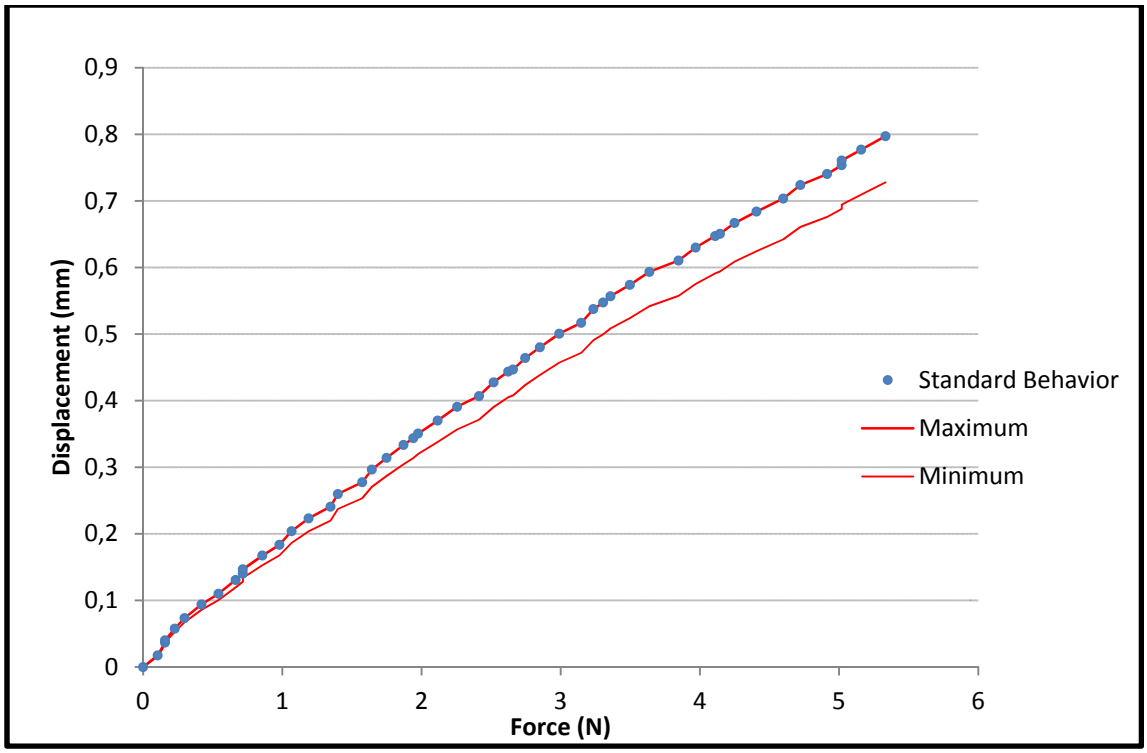

Figure 5.2d: Range of behaviors of creasing stiffness for the pill box in Experiment 2 considering the sensibility analysis of crease stiffness with a 1 N

In the experiments of Figures 5.2b and 5.2c, the behavior of the paperboard has several peaks due to imperfections of the experimental material and due to a lack of accuracy of the measurements.

Table 5.1 shows that the type of experiment has different impact on L_{crease} and L_{bend}. However, as shown in Figures 5.2a, 5.2b, 5.2c and 5.2d, the standard behavior in the four experiments was very close to the behavior with hinges as creases (maximum series). In conclusion, the standard performance of creases in the experiments was similar to the performance of hinges. Moreover, the influence of bending stiffness on the deformation is larger than the influence of the creasing stiffness. The results of the influence of bending stiffness and creasing stiffness are given in Table 5.2.

Table 5.2: Influence of bending stiffness and creasing stiffness in the maximum deformation of four experiments

	Cigarette_exp1_1N	Cigarette_exp1_5N	Pill_exp2_1N	Pill_exp2_5N
L (mm)	1,321	2,882	0,2	0,57
L_{ben} (mm)	1,105	2,498	0,183	0,541
L_{crease} (mm)	0,216	0,384	0,018	0,029
L_{ben}/L (%)	83,6	86,7	91,3	94,8
L_{crease}/L (%)	16,4	13,3	8,7	5,2

5.2 Sensibility analysis of bending stiffness.

Four simulations with different bending stiffness were carried out for four experiments on the square box. In order to change the bending stiffness of the paperboard, E_1 and E_2 were varied in the same way. The bending stiffness, S_b, is proportional to E_1 and E_2 and the properties E_3, G_{12}, G_{13}, G_{23}, V_{12}, V_{21}, V_{13}, V_{31}, V_{23} and V_{32} were calculated according to the procedure described in Section 2.1.2. For the same experiment the load was fixed to 1N or 5N. The results are given in Figure 5.3.

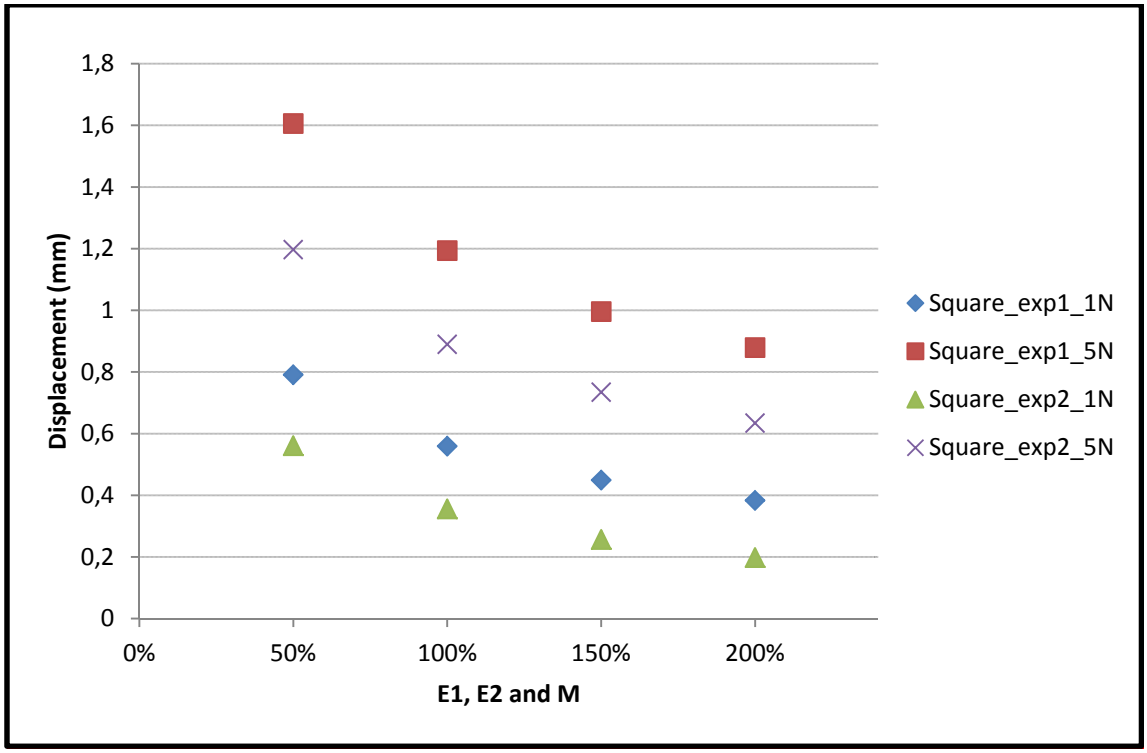

Figure 5.3: Sensibility analysis of bending stiffness for four experiments. The horizontal axis indicates the values of in-plane Young's modulus and bending stiffness relative to the nominal values.

The results in the four experiments are very similar. If the bending stiffness tends to zero, the maximum displacement tends to infinity while if the bending stiffness tends to infinity, the displacement tends to zero. In conclusion, the maximum displacement is approximately inversely proportional to the bending stiffness. If Figure 4.2.C2 and Figure 4.2.C4 are compared with the results of Table 2.7 (three layers), the same conclusion is deduced: the more bending stiffness the less maximum displacement. The maximum displacement in the test C2 is about 1.2 mm (see Figure 4.C2) corresponding to a bending stiffnesses of 16.6 Nmm in MD and 7.3 Nmm in CD (see Table 2.6), respectively, while the maximum displacement in test C4 is about 1.5 mm corresponding to bending stiffnesses of 12.7 Nmm in MD and 4.3 Nmm in CD. These results match the simulations of Experiment 1 of the square box with an applied force of 5 N shown in Figure 5.3.

6. Checkouts

In this chapter, the assumptions made in the previous chapters are analyzed.

In the material model, the influence of the coating layer was neglected and the material was considered linear elastic without any plastic behavior (Section 2.1). In order to check that the paperboard materials did not reach the plastic regime, the stress levels of the experiments were checked. In Figures 6.1a, 6.1b and 6.1c, contour plots of the maximum in-plane principal stress are shown for each type of box.

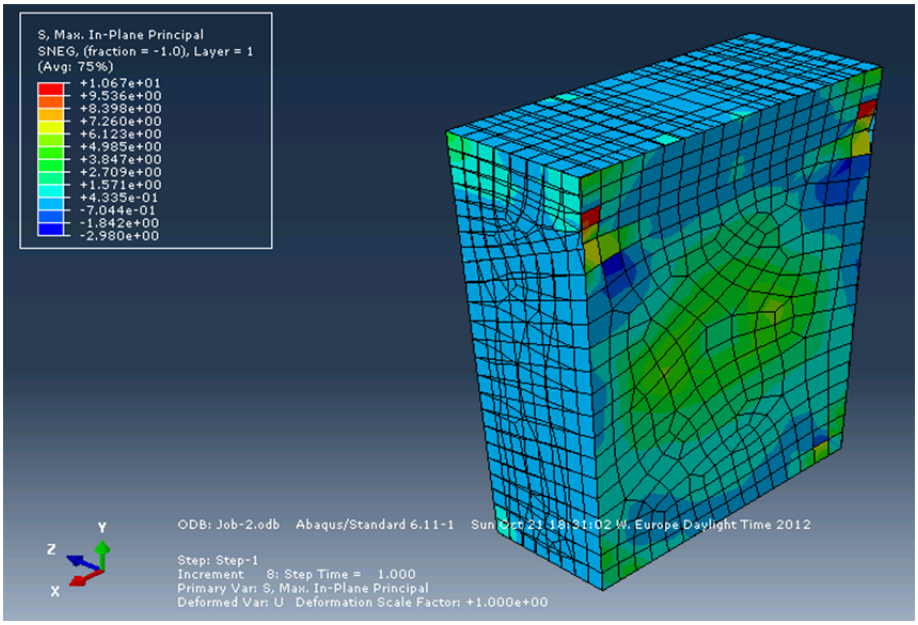

Figure 6.1a: Stress contour plot of the maximum in-plane principal stress for the cigarette box in Experiment 1 with a 5.5 N load.

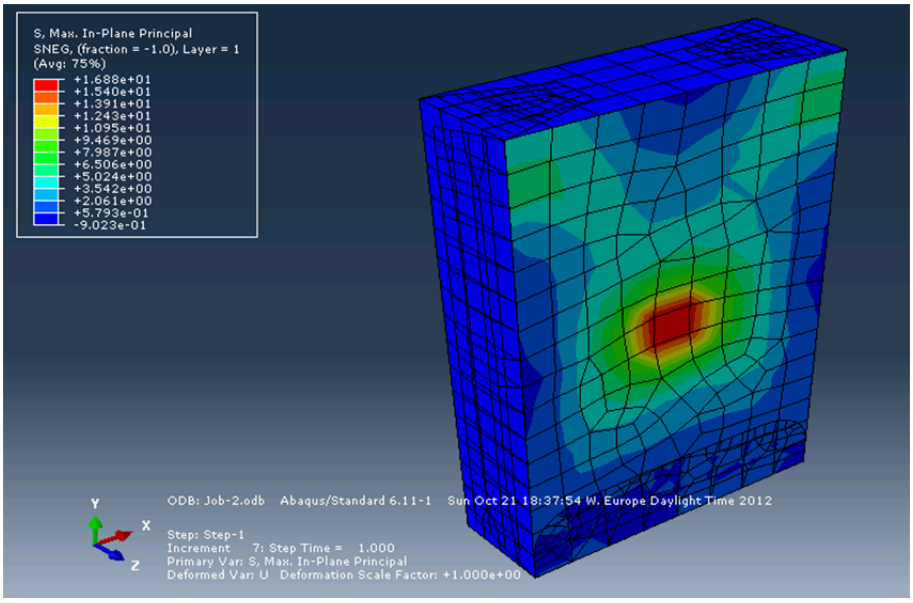

Figure 6.1b: Stress contour plot of the maximum in-plane principal stress for the pill box in Experiment 1 with a 5.5 N load

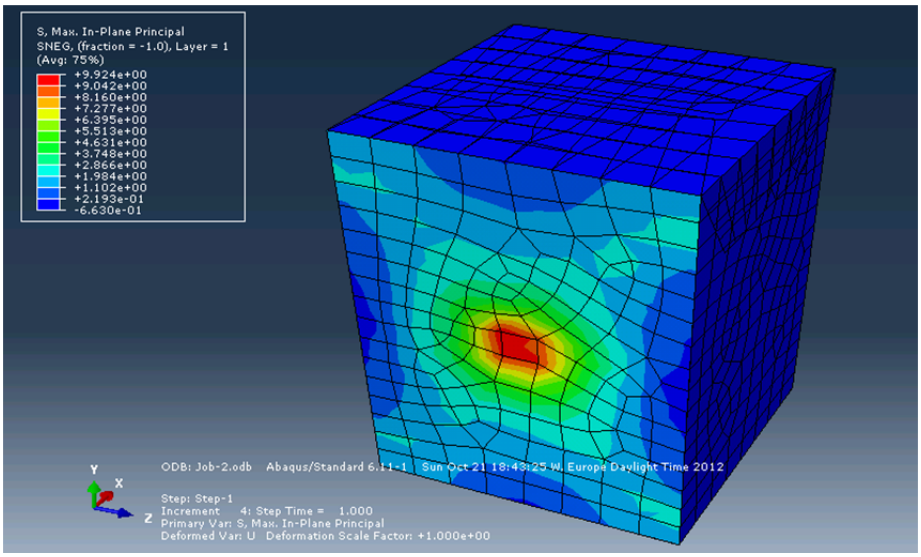

Figure 6.1c: Stress diagram for the square box in Experiment 1 with a 5.5 N load

The maximum principal stress for all the experiments was 16.8 N/mm^2 which is lower than the yield strength of the paperboard material, which is approximately 45 N/mm^2 [19]. Thus, this suggests that the paperboard does not permanently deform in any of the experiments.

In Section 2.4.1, the creasing angle of the crease was supposed to remain between 80 and 100 degrees. It was checked if that angles of all creases remained between these two values in all the experiments. The worst cases were analyzed and the angle θ was found as shown in Figure 6.2. The angle θ is an approximate value of the simulation angle.

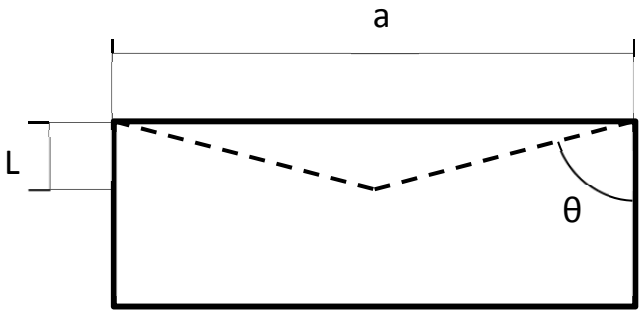

Figure 6.2: simplified sketch of the deformed shape of a typical box

The angle θ was calculated

$$\theta = \tan^{-1}\frac{a}{2 \cdot L} \qquad (6.1)$$

The results of the simulation angles are given in Table 6.1.

Table 6.1: Approximate angles of the creases of the deformed shape

	Cig_Exp1	Cig_Exp2	Pill_Exp1	Pill_Exp2	Square_Exp1	Square_Exp2
a (mm)	54	22	42	14	46	46
L (mm)	2,89	1,89	2,31	0,98	2,75	2,92
θ (degrees)	86,9	85,1	86,9	86,0	86,6	86,4

As stated in Section 2.4.1 the element sizes have an effect of the value of the creasing stiffness K_{44} and this section it is found that the variance of the element size of the meshes is negligible. For the pill box mesh, Z = 4 mm, a typical dimension was 3 mm for the smallest elements and 5 mm for the biggest. This means that all the elements of the mesh were between 3 mm and 5 mm. According to Figure 2.9 and the range of the elements sizes, K_{44} could take values between 0,015 and 0,025; in logarithmic scale, between -1,82 and -1,6. The corresponding displacements were estimated according to Figure 6.3.

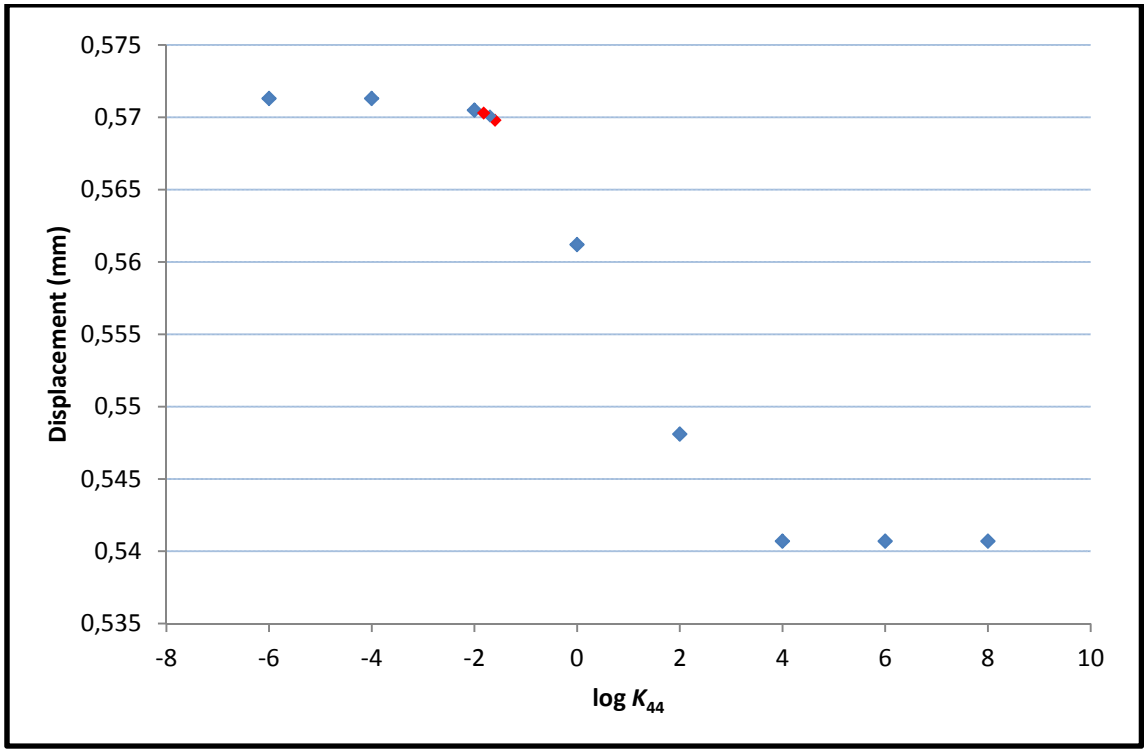

Figure 6.3: Sensibility analysis of creasing stiffness for the pill box in Experiment 2 with a 5 N force. The red dots are the estimated displacements according to the limits of K_{44} with for minimum and maximum element sizes, respectively, of the mesh.

The displacements corresponding to K_{44} = 0.015 and K_{44} = 0.025 are 0.5698 and 0.5703 mm respectively. If both displacements are compared with the original displacement, 0.5701, the error is around 0.04% for both cases, thus negligible. For this reason, K_{44} was calculated from the mean element size, Z.

7. Conclusions

Firstly, two assumptions made in previous chapters are recaptured. In the model, the gluing zones were considered as rigid. In Section 2.1, it was explained why the gluing zones should allow for deformation. Moreover, five degrees of freedom of the creases were eliminated (Section 2.4) and for the analysis in Chapter 5, the model was considered to be applicable. In the sensibility analysis of the creasing stiffness (Section 5.1) two assumptions were made. Firstly, the deformation due to in-plane stiffnesses was considered to be negligible, $L_{tensile} = 0$, which is also related with the assumption of neglecting five degrees of freedom of the creases and secondly, the deformation due to bending, L_{bend}, was considered constant although the stiffness of the creases was changed.

Considering the previous assumptions and approximations, the main conclusion of the project is that the maximum deformation depends on primarily on the bending stiffness rather than the creasing stiffness. The deformation due to the bending stiffness was around 90% of the total deformation and the deflection due to the stiffness of the creases was around 10%.

8. Topics for further studies

- Additional creasing tests should be done. The creasing stiffness may depend on other features apart from the angle of the crease and the paperboard material as stated in Section 2.4. Particularly, possible time-dependence of the creasing stiffness and the times that the crease has been folded.
- The influence of the coating layer was neglected, but it would be of interest to test its influence on the global stiffness performance of boxes.
- The model results did not perfectly fit the real behavior of some of the box experiments. As stated in Section 4.2, the neglect of the glue deformation was probably the main problem. The deformation behavior of the glue should be investigated and added to the model to solve this issue.
- More tests to verify the model should be done. Moreover, statistic studies could be carried out in order to find which parameters are most significant for the final performance of the box.

References

[1] Iggesund Paperboard AB (2004). *Paperboard Reference Manual.* Paperboard company

[2] Ugural A.C., Fenster S.K. (2003). *Advanced Strength and Applied Elasticity.* Elsevier publisher

[3] Strang, G. and Fix, G. (1973). *An Analysis of the Finite Element Method*. Prentice Hall

[4] Blanchard, P., Devaney R. L. and Hall G. R. (2006). *Differential Equations*. Thompson

[5] Atkinson F.V. and Kendall A. (1989). *An Introduction to Numerical Analysis*, Courier Dover

[6] Hrennikoff A. (1941). *Solution of Problems of Elasticity by the Frame-Work Method*. ASME J. Appl. Mech.

[7] Stein E. (2009). *Olgierd C. Zienkiewicz, a pioneer in the development of the finite element method in engineering science*. Steel Construction

[8] Anonymous (2012). *Http://en.wikipedia.org/wiki/Computer-aided_design*

[9] ABAQUS (2007). *ABAQUS User's Manual*. Abaqus Inc, Providence

[10] Chen W. F. (2008). *Limit Analysis and Soil Plasticity*. J. Ross Publishing

[11] Innventia (2012). Personal communication

[12] Czichos H. (2006). *Springer Handbook of Materials Measurement Methods*. Springer

[13] Beldie L. (2001). *Mechanics of paperboard packages - Performance at Short Term Static Loading*. Lund, Master thesis

[14] Carlsson, L.A. and Fellers, C.N. (1980). *Flexural stiffness of multi-ply paperboards*, Fibre Science and Technology, 13(3):213-223.

[15] Nygårds, M. (2008). *Identification of paperboard deformation mechanisms*. Technical Report 339, STFI-Packforsk

[16] Wyser Y., Pelletier C. and Lange J. (2002). *Predicting and Determining Bending Stiffness of Thin Films and Laminates*. John Wiley & sons

[17] Huang H. (2008). *Folding of Paperboard Numerical Analysis*. Lund, Master of Science Thesis

[18] Nygårds, M., Hallbäck, N., Just, M., and Tryding, J. (2005). *A finite element model for simulations of creasing and folding of paperboard*. In ABAQUS Users's Conference

[19] Flinn, Richard A.; Trojan, Paul K. (1975). *Engineering Materials and their Applications*. Boston: Houghton Mifflin Company

Appendix 1

In this Appendix the creation of the paperboard box modeled is described. The cigarette box, the pill box and the square box were modeled using the following steps:

- *Module > Part > Create part*

The configuration was introduced as shown in Figure 1 and the different parts were sketched with its corresponding measures as shown in Appendix 3. If two surfaces of the same box have the same dimensions, there was no need to create two different parts.

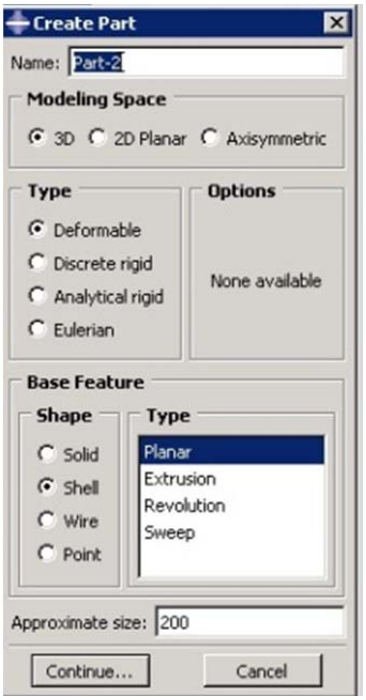

Figure 1: How to create a part

- *Module > Part > Create Material*

The different paperboard materials were represented with engineering constants as shown in Figure 2. The values of the properties of Materials F and S are given in Section 2.1.2.

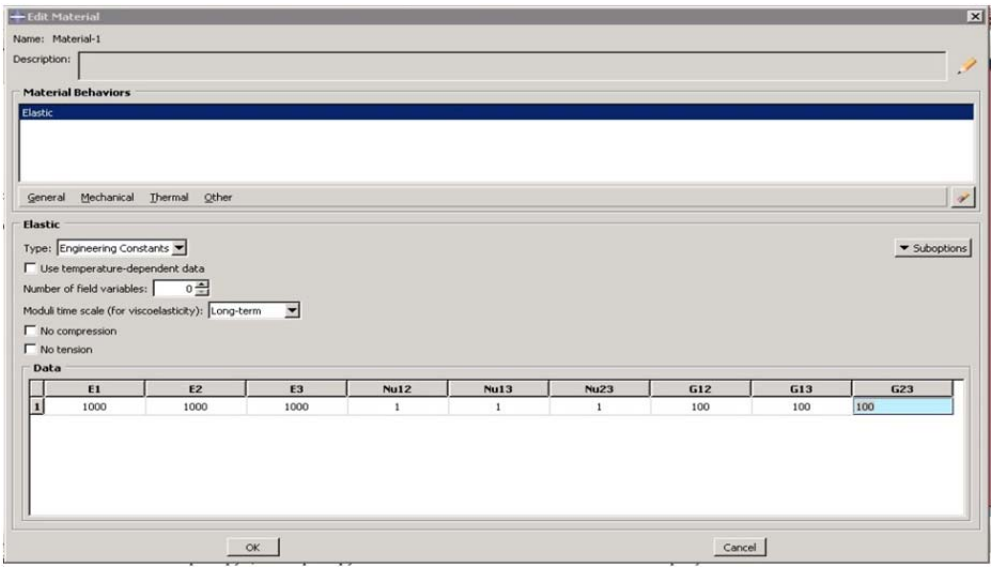

Figure 2: Definition of the material properties

- *Module > Part > Create section*

In order to create the model of the paperboard structure, the category "Shell" was chosen as illustrated in Figure 3. Homogeneous structure was created choosing "Homogeneous" type while the three layer structure was created choosing "Composite" type.

Figure 3: How to create the structure of a paperboard

- *Module > Part > Section assign*

After creating the sections of the paperboard, they were assigned to the different parts. The window in Figure 4 shows the section assignment for one part with the general configuration.

Figure 4: How to assign the paperboard structure to one part

- *Module > assembly > Create instance*

How the instances were created is shown in Figure 5. Each instance has its corresponding part. If two different instances have the same shape and structure, both instances have the same corresponding part.

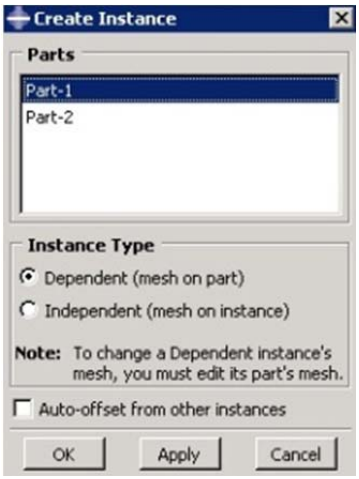

Figure 5: How to create an instance from one part

- *Module > assembly > Rotate instance*
- *Module > assembly > Translate instance*

The instances were placed using two functions: rotate instance and translate instance.

- *Module > Mesh > Seed part*
- *Module > Mesh > Seed edges*

In order to mesh a general part, the approximate global size of the elements of the mesh was chosen as shown in Figure 6. The edges can take a local element size using local seeds function as illustrated in Figure 7.

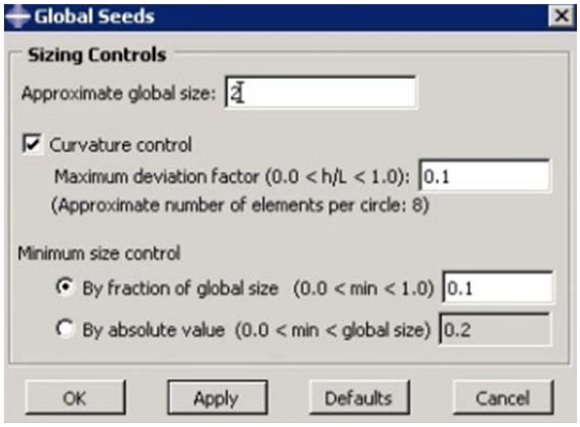

Figure 6: How to set the global size of the elements

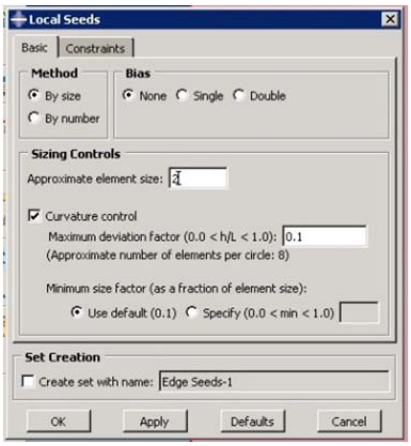

Figure 7: How to set the local size of the elements of one edge

- *Module > Mesh > Mesh parts*

The function “Mesh parts” meshes a general part considering the global element size and the local element size on the edges.

- *Module > Interaction > Create connector section*

In order to join two different surfaces through their edges, a connector section was created with the connection type “Hinge” as illustrated in Figure 8. This type of

connector restricts all the degrees of freedom between two nodes except from degree of freedom 4 as shown in Figure 9.

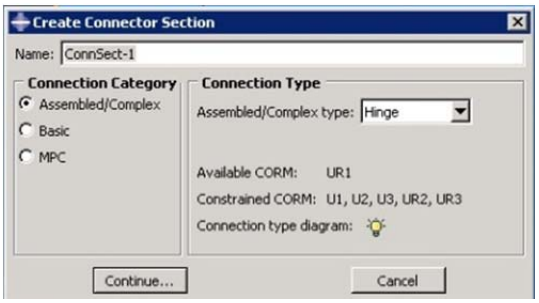

Figure 8: How to create the connector section

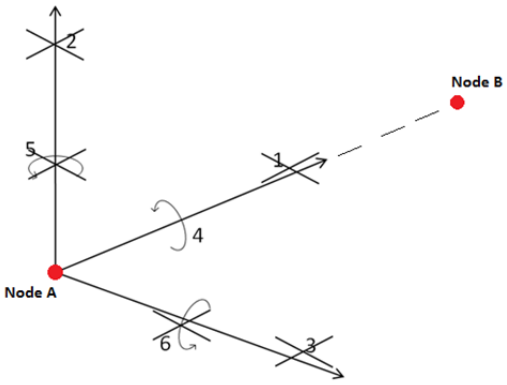

Figure 9: Degrees of freedom of one connector of type “Hinge”

One condition of the present connection of surfaces is that both surfaces must have the same number of nodes and they must be placed in the same position. In Figure 10, the nodes of both surfaces coincide.

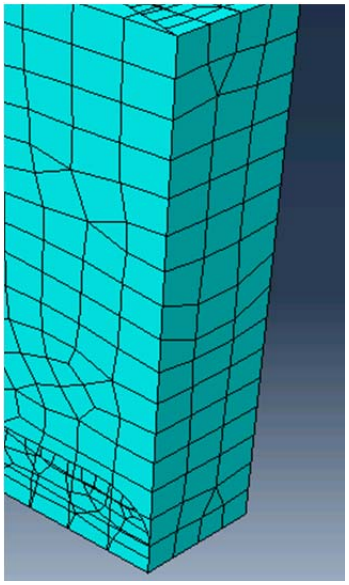

Figure 10: The nodes on the edge of both surfaces coincide.

Several connectors with a concrete distribution were added in every modeled crease as shown in Figure 11. The number of connector is lower than the number of nodes because more number of connectors would involve more restrictions than degrees of freedom for nodes with several connectors. The corners of the crease are also rid of conditions for the same reason.

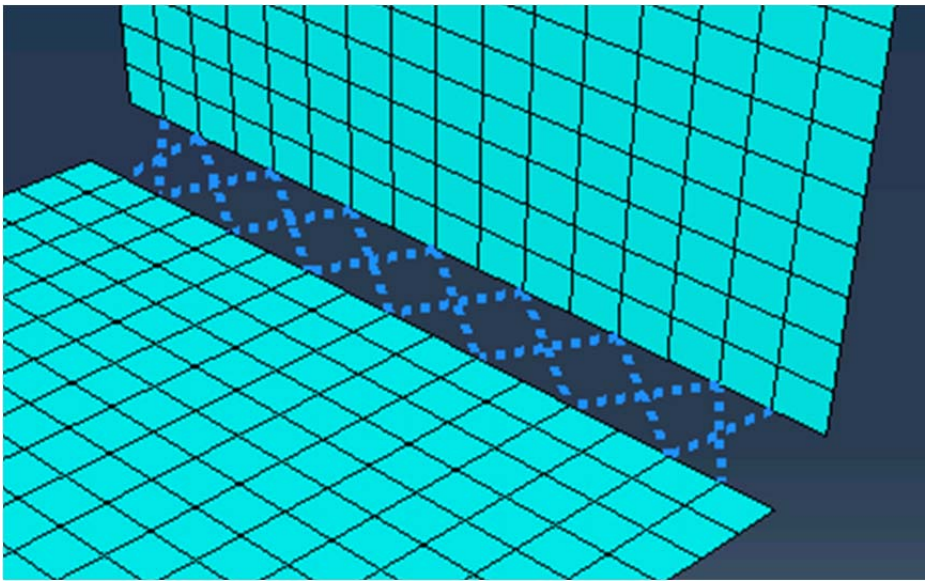

Figure 11: Connectors between two surfaces that form a crease

The elastic behavior of the connector was added as illustrated in Figure 12.

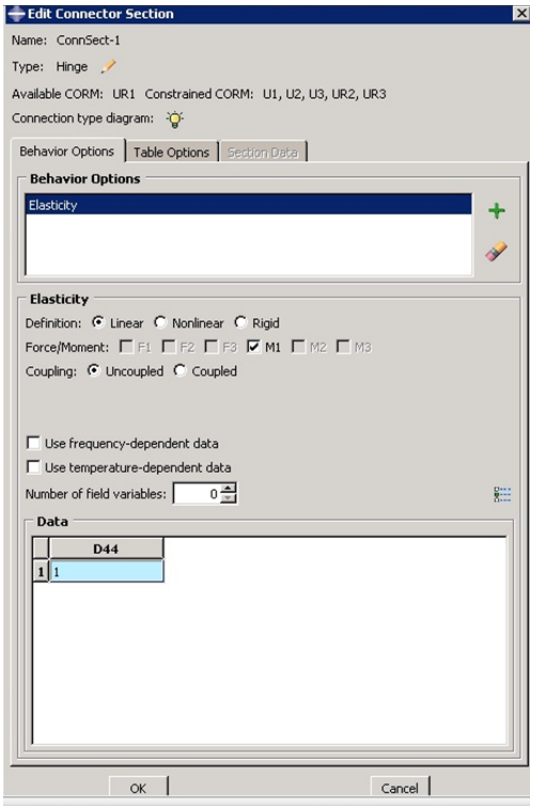

Figure 12: How to create the connector section

- *Module > Interaction > Connector builder*

How to create a connector with a concrete connector section is shown in Figure 13.

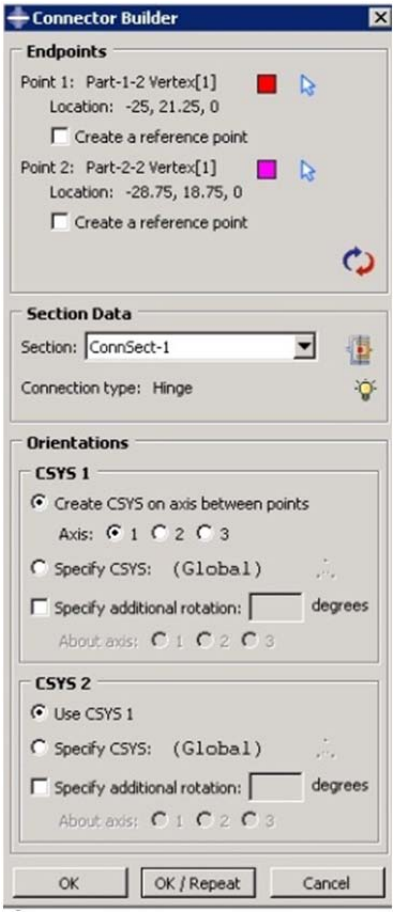

Figure 13: How to create a connector with a concrete connector section

Module > Interaction > Create constraint

The type of constraint that ties two surfaces is “Tie” as illustrated in Figure 14

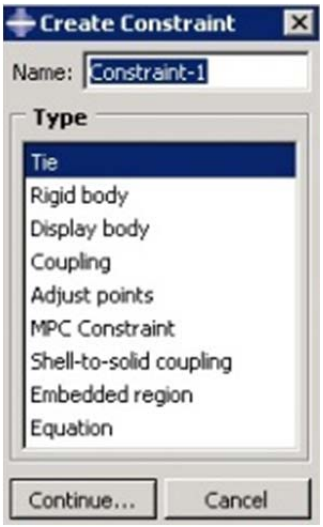

Figure 14: How to create a “Tie” constraint

- *Module > Step > Create Step*

The type of step is “Static, General” with the standard set as shown in Figures 15 and 16. The parameter NLGEOM was on in all the simulations as stated in Section 2.6.

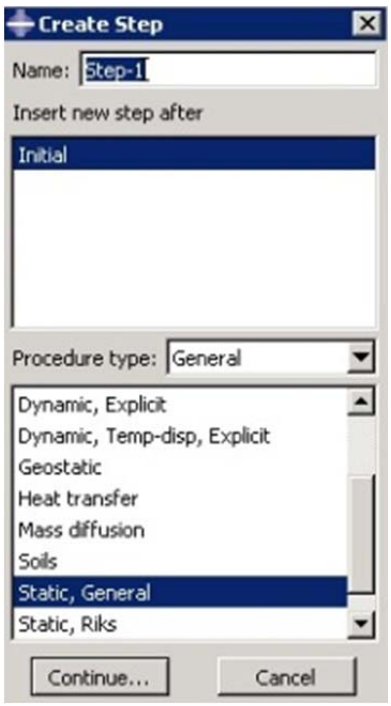

Figure 15: How to create a “Static, General” step

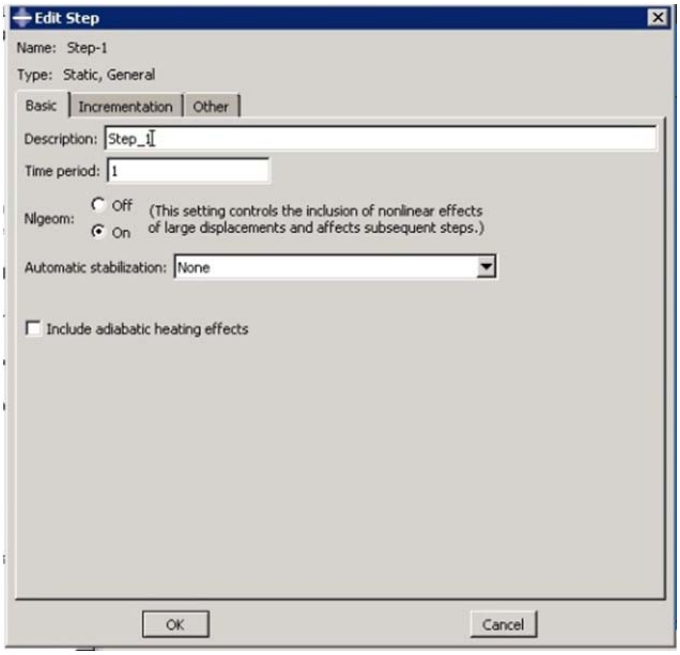

Figure 16: How to set Nlgeom on

- *Module > load > Create load*

How to apply pressure loads is shown in Figure 17.

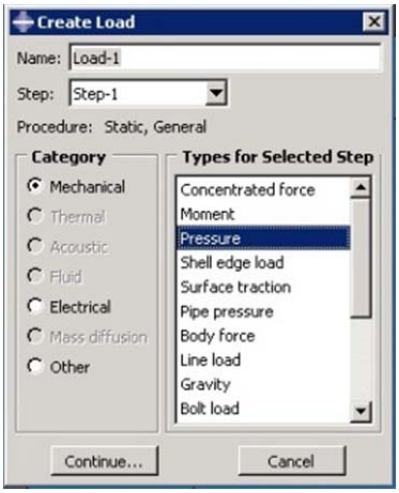

Figure 17: How to add pressures

- *Module > load > Create boundary condition*

How to introduce boundary conditions is shown in Figure 18.

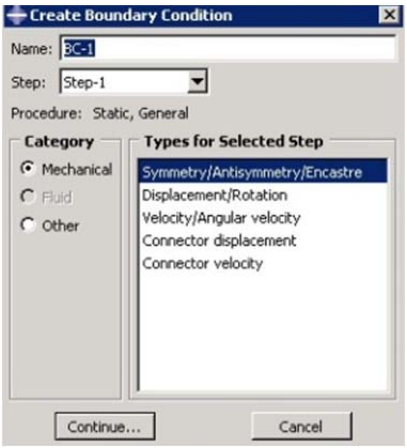

Figure 18: How to add boundary conditions

Appendix 2

The results of the four folding tests are given in Figure A, B, C and D, see Section 2.4.1.

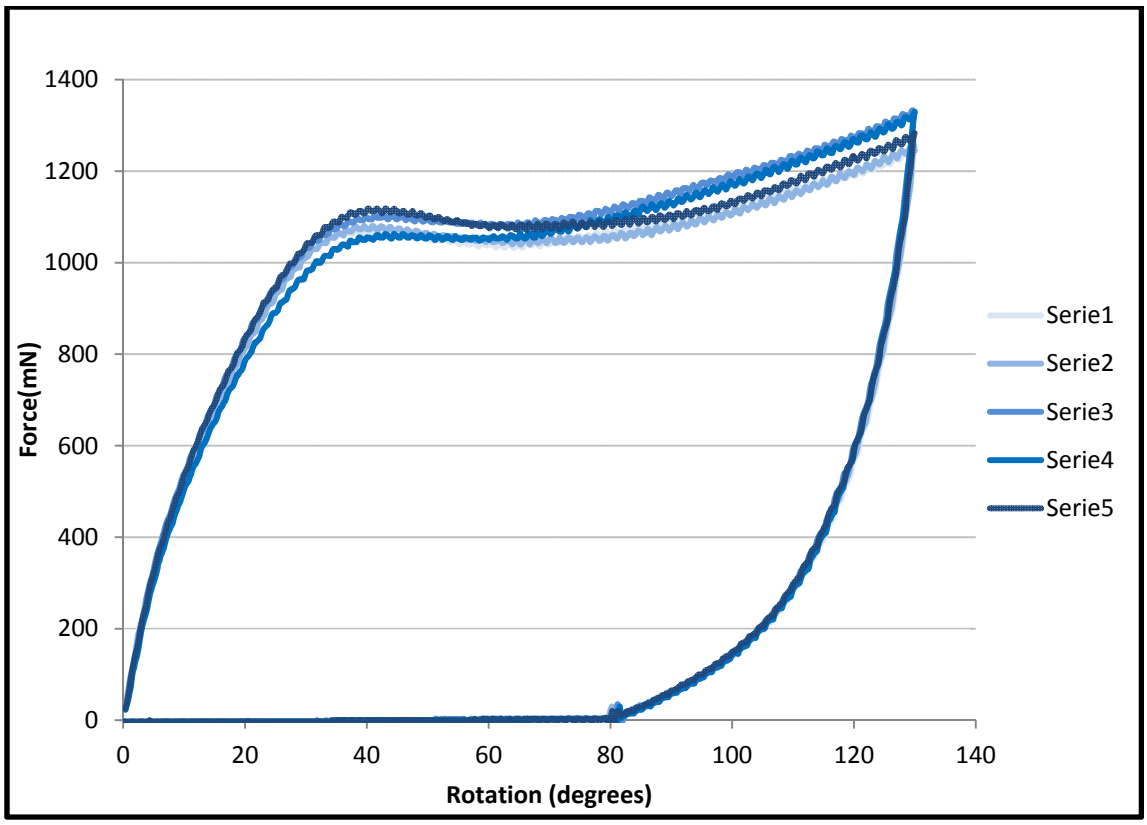

Figure A: Five force-displacement curves for the creasing tests in MD for material S.

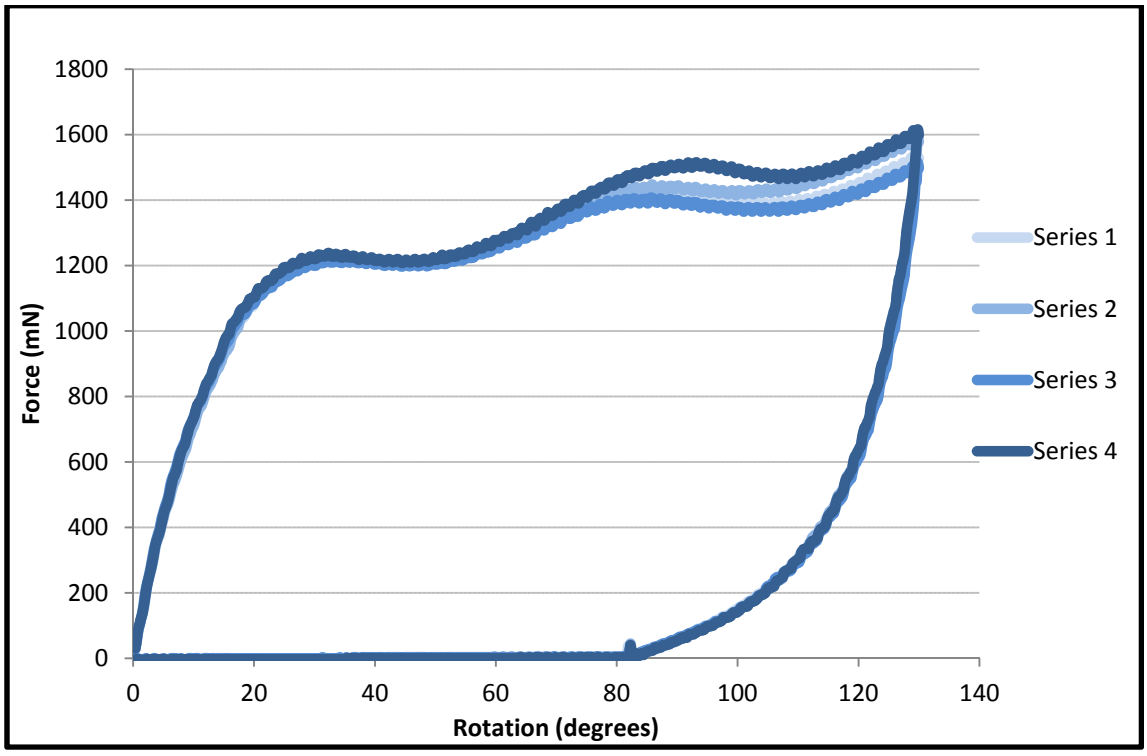

Figure B: Five force-displacement curves for the creasing tests in CD for material S.

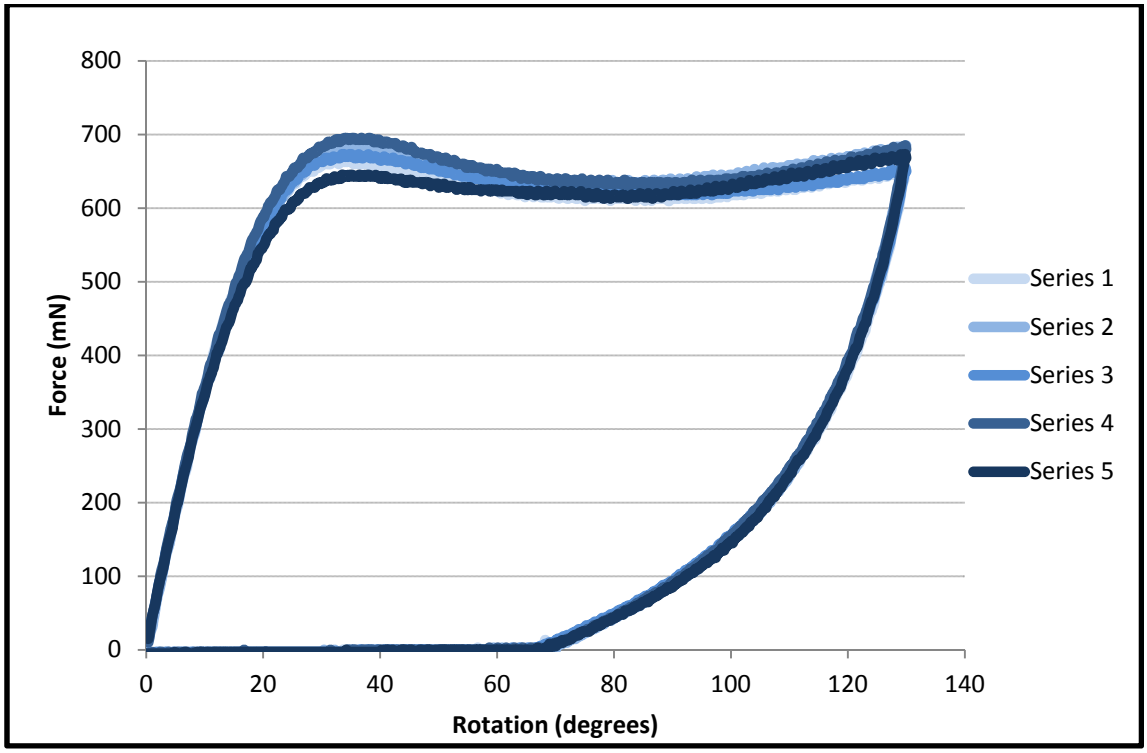

Figure C: Five force-displacement curves for the creasing tests in MD for material F.

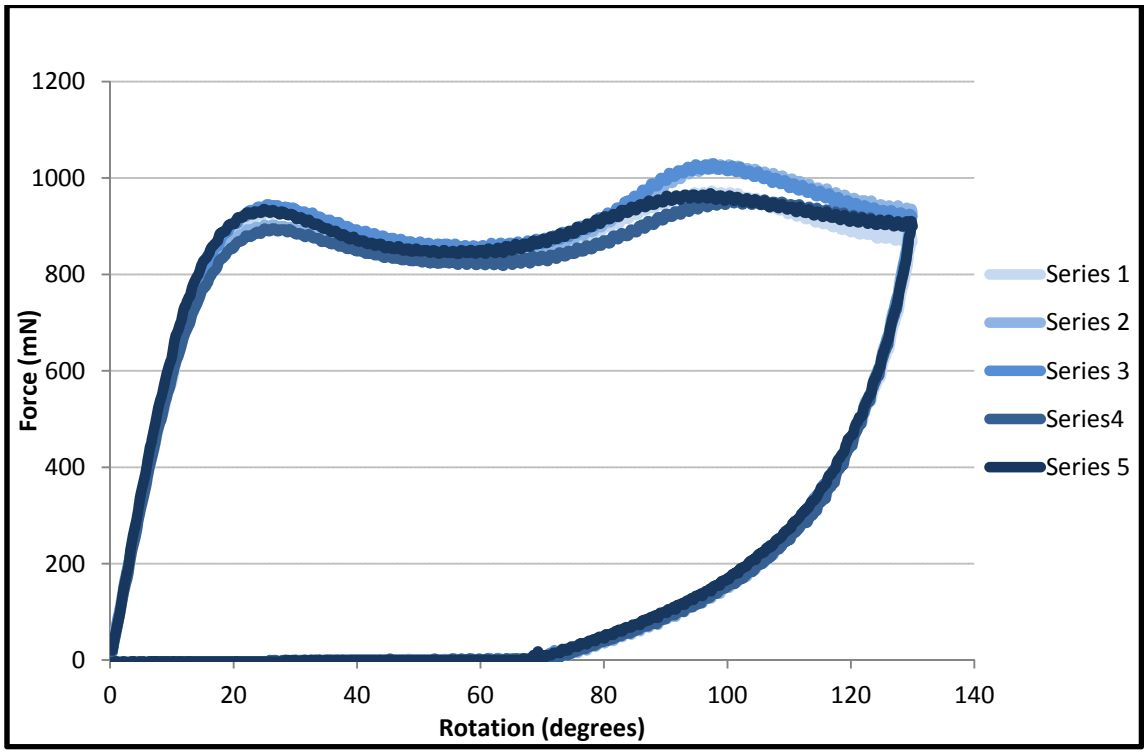

Figure D: Five force-displacement curves for the folding tests in CD for material F.

The final results of the four folding test are given in Figures E, F, G and H (Section 2.4.1).

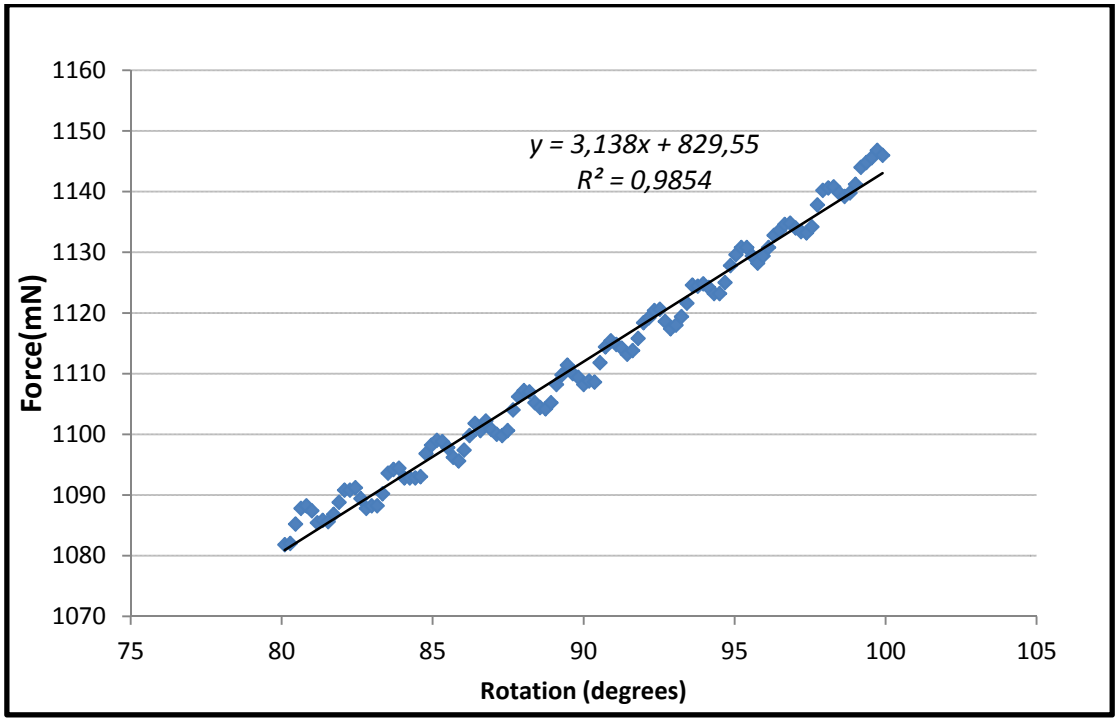

Figure E: Mean values of the five folding tests from 80 to 100 degrees with a linear trend line (material S in MD)

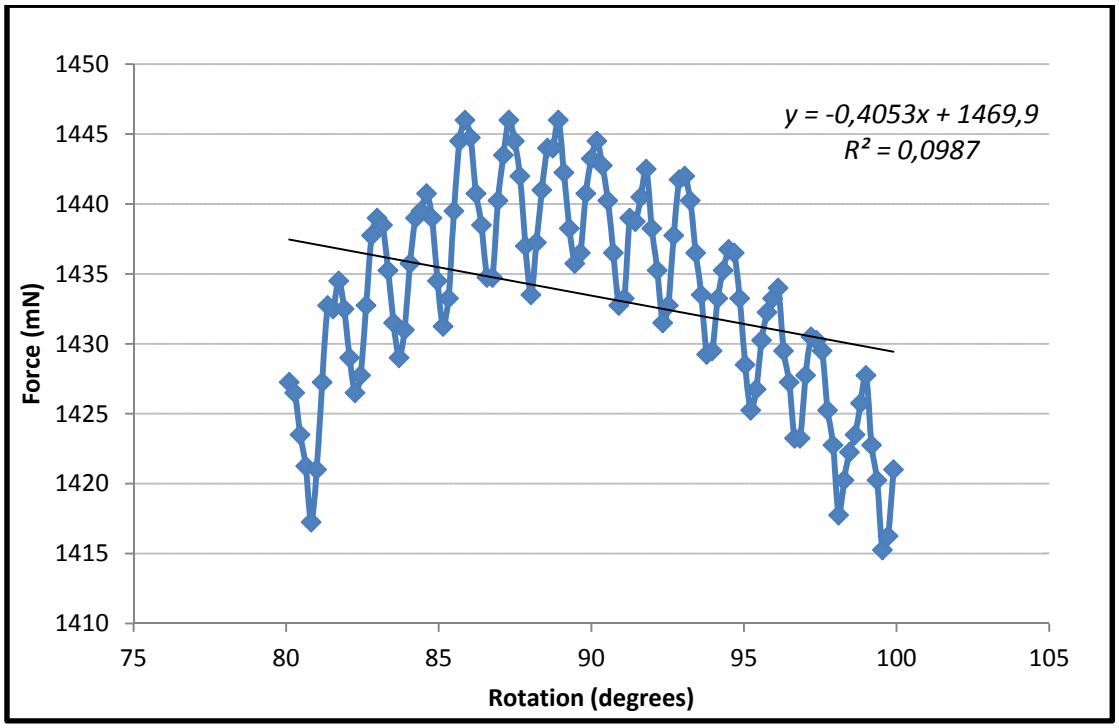

Figure F: Mean values of the five folding test from 80 to 100 degrees with a linear trend line (material S in CD)

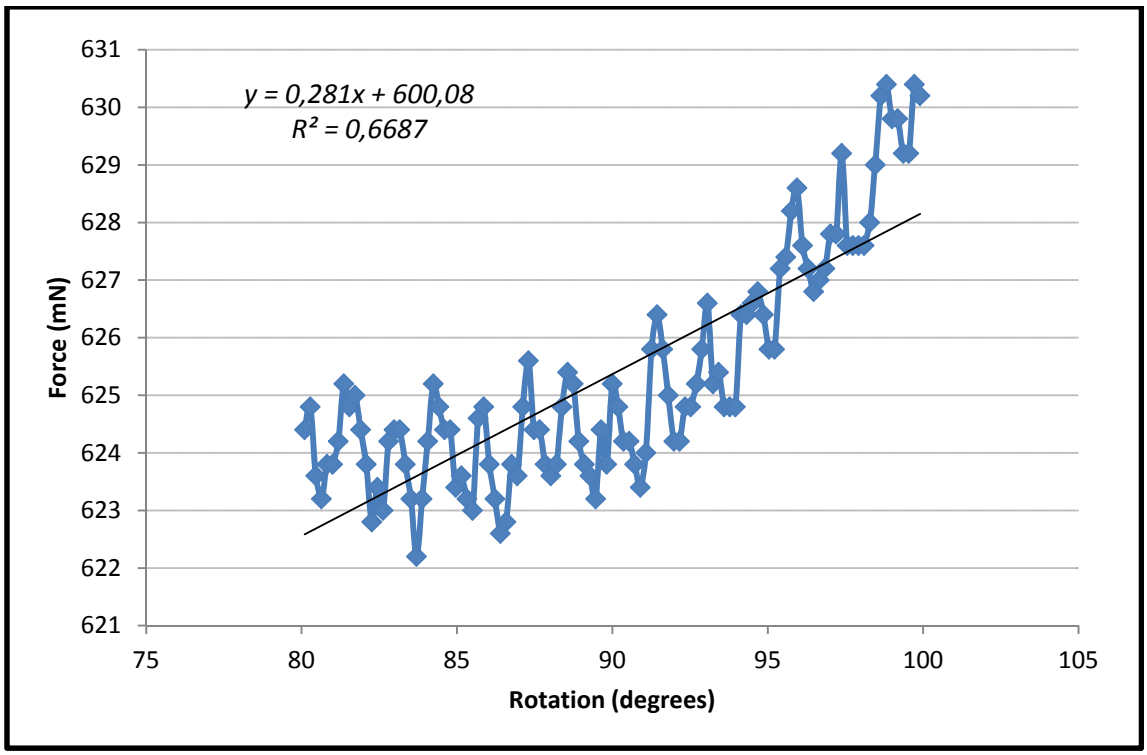

Figure G: Mean values of the five folding tests from 80 to 100 degrees with a linear trend line (material F in MD)

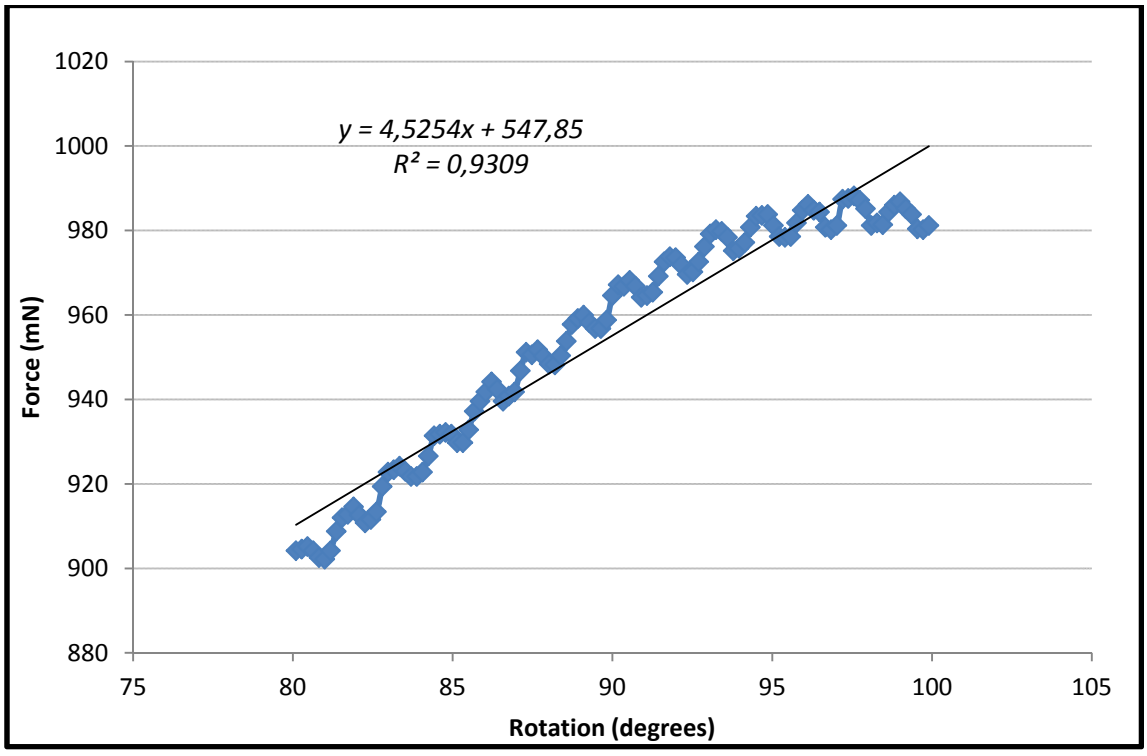

Figure H: Mean values of the five folding tests from 80 to 100 degrees with a linear trend line (material F in CD)

The basic results of the twelve experiments described in Chapter 4 are given in Figures I to T.

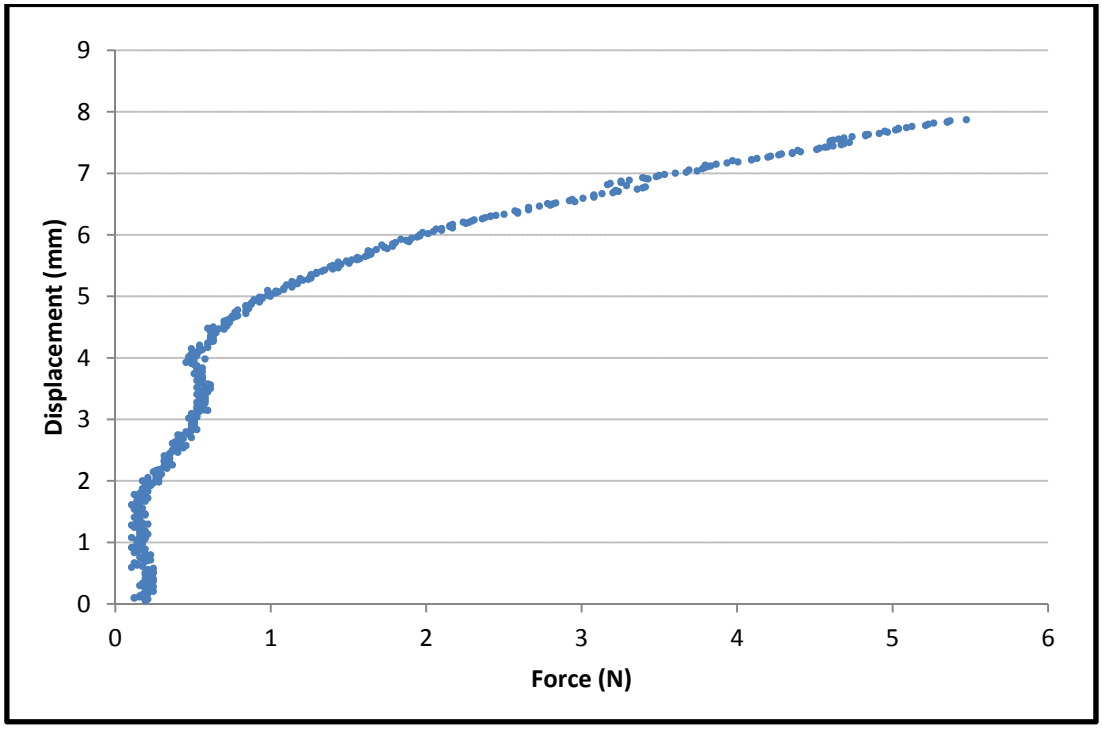

Figure I: Basic force-displacement curve for a fully glued cigarette box in Experiment 1 (test A1)

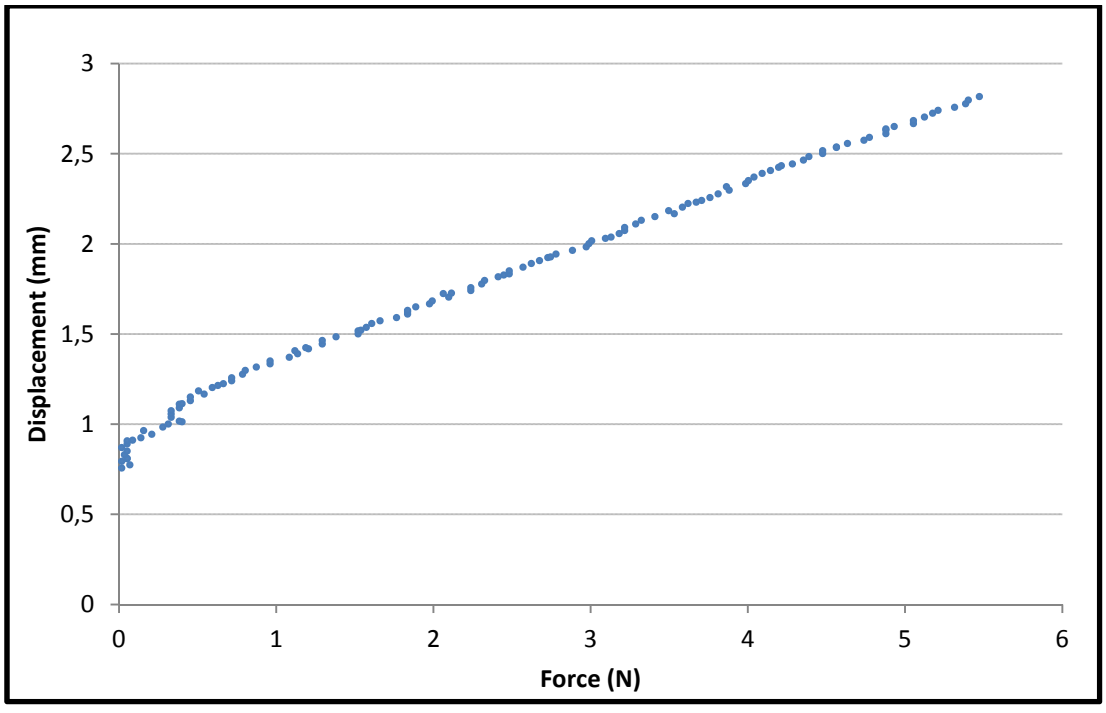

Figure J: Basic force-displacement curve for a fully glued cigarette box in Experiment 2 (test A2)

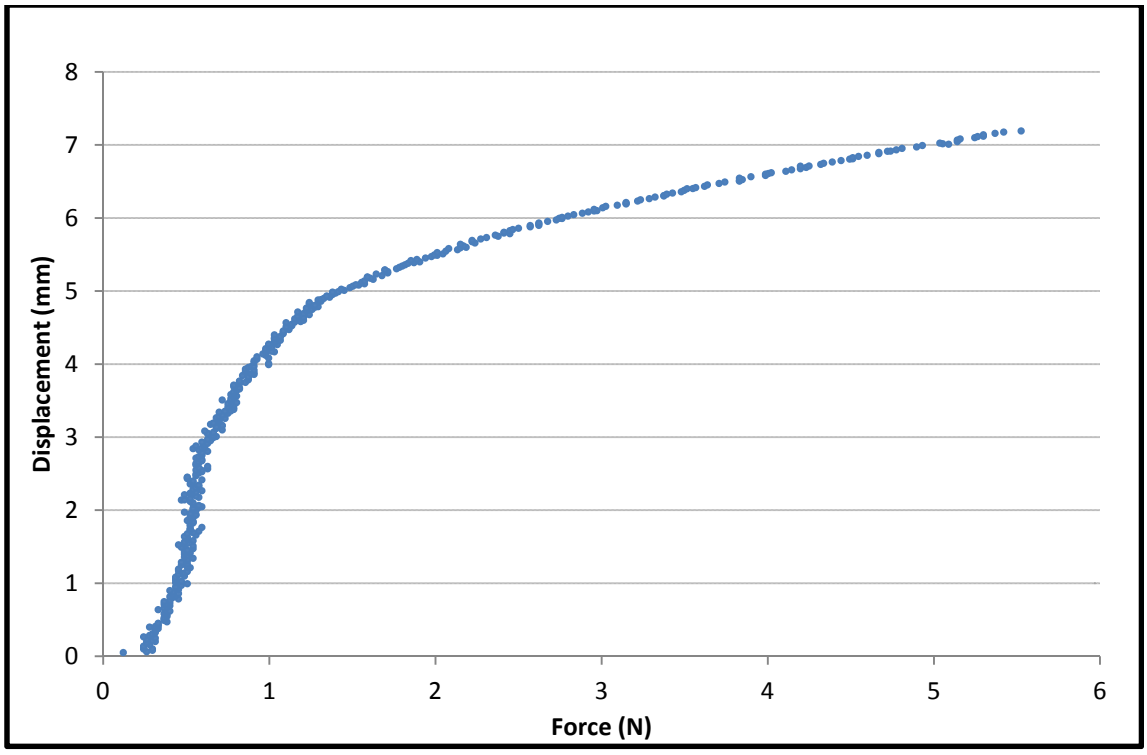

Figure K: Basic force-displacement curve cigarette box with half glue of in Experiment 1 (test A3)

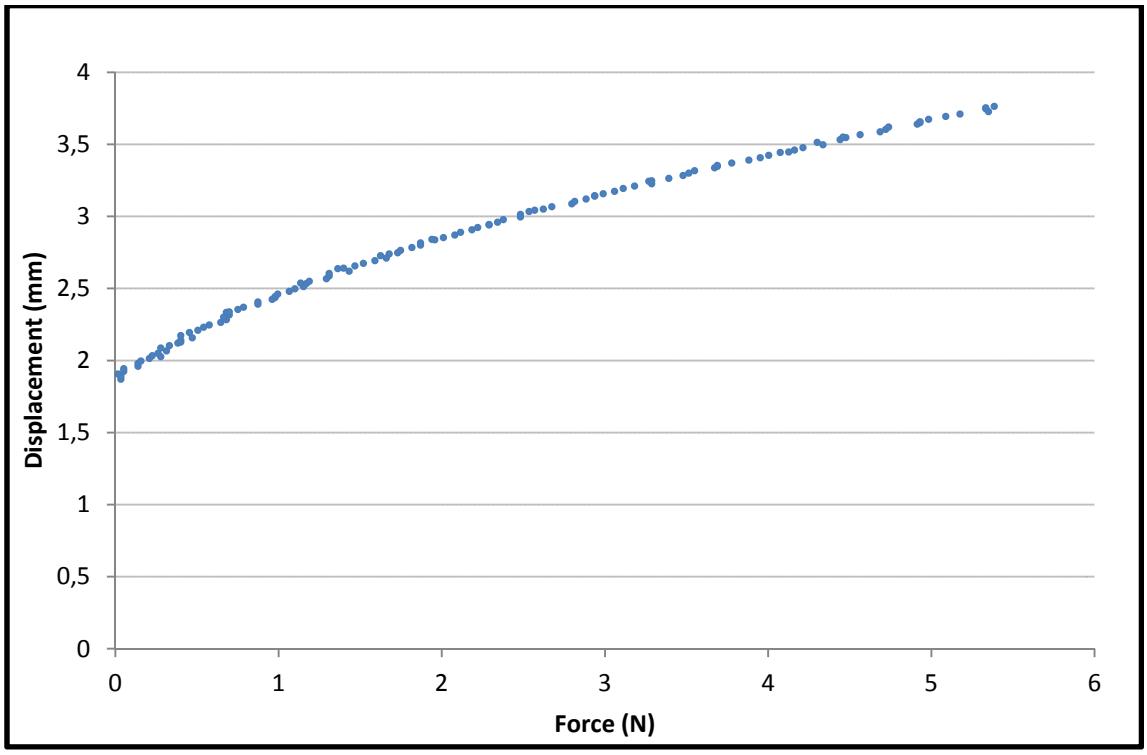

Figure L: Basic force-displacement curve cigarette box with half glue of material S in Experiment 2 (test A4)

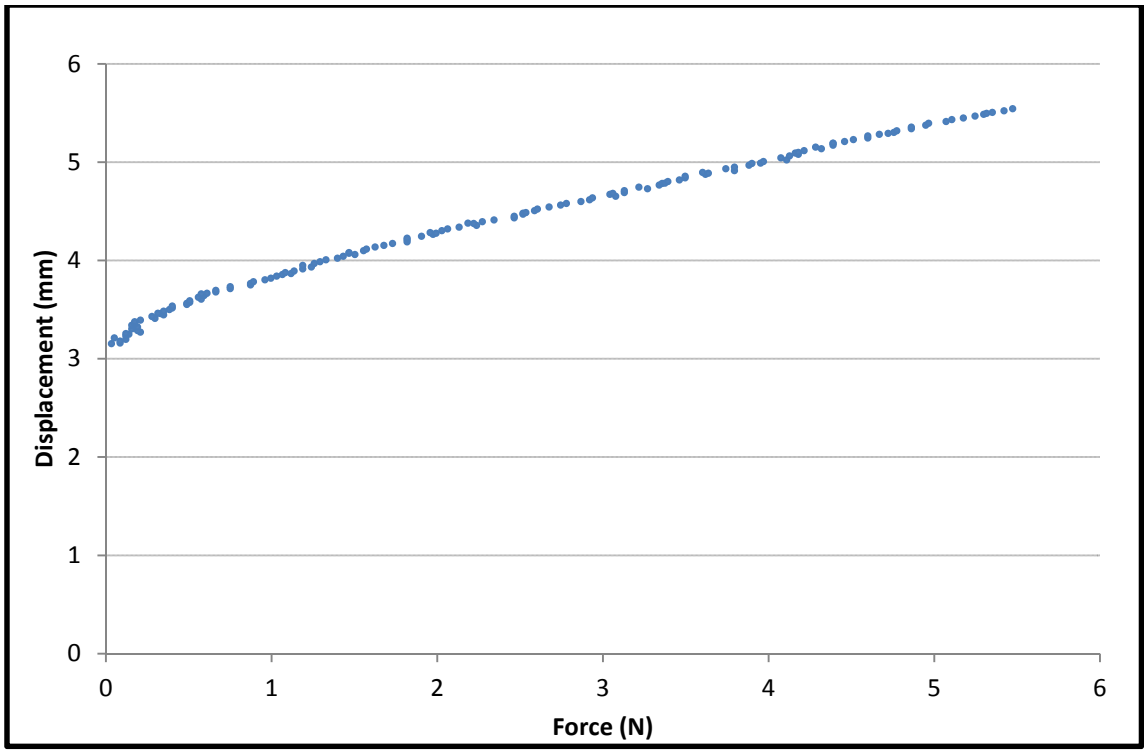

Figure M: Basic force-displacement curve pill box of with stiff creases in Experiment 1 (test B1)

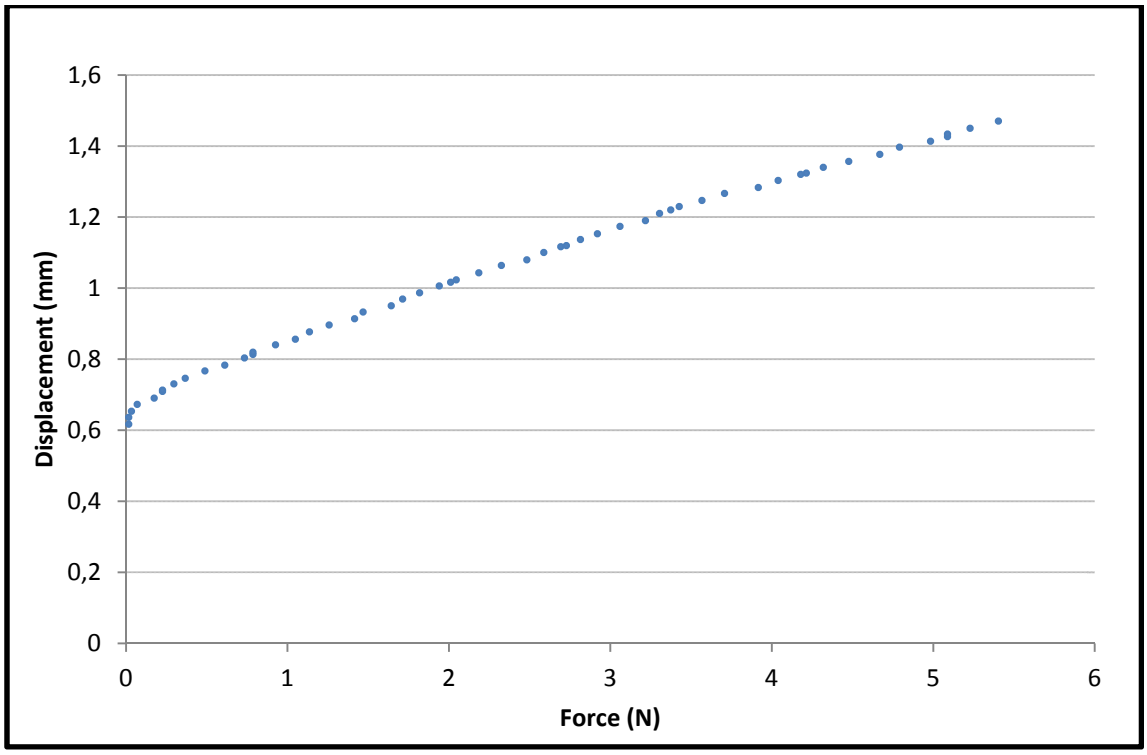

Figure N: Basic force-displacement curve pill box of with stiff creases in Experiment 2 (test B2)

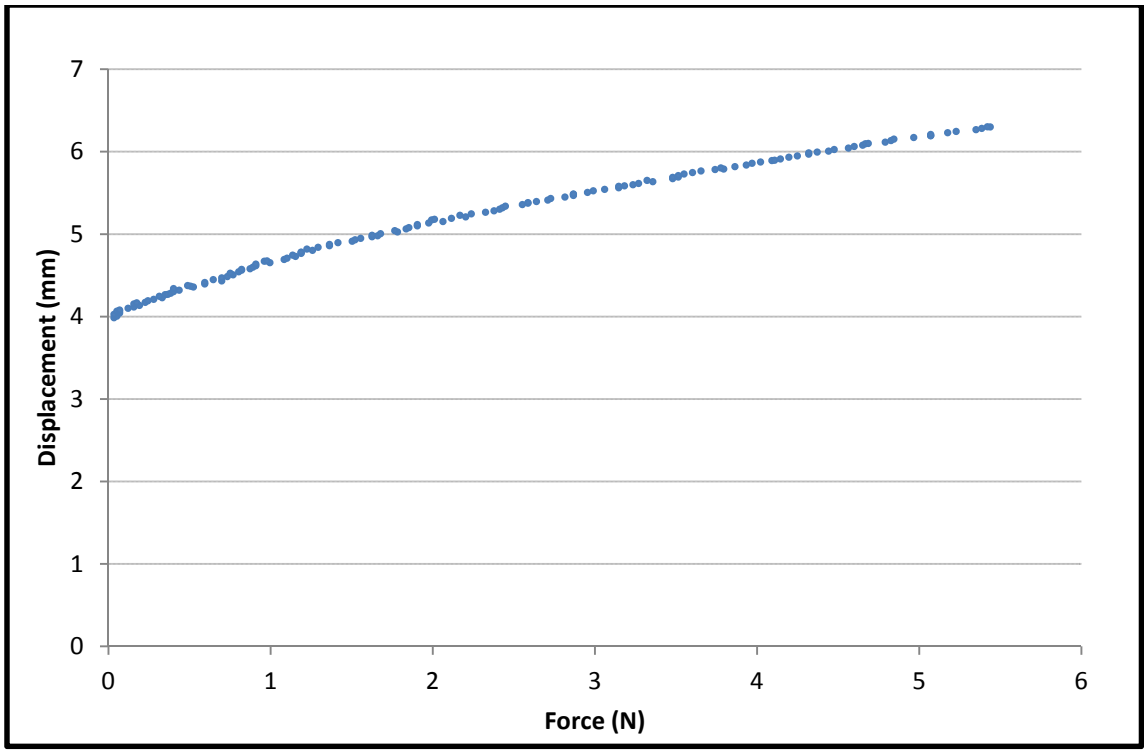

Figure O: Basic force-displacement curve pill box of with hinges as creases in Experiment 1 (test B3)

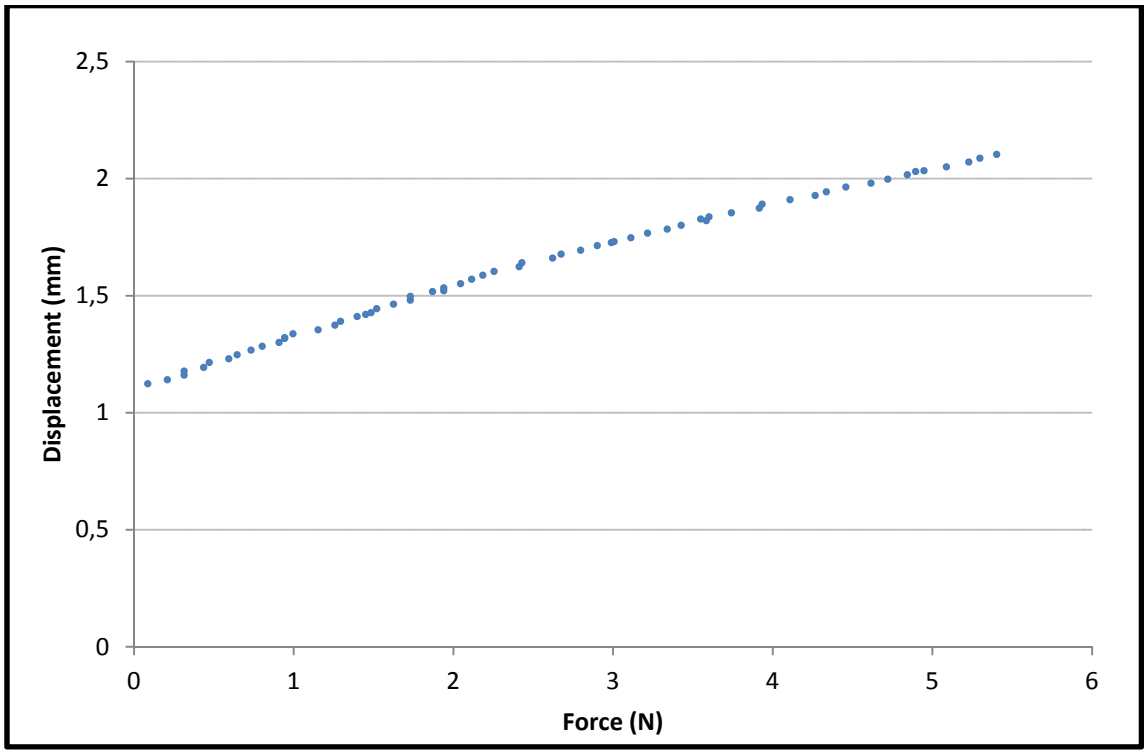

Figure P: Basic force-displacement curve pill box of with hinges as creases in Experiment 2 (test B4)

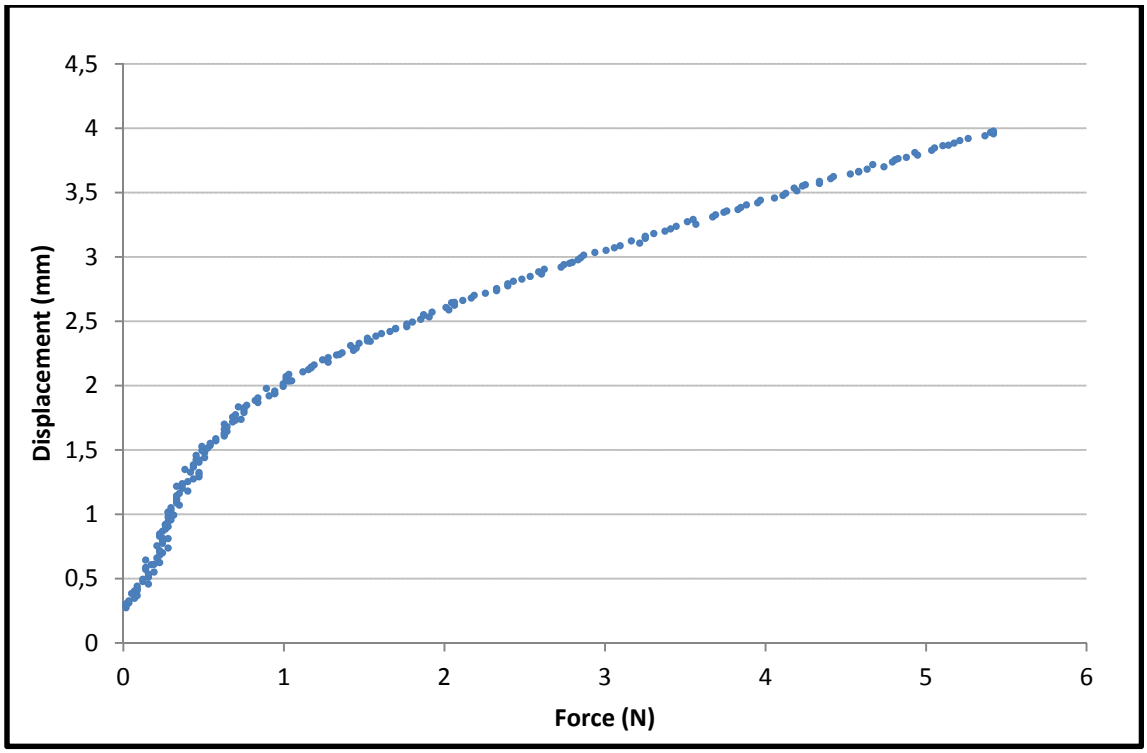

Figure Q: Basic force-displacement curve square box of material S in Experiment 1 (test C1)

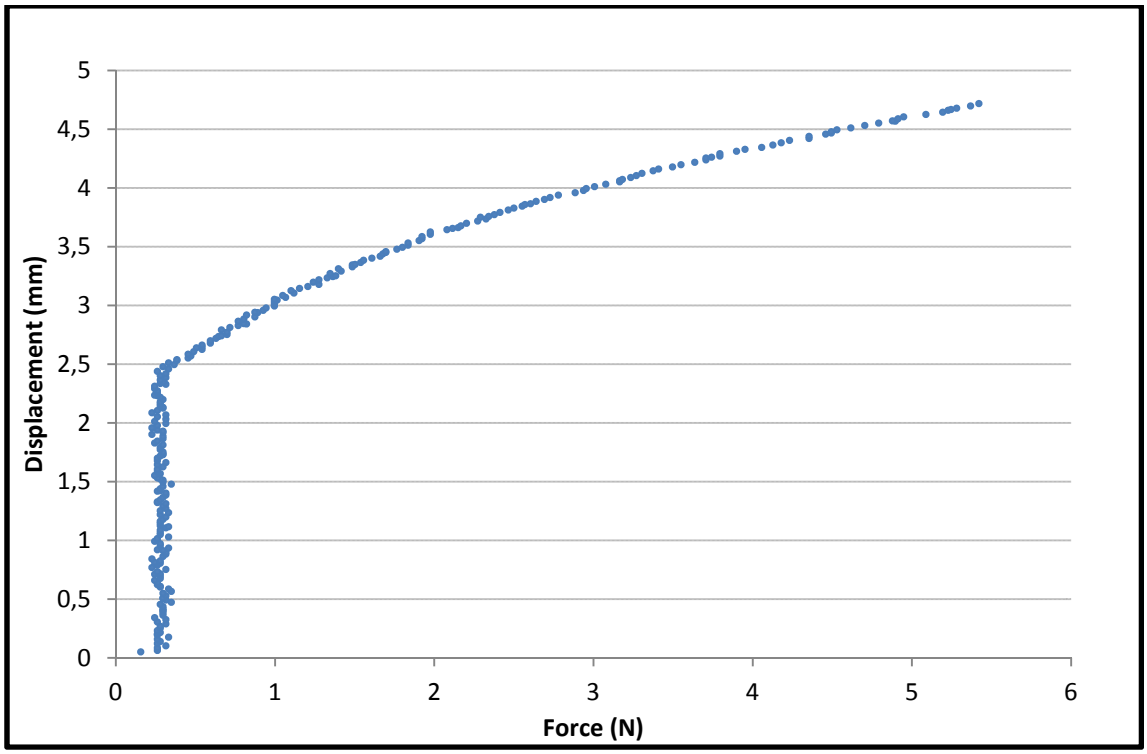

Figure R: Basic force-displacement curve square box of material S in Experiment 2 (test C2)

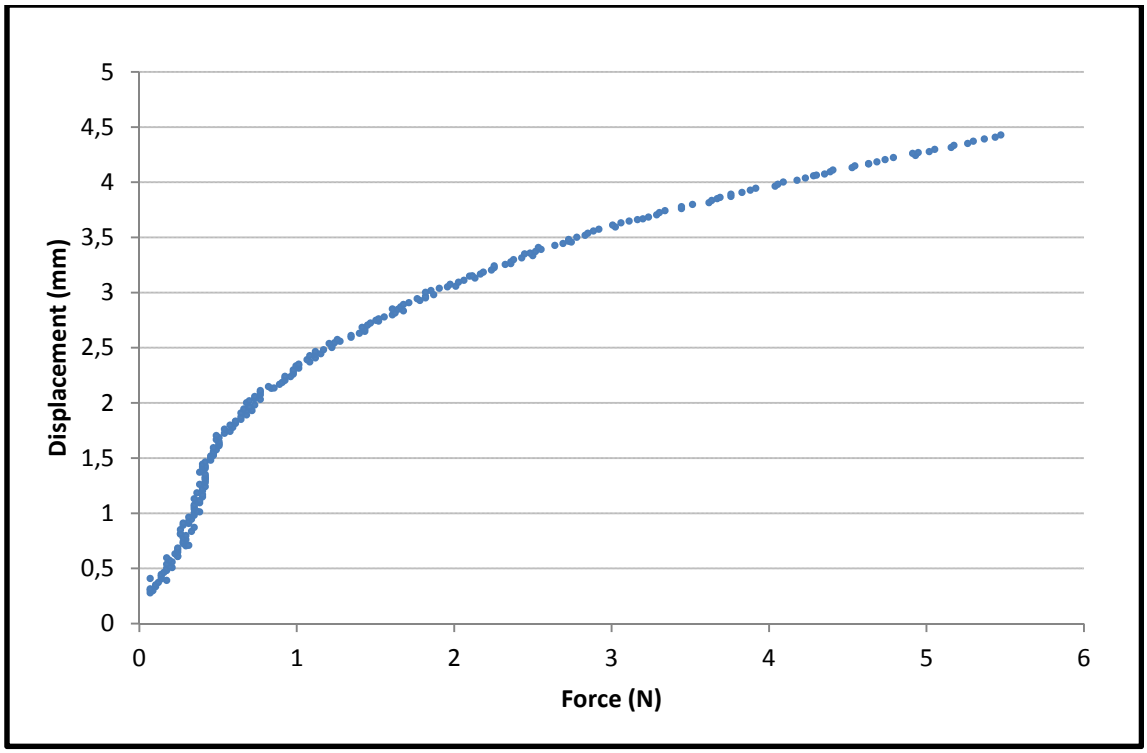

Figure S: Basic force-displacement curve square box of material F in Experiment 1 (test C3)

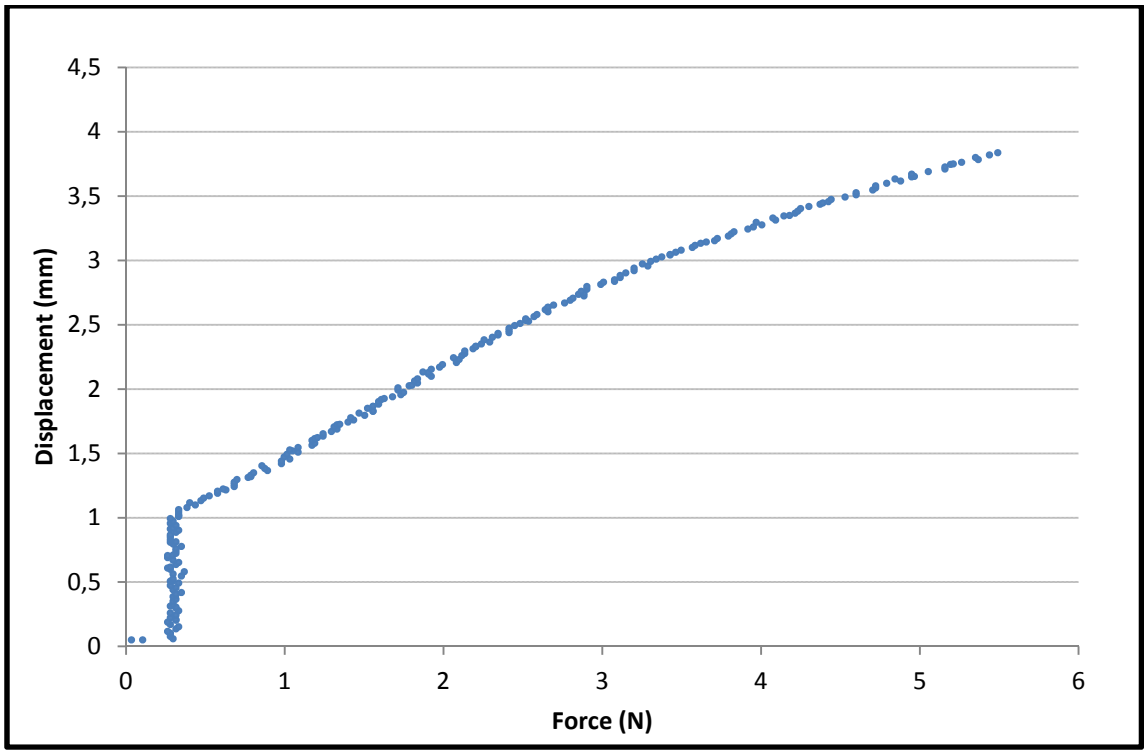

Figure T: Basic force-displacement curve square box of material F in Experiment 2 (C4)

Appendix 3

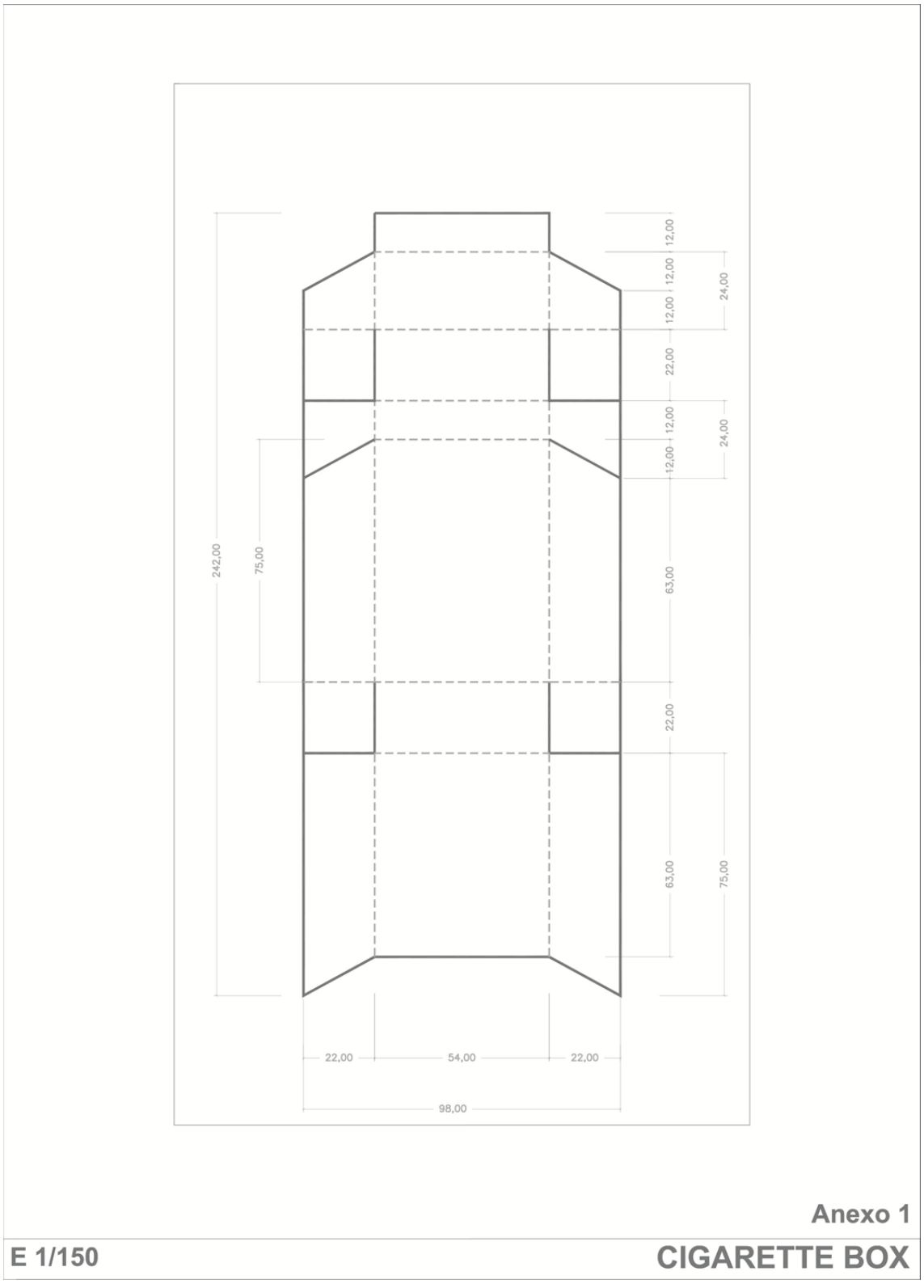
12,00
12,00
12,00
24,00
22,00
12,00
12,00
24,00
242,00
75,00
63,00
22,00
63,00
75,00
22,00
54,00
22,00
98,00
Anexo 1
E 1/150
CIGARETTE BOX

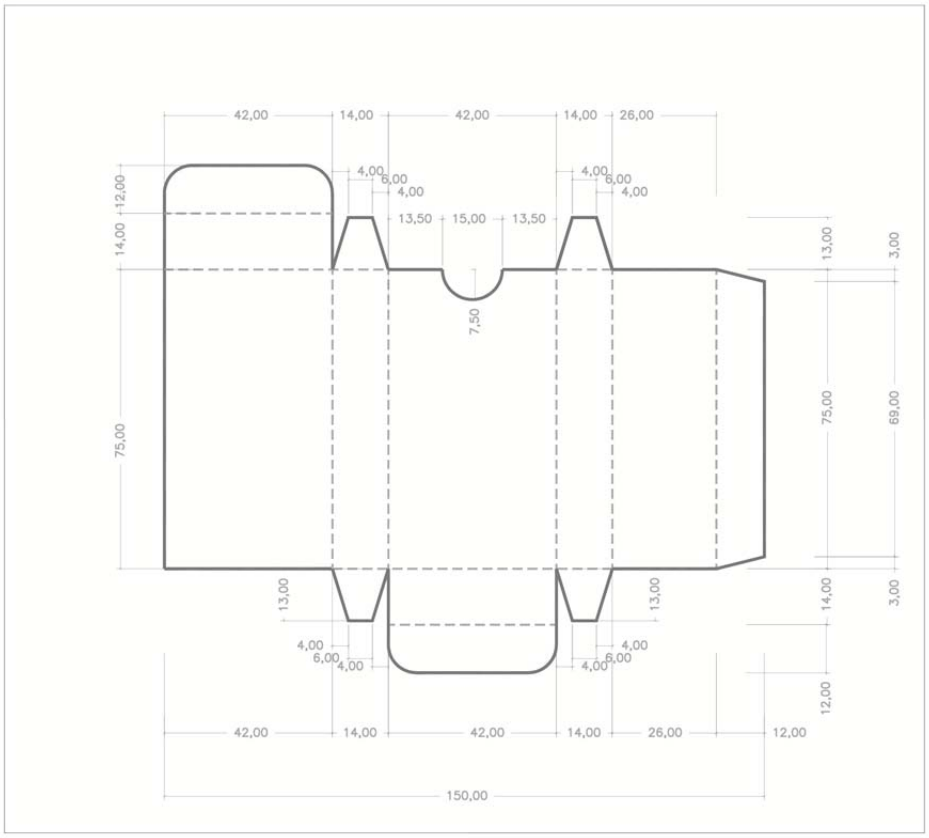

Anexo 1

E 1/150 **PILL BOX**

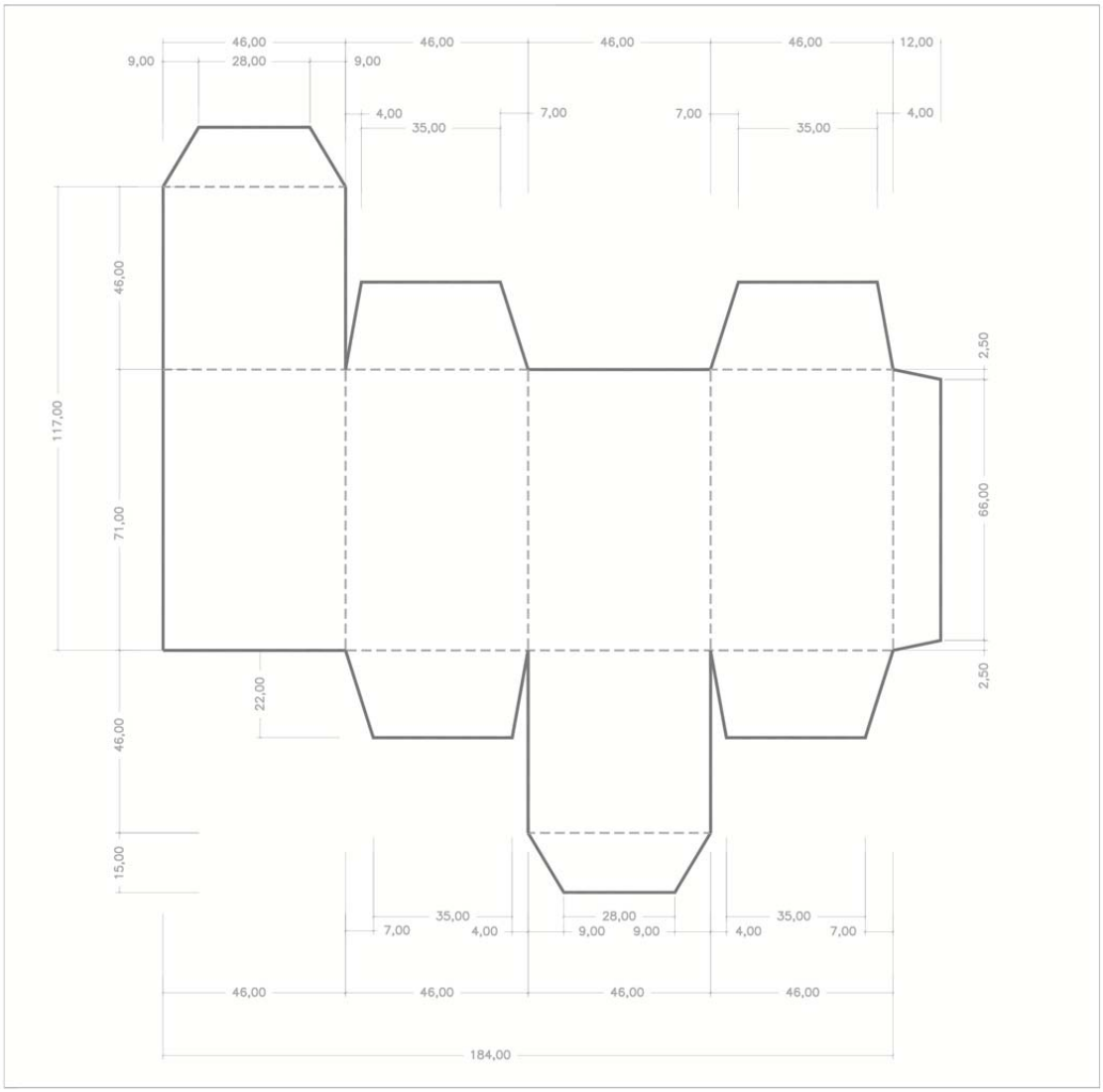

Anexo 1

E 1/150

SQUARE BOX